UTILIZING GENETICALLY ENGINEERED MOUSE MODELS OF PANCREATIC CANCER: EVALUATING THE ROLE OF CATHEPSIN B AND THE EFFICACY OF FARNESYL THIOSALICYLIC ACID

AARTHI GOPINATHAN

A DISSERTATION

In

Cell and Molecular Biology

Presented to the Faculties of the University of Pennsylvania

In Partial Fulfilment of the Requirements for the

Degree of Doctor of Philosophy

2010

Supervisor of Dissertation

David A. Tuveson, MD, PhD, Senior Group Leader

Graduate Group Chairperson

Daniel S. Kessler, PhD, Associate Professor

of Cell and Developmental Biology

Dissertation Committee

Martin P. Carroll, M.D, Associate Professor of Medicine

Margaret M. Chou, Ph.D, Associate Professor of Pathology and Laboratory Medicine

Richard K. Assoian, Ph.D, Professor of Pharmacology

Joseph L. Kissil, Ph.D, Assistant Professor

UTILIZING GENETICALLY ENGINEERED MOUSE MODELS OF PANCREATIC CANCER: EVALUATING THE ROLE OF CATHEPSIN B AND THE EFFICACY OF FARNESYL THIOSALICYLIC ACID

ACKNOWLEDGEMENTS

Firstly, I would like to thank David Tuveson for providing the support, funding, advice and opportunity to make this work possible.

A number of people have been involved in this work, and I would like to thank them for their contributions: Gina DeNicola, Florian Karreth, Kenneth Olive, Kristopher Frese, and Natalie Cook. My appreciation also goes to Michelle Rudek and everyone at the Analytical Pharmacology Core laboratory at the Kimmel Cancer Centre at Johns Hopkins for developing and conducting the FTS pharmacology assays. A big thank you to Frances Connor, Paul Mackin and Lisa Young for their contribution towards the therapeutics effort. I extend my thanks to Thomas Reinheckel for providing the cathepsin B null mice and for much valuable input and feedback. I would also like to thank Yoel Kloog, Adrienne Cox and Manuel Hidalgo for their assistance and input on FTS.

I would like to acknowledge the members of my thesis committee: Martin Carroll, Margaret Chou, Rick Assoian and Jo Kissil for their input and critical feedback. I would also like to thank Val Weaver and Barry Ziober for their input.

Thank you to the entire Tuveson laboratory for all of your help, feedback and support through the duration of my PhD. It has been an interesting and enjoyable journey.

I would like to thank all of my friends and family for their patience, particularly my parents and Preethi for their encouragement, and Florin who has provided me with unstinting support.

ABSTRACT

UTILIZING GENETICALLY ENGINEERED MOUSE MODELS OF PANCREATIC CANCER: IDENTIFICATION OF CATHEPSIN B AS A THERAPEUTIC TARGET AND EVALUATING THE EFFICACY OF FARNESYL THIOSALICYLIC ACID

Aarthi Gopinathan

David A. Tuveson

I have utilized genetically engineered mouse models of pancreatic cancer to identify a potential new therapeutic target, and to test the efficacy of a putative ras inhibitor. In the first part, I show that cathepsin B is upregulated during disease progression in the mouse pancreas, as is overall cathepsin activity. Loss of cathepsin B decreases preinvasive disease burden and imparts a significant survival benefit, with a consistent decrease in proliferation. In addition, lack of cathepsin B also decreases the burden of liver metastasis. Phospho-Erk localization appears to be affected by cathepsin B loss, which may account for the defect in proliferation. Cathepsin B null tumours also have increased active cathepsin L, which may compensate for cathepsin B in tumour progression and metastasis. Finally, a cysteine protease inhibitor in combination with gemcitabine confers a significant increase in survival in tumour-bearing mice. In the second part of this work, I have investigated the effect of farnesylthiosalicylic acid (FTS) in pancreatic tumour-bearing mice. In combination with gemcitabine, FTS significantly increases survival and decreases tumour kinetics and proliferation, and inhibits liver metastasis. Although FTS has previously been reported as a ras inhibitor, there is no evidence of modulation of ras activity or signaling in primary tumours after long-term or short-term intervention, or in liver metastases. In short, the therapeutic effects of FTS in this mouse model of pancreatic cancer do not appear to be ras-related, and the target of FTS remains to be elucidated.

CONTENTS

LIST OF TABLES

LIST OF FIGURES

LIST OF APPENDICES

INTRODUCTION

Pancreatic ductal adenocarcinoma

Pancreatic ductal adenocarcinoma (PDA) is a lethal disease with a median survival of < 6 months and a 5-year survival rate of < 5%. It is the fourth-leading cause of cancer-related deaths in the United States, with an estimated 42,000 new cases and 35,000 deaths in 2009 [(1)]. It is the most frequent type of pancreatic malignancy, accounting for >85% of cases [(2)]. Risk factors for PDA include chronic pancreatitis, diabetes, obesity, advanced age and smoking [(3-8)]. Approximately 10% of PDAs are associated with familial syndromes that confer an increased risk, corresponding with germline mutations that target tumour suppressors such as *Brca2*, *Ink4a* and *Lkb1* and the DNA repair gene *Mlh1* [(9-11)].

Chronic pancreatitis, a fibroinflammatory disease of the pancreas that causes irreversible loss of exocrine and endocrine function [(12)], is caused by various factors including excessive alcohol consumption, smoking, autoimmune disorders and genetic mutations. Long-standing chronic pancreatitis greatly increases the risk of developing pancreatic cancer [(13)]. Genes associated with pancreatitis are often linked to increased occurrence of PDA. Germline mutations in *Prss1* which cause hereditary pancreatitis are associated with a 53-fold increase in PDA occurrence [(14)]. In addition mutations in the cystic fibrosis transmembrane conductance regulator and Spink1 genes, both of which are associated with pancreatic disease, may increase the risk of PDA [(15, 16)]. Pancreatitis may promote tumorigenesis due to the release of growth factors and cytokines and the induction of reactive oxygen species, which in-turn would stimulate proliferation and selection of oncogenic mutations. Indeed, up to one-

third of patients with chronic pancreatitis carry activating mutations in the *Kras* oncogene [17].

Contributing to the dismal diagnosis of PDA is the difficulty in detecting early tumours, with a large number of patients presenting with advanced and metastatic disease [reviewed in 2, 18]. Only an estimated 10 - 15% of patients at first diagnosis possess tumours that can be resected by radical pancreatico-duodenectomy. In this subset of patients, disease almost always recurs and 5-year survival does not exceed 10 – 25% [19]. The majority of patients present with non-specific symptoms including jaundice and back pain, relating to the location of the primary tumour. Manifestations of more advanced disease include ascites, weight-loss, cachexia, obstruction of the gastric outlet and thromboembolic disease [20].

Primary tumours are commonly located at the head of the pancreas, and infiltrate surrounding organs including the spleen, lymph nodes and peritoneal cavity, with metastasis to the liver and lungs. PDAs primarily exhibit glandular histology, although others such as sarcomatoid, colloid and adenosquamous are also found [21]. Tumour heterogeneity results in multiple histologies and differentiation grades within a single tumour. The tumours are characterized by a dense desmoplastic reaction with fibroblasts and immune cells as well as deposition of an extracellular matrix consisting of proteins such as collagens, laminin and fibronectin among others [reviewed in 22,23]. PDAs tend towards early dissemination, and even small primary tumours exhibit lymphoid, vascular and perineural invasion [24].

Genetics and histology of pancreatic cancer

The genetic and histologic progression of pancreatic cancer has been analyzed from resected tumour specimens, giving insight into the mechanism of disease initiation and progression. Histologically, the model for disease progression describes increasing grades of preinvasive Pancreatic Intraepithelial Neoplasia (PanIN), characterized by a range of morphological alterations which suggest increasing grades of dysplasia. Normal pancreatic ducts consist of a single layer of cuboidal ductal epithelial cells with basally localized nuclei. The earliest preneoplasm is the PanIN1A, where the epithelial cells are columnar and comprised of an enlarged mucinous apical cytoplasm. In PanIN1Bs, the ducts start to develop papillary projections. PanIN2s are characterized by nuclear atypia, with nuclei losing their basal localization. The highest grade of preneoplasm is the PanIN3, described as ductal carcinoma *in situ,* with epithelial cells forming multiple layers and detaching into the lumen. This is followed by frank carcinoma, with invasion of the surrounding basement membrane. [25, 26]. Activating mutations in the *Kras* oncogene have been identified as the initiating event, present in >90% of tumours. Other common genetic events include the inactivation of the *Ink4a/Arf* locus, point mutations in the tumour suppressor *Trp53,* and mutations or deletions of *Smad4* [18] (Fig I.1).

Mouse models of pancreatic cancer

Mouse models of PDA have been described with $Kras^{G12D}$ as the initiating mutation that recapitulate the progression of the human disease, a process that is accelerated by the concomitant expression of a point-mutant *Trp53* allele [27, 28]. The $Kras^{G12D}$ allele is introduced as a conditional mutation, under the control of a floxed transcriptional

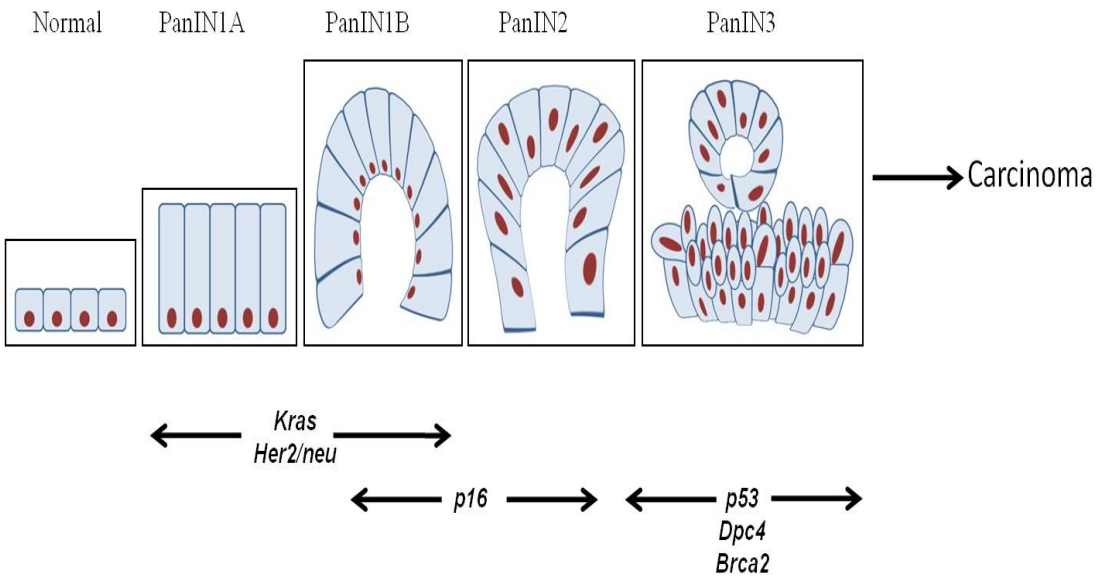

Figure I.1 Model showing the genetic and histologic progression of pancreatic cancer. The progression from normal ducts to PDA involves a progression with varying grades of dysplasia. Normal ducts consist of a single layer of cuboidal ductal epithelial cells. The path to carcinoma involves various grades of preinvasive Pancreatic Intraepithelial Neoplasia (PanIN), encompassing altered morphology, nuclear atypia and carcinoma *in situ*, followed by invasion into the basement membrane to form frank PDA. The initiating genetic event is mutation of the *Kras* oncogene, which is the earliest and most frequent event. Alterations in tumour suppressors such as p16, p53, DPC4 and Brca2 contribute to progression.

and translational stop cassette. Expression of cre recombinase is directed to the pancreas by the use of pancreas-specific promoters such as Pdx-1 and Ptf1-p48. When the stop cassette is excised, the oncogenic allele is expressed at physiological levels from its endogenous promoter. Expression of oncogenic Kras in the mouse pancreas causes the complete spectrum of preinvasive PanINs described above, and with a prolonged latency the spontaneous development of pancreatic cancer with low penetrance [27].

Additional mouse models have also been developed utilizing the incorporation of tumour suppressor gene mutations such as in the context of oncogenic Kras. The concomitant expression of a conditional point mutant *Trp53* allele in this system accelerates tumorigenesis. In this model, PDA develops with a much shortened latency, and with all of the clinical and pathological features of advanced disease, including cachexia, haemorrhagic ascites, and metastases to the liver, lungs, peritoneum and lymph nodes [28]. The conditional deletion of the *Ink4a/Arf* locus or of *Dpc4* also engenders rapid progression of metastatic PDA [29, 30]. These tumour suppressors do not cause pancreatic cancer without the coordinate expression of oncogenic Kras. The observations in mouse models support the role of oncogenic Kras in the initiation of PDA and the tumour suppressors *Ink4/Arf* and *Trp53* in disease progression, and fit well within the PanIN progression model. These mouse models provide a platform to study various facets of pancreatic cancer biology and are ideal to test therapeutic agents.

Utilizing genetically engineered mouse models in cancer biology and therapeutics

To date, the vast majority of preclinical efficacy studies of various therapeutic agents have been carried out in xenograft models. Xenograft tumour models are generated in immunodeficient mice following the implantation of tumour cells or tumour tissue into ectopic (e.g. subcutis, renal capsule) or orthotopic sites. The commonly stated advantages of tumour xenografts are the ease of model generation and the fact that therapeutic assessment occurs in human cancer tissue as opposed to another species. Furthermore, patient-specific xenografts have recently been described as a means to develop personalized therapies for some malignancies [31, 32]. Unfortunately, the results obtained from a number of xenograft studies [33, 34] have not translated well into the clinic [35, 36].

Genetically engineered mouse (GEM) models are a promising alternative to xenograft models for biological and therapeutic investigations. GEM models are generated through the introduction of genetic mutations associated with particular human malignancies, and have been reviewed previously [37]. One such example is the Kras and Trp53-driven models of pancreatic cancer described above. The initiating genetic lesion in a GEM, expressed through the use of conditional systems, occurs in the tissue that is relevant to the type of tumour being modelled. As a result, tumour initiation and progression occur in the correct cell type and in the relevant in situ environment. The result may be a pattern of expression whereby mutant cells are surrounded by normal cells, as is the case with tumour initiation in humans. In addition to the initiating molecular events, location of the preneoplasm within a particular cellular microenvironment or region of the organ may affect tumour

development. Primary PDAs, for instance, occur very frequently at the head of the pancreas, although the reasons for this are not understood. Tumour initiation in xenografts is very different, consisting of fully transformed, rapidly proliferating tumour cells grown in an environment that is not its normal milieu, and resulting in tumours that differ from corresponding human cancers.

The kinetics of tumour development in vivo are generally considered to be rather slow, occurring over several years and requiring multiple rounds of selection for cells with additional mutations that render a survival or proliferative advantage. The result is a primary tumour that is heterogeneous and polyclonal. From the therapeutic standpoint, this variation is important because of inherent differences in the populations of tumour cells that may confer a more resistant phenotype to intervention than others. This variability is often lacking in xenografts, as the tumours develop very rapidly and are usually derived from homogeneous or oligoclonal populations of cells. GEM models that have a long latency to tumour development may possess such variability, and will permit the study of pathways and mechanisms of resistance to various therapies. Indeed, our Kras;Trp53 GEM model of ductal pancreatic cancer harbours an underlying chromosomal instability phenotype that may produce a similar genomic heterogeneity to that observed in primary human PDA. Conversely, certain GEM models in which cancers develop rapidly may circumvent some of these stages and may not be effective models of the human disease.

One of the major drawbacks of xenograft models is the impairment of the immune system. Numerous studies have reported that the host immune system plays an important role in tumour development [(reviewed in 38, 39)]. GEM models have the distinct

advantage of producing tumours with a well-developed stromal compartment. The stroma consists of extracellular matrix proteins, such as collagen, which lends rigidity to tumours, and a number of different cell types that are recruited during tumour development including activated fibroblasts and immune cells. This allows tumour-microenvironment interactions to be modelled, in particular the role of non-cell autonomous processes and their relevance to tumour development and survival. In preclinical testing, understanding the effect of drugs on the tumour microenvironment, as well as the role of the immune system in the response to therapies, is of primary importance. GEM models can also be used to study the effect of immune-directed therapies.

Accurate GEM models histologically mimic their cognate human malignancy. Tumours from xenograft models, as well as those from a number of early GEM models, are often histologically distinct when compared with tumours found in human malignancies. These differences in tumour structure and composition may skew the results of drug tests, and affect the response of the tumour to the therapy. For example, PDA xenograft tumours are often exquisitely sensitive to anti-angiogenic agents owing to the neovasculature that develops in xenografts [40, 41]. However, there is less evidence that such a vascular composition is relevant in the cognate human tumour, as exemplified by the clinical failure of anti-vascular approaches in PDA.

Tumour metastasis represents a major clinical problem for which there are few effective therapies. This process is often difficult to model in xenografts owing to the rapid growth of primary ectopic tumours, although orthotopic implantation followed by resection [42] and direct intravascular tumour cell injection can generate models of

distant spread. Nonetheless, xenograft models cannot recapitulate the myriad of processes required for metastasis from a primary tumour. GEM models that develop tumours that metastasize from the native site should, therefore, offer the optimal manner to study metastasis and evaluate therapeutics directed against this process.

The development of approaches that accurately describe tumour burden and tumour biology during drug treatment is imperative for successful clinical translation. Given the multiple biological differences between xenografts and autochthonous human tumours, it is therefore not surprising that such methods are routinely developed in clinical investigation rather than during preclinical investigation. Indeed, GEM models should prove advantageous over xenograft models in this regard. For example, high resolution imaging modalities can be developed in GEM models to monitor therapeutic response. These include anatomic methods such as magnetic resonance imaging, computed tomography, and sonography, and functional methods that investigate tissue perfusion or metabolism. In contrast to PDA xenograft models, the Kras-driven GEM model of pancreatic cancer closely recapitulates the radiographic features of human PDA [(43)]. Additionally, plasma proteomic profiling in GEM models can provide new candidates for tumour detection and monitoring in patients, as recently demonstrated with a mouse model of pancreatic cancer [(44)]. As tumour tissue is readily available, GEM models enable the direct correlation between radiological responsiveness, drug levels, and molecular and cellular parameters. This is one of the least explored facets of therapeutic development, owing to the paucity of tumour tissue available from patients undergoing treatment.

Evidence supporting the usefulness of GEMs

To date, GEM models of breast, lung and pancreatic cancer have been used in preclinical evaluations of therapeutic agents. Similar to clinical experience, lung adenocarcinomas arising as a result of mutant epidermal growth factor receptor (EGFR)-expression regressed on treatment with erlotinib and cetuximab [45, 46]. In another study, the response of mammary tumours in *p53*-and *Brca1*-deficient mice to the chemotherapeutic agents doxorubicin, docetaxel and cisplatin was evaluated [47]. Breast tumours in this model demonstrated sensitivity to the chemotherapeutic agents and acquired resistance in a manner that mimicked clinical experience [reviewed in 48]. The use of GEM models of PDA, which do not respond to the chemotherapeutic gemcitabine, suggested a new paradigm in pancreatic cancer therapeutics by stromal depletion using hedgehog inhibitors [43]. This type of analysis would not have been feasible in xenograft models given the paucity of stromal content. Therefore, these early results obtained with GEM models suggest they can provide similar therapeutic responses to those observed in clinical practice.

The work presented here utilizes GEM models of pancreatic cancer to study the biology of the disease, as well as to study the effect of therapeutic agents. I have evaluated the relevance of the lysosomal protease cathepsin B in the initiation and development of PDA, and have identified cathepsin B as a potential therapeutic target of interest in pancreatic cancer. In addition I have evaluated the efficacy of farnesylthiosalicylic acid, a small molecule described as a Ras inhibitor, in the GEM model of PDA to determine its usefulness as a pancreatic cancer therapy.

CHAPTER I

CATHEPSIN B PROMOTES THE PROGRESSION OF PANCREATIC DUCTAL ADENOCARCINOMA IN MICE

INTRODUCTION

The cysteine cathepsin family of lysosomal proteases

The cathepsins are a large family of lysosomal proteases. They are involved in a number of biological processes including protein turnover, antigen processing and immune responses, hormone activation, apoptosis and extracellular matrix remodelling [49, 50, 51]. Cathepsins are classified according to catalytic site residues – cathepsins A and G are serine cathepsins, E and D are aspartate cathepsins, and the 11cysteine cathepsins (B,C, F, H, K, L, O, S, V, W and X) comprise the largest subgroup and belong to the papain family of proteases [reviewed in 52].

Cathepsin activity is tightly regulated, with all members of the family being synthesized as inactive zymogens. During transport to the endoplasmic reticulum, the prepeptide is removed. The propeptide is required for proper targeting, stability and folding [53-55]. It also inhibits the activity of the enzymes by restricting access to the active site. The cathepsins are transported to lysosomes via the mannose-6-phosphate receptor pathway, where the procathepsins undergo proteolytic cleavage due to the reducing, acidic environment, giving rise to the active mature enzymes [56, 57].

Cathepsins B and L are known to be ubiquitous and constitutive and are thought to participate in protein turnover. Other members of the cysteine cathepsin family exhibit more specific expression patterns: cathepsin S, for instance is expressed in immune cells and is involved in major histocompatibility complex II antigen presentation and cathepsin K is osteoclast-specific and involved in bone remodelling [reviewed in 58]. The generation of knockout mice has allowed a more in-depth analysis of the role of cathepsins in various processes, and has highlighted some redundancies in

the family. Although cathepsin L knockout mice demonstrate phenotypes in skin and cardiac muscle, and cathepsin B-deficient mice are impaired in tumour necrosis factor alpha-induced hepatocyte apoptosis [59-61], these individual knockouts are viable. The combination of the two deficiencies, however, results in the apoptosis of cerebral and cerebellar neurons and death at 2-4 weeks [62].

Disturbances in cathepsin activity lead to pathological conditions such as rheumatoid arthritis, cancer, osteoporosis, neurological disorders and lysosomal storage diseases, and are thus being studied as therapeutic targets for a number of diseases[reviewed in 63, 64].

Cathepsin B

Structure and activation

Cathepsin B is a ubiquitous member of the cysteine cathepsin family, and is considered a housekeeping gene. In humans, the gene is located on chromosome 8p22, and consists of 12 exons [65]. The inactive protein consists of 339 amino acids (43 kda) and the active single chain form is 31kda [57]. Structurally, cathepsin B consists of two distinct domains, the left-hand "L" domain and the right-hand "R" domain. The L domain consists mostly of alpha-helices and the R domain is composed of a beta-barrel motif. The amino and carboxy termini function to hold the domains together. The protein is approximately disc shaped with an obvious incision representing the active site cleft. Catalytic residues in the active site are cysteine 108, histidine 278 and asparagine 298 (Fig I1.1A). In the proenzyme, the propeptide occupies the active site and prevents its accessibility to substrates (Fig I1.1B) [66]. Cathepsin B is an endopeptidase like most other members of the family. In addition,

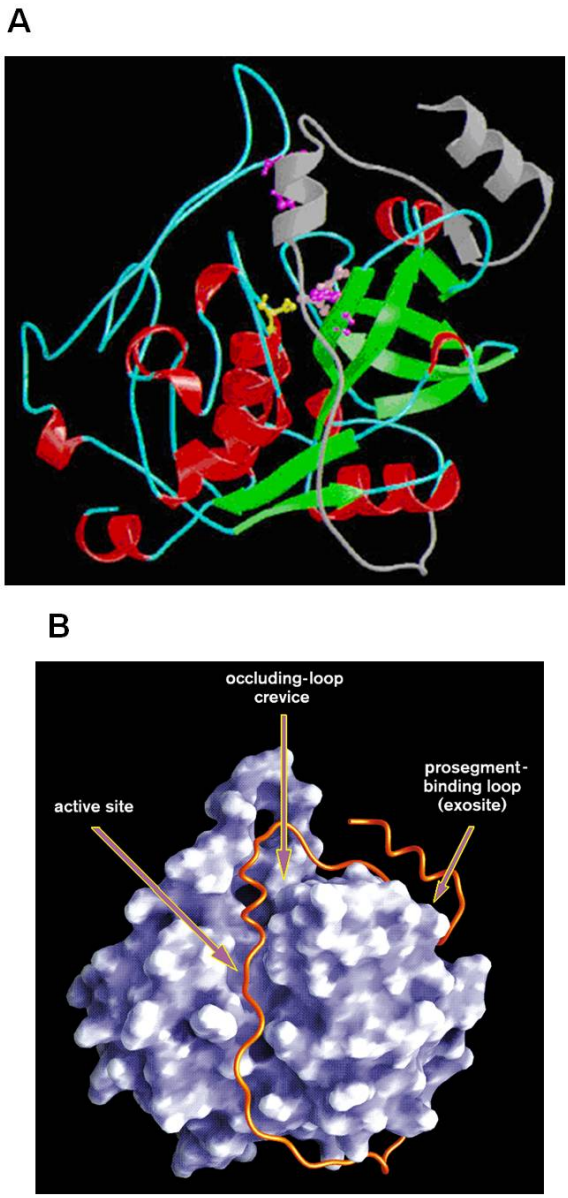

Fig I1.1 Crystal structure of cathepsin B. The diagram of procathepsin B (A) depicts the propeptide in grey. Catalytic residues are depicted – the active site Cys108 is in yellow, His278 in purple, and Asn298 in pink. Histidine residues on the occluding loop are depicted in purple. Structure obtained from MEROPS – the peptide database C01.060 (A). The active site cleft is visible in this depiction of the three-dimensional structure of cathepsin B, along with its occupation by the propeptide. Image obtained from Cygler *et al.* Structure 1996:4(4) (B).

however, it is also a carboxypeptidase, due to the presence of an occluding loop formed from residues 104 – 126. Two cysteine residues, cys108 and cys119, form a disulphide linkage that encloses the included residues in a circle, and the histidine residues his110 and his111 serve to stabilize the terminal carboxylate of a peptide. Together, this structure accounts for the dipeptidyl carboxypeptidase activity [(reviewed in 67)].

Activation of the enzyme is precipitated by a decrease in pH. This decrease substantially weakens the interactions between the active cleft and the propeptide [(68)]. Glycosaminoglycans, which facilitate autoactivation, are also capable of inducing a conformational change resulting in the weakening of the propeptide-active cleft interaction [(69)]. The occluding loop of cathepsin B is involved in displacing the propeptide once it is less tightly bound to the active site [(70)]. Since propeptides exhibit a small amount of intrinsic catalytic activity, this may be sufficient to initiate a chain reaction of propeptide cleavage. However, other proteinases may also have a role in initiation of activation. Once the chain is begun, the process rapidly continues due to the increasing numbers of active molecules [(71)].

Cathepsin B in cancer

Cathepsin B expression is upregulated in a number of human malignancies. Cathepsin B levels in serum and tumour tissue are under investigation as prognostic indicators in a variety of tumour types including colon , endometrial , non-small cell lung, glioblastoma, pancreatic cancer, breast carcinoma and melanoma which are summarized in Table I1.1 [(72-79)].

Cancer type	Relation of cathepsin B expression to outcome
Colon cancer	Associated with higher risk of mortality.
Endometrial cancer	Predictive of aggressive tumour behaviour.
Non-small cell lung cancer	Associated with poor outcome.
Glioblastoma	Strong predictor of survival.
Gastric cancer	Associated with advanced tumour stages and progressive disease.
Pancreatic adenocarcinoma	Strong prognostic marker in resectable pancreatic cancer, predictor for early recurrence after resection.
Breast carcinoma	Good prognostic indicator in lymph node-negative patients.
Oral cancer	Prognostic marker – relationship between expression levels and invasive and metastatic growth.
Melanoma	May serve as a prognostic factor in advanced disease

Table I1.1 Correlation of cathepsin B in serum or tumour tissue with disease outcome

Upregulation occurs via several different mechanisms. In oesophageal and gastric adenocarcinomas, a novel amplicon has been identified that results in the overexpression of cathepsin B [80, 81]. Tumour cells express cathepsin B transcript variants, through alternative promoters and splicing [82, 83]. In fact, cathepsin B transcripts lacking exon 2 appear to be more efficiently translated, and may be responsible for the increased expression of cathepsin B in a number of human malignancies [65, 84, 85]. Cathepsin B transcription appears to be controlled by the Sp1 and Ets1 transcription factors in cancer, with expression levels correlating with levels of Sp1 in glioma cells [82, 86, 87]. In addition, the mRNA stability of cathepsin B can be altered – for instance, phorbol ester treatment of the HL60 human leukaemia cell lines results in increased mRNA half-life on differentiation into macrophages [88].

Cathepsin B is not just upregulated but also mislocalized. Expression in tumour cells is in lysosomal and endosomal vesicles, but it is also on the plasma membrane and secreted into the extracellular space. So far, cathepsin B is the only cysteine cathepsin that has been localized to a membrane microdomain. Procathepsin B binds directly to S100A10, the light chain of the annexin II heterotetramer (AIIT), and this interaction mediates the localization of cathepsin B to caveolae of human colon carcinoma cells [89, 90]. The localization of cathepsin B to caveolae also appears to be influenced by mutant Kras, which results in increased pericellular activity [91]. In addition, interactions of cells with extracellular matrix components such as collagen I increase cathepsin B secretion as does decreased extracellular pH, the latter potentially through lysosomal exocytosis [92, 93].

Cathepsin B, through the degradation of extracellular matrix components such as collagen IV, laminin and fibronectin, is thought to participate in malignant progression. This degradation occurs either directly, or through the activation of proteolytic cascades on the cell surface. Proteases such as urokinase plasminogen receptor (uPA) and its receptor uPAR, and the matrix metalloproteases MMP-2 and MT1-MMP are localized to caveolae [94-96]. Cathepsin B can activate uPA and MMPs, thus initiating protease cascades that contribute to matrix degradation and the tumorigenic process (Fig I1.2).

Cathepsin B in mouse models of cancer

Mouse models of islet, mammary and intestinal carcinomas have elucidated the importance of cathepsin B in various tumour types. In the RIP-Tag model of islet carcinogenesis, lack of cathepsin B retards tumour growth and impairs proliferation

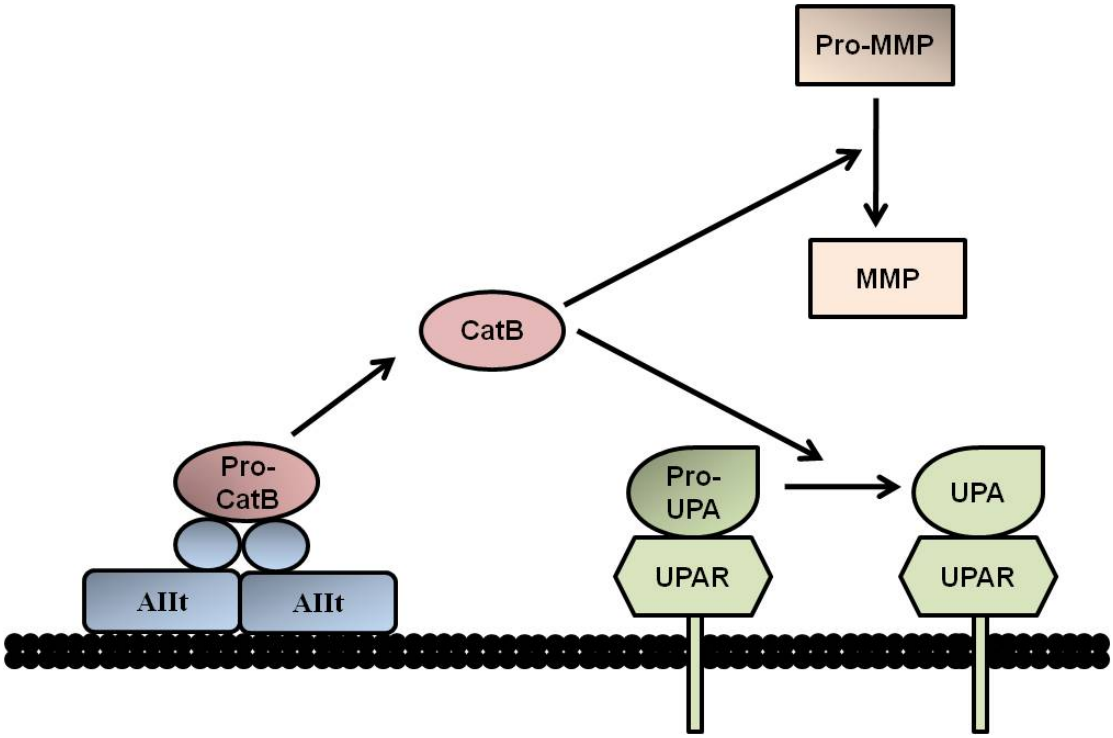

Fig I1.2 Cathepsin B activates proteases extracellularly. Cathepsin B may be exported in cancer cells. One mechanism for this occurrence is through interactions with Annexin II heterotetramers. Once cathepsin B is activated outside the cell, it is involved in the initiation of proteolytic cascades, by activating MMPs and converting Pro-Urokinase plasminogen activator (Pro-UPA) to active UPA.

and invasion [97, 98]. The overexpression of cathepsin B in the polyoma middle T-induced mammary carcinoma model enhances tumour progression and metastasis, with increased immune infiltration and angiogenesis [99]. Cathepsin B loss in the mouse mammary tumour virus – PyMT model impaired the development of high-grade carcinomas, with a significantly decreased tumour proliferation [100]. The genetic ablation of cathepsin B in the Adenomatous Polyposis Coli (APC) model results in decreased polyposis [101]. Cathepsin B loss impinges upon various facets of tumour development including initiation, proliferation, apoptosis, angiogenesis and metastasis. The contribution of cathepsin B to tumour development and metastasis is not solely cell autonomous. Indeed, tumour-associated stromal cells such as fibroblasts, macrophages and neutrophils express cathepsin B [58], and a role for microenvironmental cathepsin B in metastasis has been previously demonstrated *in vivo* in the transgenic MMTV-PyMT model of mammary carcinoma [102]. In addition, cathepsin B from tumour-associated macrophages is an important contributor towards tumour growth, angiogenesis and invasion [103].

To examine the role of cathepsin B in the initiation and progression of PDA, the oncogenic Kras-driven mouse models of pancreatic cancer were utilized, concomitant with genetic ablation of cathepsin B. In these models, cathepsin B expression and cathepsin activity are upregulated in preinvasive and invasive stages of disease. As shown, Cathepsin B deficiency leads to decreased proliferation in PanINs and confers a significant survival advantage in mice that develop PDA. Additionally, pancreatic carcinomas lacking cathepsin B retain a proliferative defect that is consistent with that observed in early-stage disease. Cathepsin B loss also affects metastasis of PDA to the liver with a significant reduction in the burden of liver metastases. In addition,

cathepsin B null mice exhibit trends towards decreased incidence of liver metastasis and increased incidence of lung metastasis. Loss of cathepsin B expression correlates with decreased phospho-ERK and decreased proliferation of pancreatic cancer cell lines in subcutaneous allografts. Finally, use of a non-cell permeable broad-spectrum cysteine protease inhibitor in combination with Gemcitabine *in vivo* increases survival of tumour-bearing mice. Taken together, these results support cathepsin B as a therapeutic target in PDA.

MATERIALS AND METHODS

Mouse strains

The LSL-Kras^{G12D}, LSL-Trp53^{R172H}, Trp53$^{flox/flox}$, Pdx-1-Cre and cathepsin B null strains of mice have been previously described [27, 28, 104, 105]. These strains of mice were interbred to ensure a mixed C57BL6/129Sv background for survival studies. Mice were housed and maintained, and experiments were conducted, in compliance with UK home office regulations.

Generation of experimental animals

1. LSL-Kras^{G12D}; Cathepsin B; Pdx-1-Cre: LSL-Kras^{G12D}; Cathepsin B mice were bred with Cathepsin B; Pdx-1-Cre to generate LSL-Kras^{G12D}; Pdx-1-Cre; Cathepsin B+/+ and LSL-Kras^{G12D}; Pdx-1-Cre; Cathepsin B-/- offspring which were utilized for timepoint analysis of disease burden.

2. LSL-Kras^{G12D}; Trp53$^{flox/flox}$; Cathepsin B; Pdx-1-Cre: LSL-Kras^{G12D}; Trp53$^{flox/flox}$; Cathepsin B and Trp53$^{flox/flox}$; Cathepsin B; Pdx-1-Cre parents were mated to generate LSL-Kras^{G12D}; Trp53$^{flox/flox}$; Pdx-1-Cre; Cathepsin B+/+ and LSL-Kras^{G12D}; Trp53$^{flox/flox}$; Pdx-1-Cre; CathepsinB-/- offspring for survival studies

3. LSL-Kras^{G12D}; Trp53^{R172H}; Cathepsin B; Pdx-1-Cre: LSL-Kras^{G12D}; Trp53^{R172H}; Cathepsin B mice were interbred with Cathepsin B; Pdx-1-Cre mice. The offspring of interest were LSL-Kras^{G12D}; LSL-Trp53^{R172H}; Pdx-1-Cre; Cathepsin B+/+ and LSL-Kras^{G12D}; LSL-Trp53^{R172H}; Pdx-1-Cre;

Cathepsin B-/-, which were utilized for survival and further tumour studies.

4. LSL-Kras^{G12D}; Trp53^{R172H}; Pdx-1-Cre: LSL-Kras^{G12D}; Trp53^{R172H} and Pdx-1-Cre mice were bred together to generate experimental animals used for therapeutic studies.

Reagents

Avidin-biotin blocking kits (SP-2001), signal amplification kits (PK-6200), DAB substrate kits (SK-4100) and peroxidise-conjugated secondary antibodies for immunohistochemistry were obtained from Vector labs. Prosense 680 was obtained from VisEN Medical. E64 was obtained from Sigma-Aldrich. Secondary antibodies for western blotting were obtained from Jackson Immunoresearch. EZ-link Sulfo-NHS-SS-Biotin and neutravidin agarose from Pierce was obtained from Thermo Fisher. Tissue culture reagents were obtained from GIBCO. E64 (E3132) was obtained from Sigma-Aldrich.

Immunohistochemistry

Paraffin-embedded mouse tissue sections were dewaxed in 100% xylene (2x 5minutes), and were then rehydrated through an ethanol series (5 minutes each in 100%, 96%, 80% and 70% ethanol) followed by phosphate-buffered saline (PBS). Antigen retrieval was heat-mediated using boiling citrate buffer (10mM, pH 6.0). After cooling, endogenous peroxidise activity was blocked by incubation in 3% hydrogen peroxide for 15 minutes. The slides were then blocked for 30 minutes at room temperature in 10% serum + 1% BSA, followed by avidin-biotin blocking.

Primary antibodies were used at the dilutions indicated below in blocking buffer, and were incubated overnight at 4°C.

Slides were washed twice with TBS-T and incubated with biotinylated secondary antibodies at room temperature for 30 minutes. Signal amplification was carried out with Vectastain ABC reagents for 30 minutes, and slides were incubated with diaminobenzidine (HRP-based detection) until suitable signal developed. The slides were rinsed in tap water and counter-stained with Harris haematoxylin. They were then dehydrated through an ethanol series into xylene and coverslipped with permount mounting medium.

Antibody	Source	Dilution
Cathepsin B	R&D Biosystems	1:50
Cathepsin L	R&D Biosystems	1:50
Alpha-smooth muscle actin	Abcam	1:200
Phospho-histone H3	Cell Signaling	1:100
Ki67	Neomarkers	1:200
CD31	Santa Cruz Biotechnologies	1:100
Phospho-ERK (Thr202/Tyr204)	Cell Signaling	1:100

Table M 1.1: Antibodies for Immunohistochemistry

Masson's trichrome staining

Tissue sections were deparaffinised in xylene as described above. Sections were treated with picric acid for 30 minutes, and were then washed in running tap water. The tissue was stained with Weigert's Iron haematoxylin solution for 5 minutes and washed briefly in running water. Sections were then treated in 2% acid alcohol to differentiate, washed in running tap water and stained with acid fuchsin for 10 minutes. After rinsing in deionised water, the tissue was treated with phosphomolybdic acid for 5 minutes and then stained with methyl blue for 5 minutes. The slides were rinsed in deionised water, differentiated in 1% acetic acid and dehydrated rapidly in two changes of 100% ethanol and xylene, and mounted using a xylene-based mounting medium.

***In vivo* measurement of cathepsin activity**

Prosense 680 was diluted in 1X PBS according to the manufacturer's instructions (1.35 mls of 1X PBS added to 150 µl of probe). The probe was equilibrated to room temperature and injected at a concentration of 80nM/kg intravenously into the tail vein. After 24 hours, mice were sacrificed and the pancreas and brain were harvested. Fluorescence signal was detected using the IVIS 200 (Caliper Life Sciences, MA), and signal intensity was quantified using Living Image 3.2 as a measure of arbitrary units per gram of tissue. Brain tissue was used as a negative control.

Derivation of tumour cell lines

The establishment of cell lines from mouse pancreata has been previously described [(106)]. The pancreatic cancer cell lines used in this study were established by an abbreviated version of this protocol. In brief, mice were sacrificed and tumour pieces

were harvested into buffered G solution (HBSS + Penicillin/streptomycin, fungizone, 0.9g/L glucose). The tumour pieces were minced in 1ml of 0.25% trypsin, and were incubated at 37°C for 10 minutes. Trypsin was quenched in DMEM + 10% FBS. Cells were centrifuged, washed three times in G solution, and plated onto BD biocoat collagen plates in serum-free ductal medium (DMEM F-12, 1.22 mg/ml nicotinamide, 5mg/ml glucose, 5% ITS+, 100µg/ml gentamicin, 5% Nu-serum IV, fungizone, 25 µg/ml bovine pituitary extract, 20ng/ml epidermal growth factor, 50nM 3,3'5-Triiodo-L-thyronine, 1µM dexamethasone, 100ng/ml cholera toxin). Cells were maintained on collagen for two passages and were then transferred to plastic. Once successfully established on plastic, cell lines were maintained in DMEM + 10% FBS.

Generation of mouse embryonic fibroblasts

Cathepsin B null mouse embryonic fibroblasts (MEFs) were obtained from E13.5 day embryos. Embryos were dissected from pregnant females, the internal organs and heads were removed and the tissue was chopped up in 0.25% trypsin. Following a 45 minute incubation at 37°C, the trypsin was quenched and the cells were suspended by pipetting in DMEM + 10% FBS, and were plated onto 15 cm dishes.

Surface biotinylation of cell lines

Biotin labelling of surface proteins was carried out using 0.5 mg/ml of EZ-Link-Sulfo-NHS-SS-Biotin. The reagent was prepared fresh immediately prior to use. Cells were washed with cold 1X PBS and were labelled for 30 minutes at 4°C. Unlabelled cells to be used as a negative control were incubated with 1X PBS. Unbound biotin was quenched with 100mM glycine. Cells were rinsed and lysed with RIPA buffer. Lysates were incubated with neutravidin beads for 1 hr at 4°C. The beads were

washed in cold 1X PBS and boiled in SDS loading buffer to elute bound protein, and proteins were analyzed by western blotting.

Quantification of proliferation

Proliferation in PanINs was quantified as percentage of Ki67 positive cells. Tissue sections were stained for Ki67 and all PanINs on a given section were quantified by enumeration of positive and negative nuclei. Tumour proliferation was quantified as a measure of phospho-histone H3 positive nuclei in five 20X fields. Proliferation in allografts was quantified by measuring the number of Ki67 positive cells per 20x field.

Tumour analysis

Areas of necrosis were measured using Imagescope, and were represented as percentage of total tumour area. Mean vessel density (MVD) was measured by staining sections for CD31, and enumerating the number of vessels in five 40X fields. Area of liver and lung metastases was measured using Imagescope.

Protein extraction from tumour tissue

Tumour fragments harvested for protein lysates were snap-frozen in liquid nitrogen. Tissue was lysed in SDS lysis buffer containing protease and phosphatase inhibitors and centrifuged to remove debris.

Cloning and Transfection

The mouse cathepsin B cDNA [107] was isolated from the pSG5 backbone using BamHI and EcoRI and was cloned into the pBabehygro expression vector. The resulting expression plasmids were sequenced to verify cathepsin B cDNA integrity.

Cells were transfected with pBabehygro or pBabehygro-Cathepsin B using lipofectamine 2000 (Invitrogen) according to the manufacturer's instructions. Serum-free Opti-MEM was combined with 5µl lipofectamine and 2µg DNA to a final volume of 200µl, which was added to cells drop-wise. After 24 hours, the medium was replaced and cells were selected with 200ug/ml hygromycin for 7 days to select clones stably-expressing cathepsin B.

Cell culture

Cell lines derived from tumours were maintained in DMEM + 10% FBS. For harvesting protein, 2 x 10^6 cells were plated on 10cm dishes, grown overnight and were fed with DMEM + 1% FBS for 24 hours before use. Protein lysates were obtained using SDS lysis buffer. Culture supernatants were harvested and concentrated using Millipore centrifugal filter units.

Proliferation assays

Proliferation assays were set up by trypsinizing cells and seeding them at 2.5 x 10^5 cells in triplicate in 12-well dishes in either DMEM + 10% FBS or DMEM + 1% FBS. Cells were fed daily and cell number was determined on days 1, 3, 5 and 8 using a Z2 Coulter Counter (Beckman Coulter).

Soft agar assays

Soft agar assays were set up in 6 cm dishes. Low melting point agarose was dissolved at 2% in DMEM. This stock was diluted to 0.8% agarose, 4mls was plated onto 6 cm dishes and allowed to solidify for 30 minutes. Cells were trypsinized, and 2 x 10^4 cells were suspended in 0.4% low melting point agar and were layered over the 0.8% agar.

The agarose was allowed to set before plates were transferred to a 37°C incubator overnight. The next day, cells were fed with DMEM + 10% FBS. Colonies were allowed to develop for three – four weeks, and the cells were fed twice weekly during this period.

Cytokine arrays

Analysis of cytokine profiles was conducted using the RayBio mouse cytokine antibody array 6 (AAM-CYT-6) from RayBiotech Inc. The assay was conducted as described by the manufacturer. Snap-frozen tissue fragments and cell lines were lysed in 1X RayBio cell lysis buffer with added proteinase inhibitors (Roche), and protein concentration was quantified. Pooled tumour samples were prepared by mixing 50 µg protein each from five KPC;B+/+ and five KPC;B-/- tumours to give a total of 250 ug protein for each cohort. Samples from cell lines were similarly pooled – 100 ug each for a total of 300 ug each for cathepsin B-null and cathepsin B-reconstituted tumour lines. Pooled samples were diluted to a total volume of 2mls in 1X blocking buffer.

Array membranes were blocked with 3mls 1X blocking buffer at room temperature for 30 minutes. Blocking buffer was decanted, the samples were added to the membranes and were incubated at 4°C overnight with gentle rocking. The membranes were washed three times with 1X wash buffer I for five minutes each at room temperature, followed by two five-minute washes with 1X wash buffer II at room temperature.

Biotin-conjugated primary antibody solution was prepared by diluting it in 4mls 1X blocking buffer, 2 mls of the working solution was added to each membrane and

incubated at room temperature for 2 hours. This incubation was followed by repeated washes as described above. HRP-conjugated streptavidin was diluted 1000-fold in 1X blocking buffer, 3mls of the working solution was added to each membrane, incubated for 2 hours at room temperature and washed as described above. Detection was by chemiluminescence using the provided detection reagents and X-ray film (Amersham). The film was scanned using a GE Image Scanner III, and the spots were quantified using ImageQuant software.

Interleukin-6 enzyme-linked immunosorbent assay (ELISA)

Interleukin-6 levels in cells and tissue were measured using the Quantikine mouse IL-6 immunoassay (R&D systems, M6000B). Cells and tissues were lysed using 1X cell lysis buffer (Cell Signaling, 9803) with added protease inhibitors. Five tumour fragments each were assayed from the KPC;B+/+ and KPC;B-/- cohorts. 50µg of protein was loaded for each sample in a volume of 50 µl, with assays being done in triplicate.

Standard dilutions were prepared in calibrator diluents ranging from 0 pg/ml to 500pg/ml. 50 µl of assay diluents was added to each well, followed by 50 µl of standards, control and samples in triplicate. The plate was mixed gently and allowed to incubate at room temperature for 2 hours, followed by 5 washes with 400 µl each of wash buffer. Wash buffer was carefully decanted from all wells before proceeding to the next step. 100 µl of enzyme-linked IL-6 polyclonal antibody was added to each well and incubated for two hours at room temperature, followed by washes as described above to remove unbound antibody. Signal was generated by incubating with 100 µl of substrate solution for 30 minutes at room temperature in the dark, and

the reaction was halted with the acidic stop solution. The optical density was read using the Tecan Infinite M200 microplate reader. Sixteen spots were read per well at 450nm, with a background correction of 570nm. Optical density values were plotted on the standard curve to generate interleukin-6 concentrations.

Ras-GTP assays

Ras activity was measured with a kit (Millipore) following the manufacturer's instructions. Cells were rinsed twice with ice-cold 1X PBS and lysed in ice-cold Mg2+ lysis buffer (25mM Hepes pH 7.5, 150 mM NaCl, 1% Igepal CA-630, 10mM $MgCl_2$ and 2% glycerol). Lysates were incubated with 10 µl Raf-1 RBD agarose beads for 30 minutes at 4°C. The beads were washed carefully three times with cold lysis buffer, and were boiled in SDS loading dye to elute proteins. Ras-GTP levels were measured by western blotting.

Western blotting

Proteins were boiled in SDS loading buffer, separated at 80 – 100V on 4-12% Nupage gels (Invitrogen) using MES running buffer (Invitrogen). Proteins were transferred onto PVDF membranes (Millipore) in transfer buffer (25mM Tris, 192mM glycine, 20% ethanol) at 70V for 2.5 hours. Membranes were blocked for one hour with 5% milk in TBST (10mM Tris, 150mM NaCl, 0.1% Tween-20) and were incubated with relevant primary antibodies at 4°C overnight. Membranes were washed with TBST

Antibody	Source	Dilution
Cathepsin B	R&D Biosystems	1:1000

Cathepsin L	R&D Biosystems	1:1000
Actin (I-19)	Santa Cruz Biotechnologies	1:5000
EGFR	Cell Signaling	1:1000
ERK	Cell Signaling	1:1000
Stat3 (Tyr705)	Cell Signaling	1:1000
Phospho-Akt (Ser 473)	Cell Signaling	1:1000
Phospho-Rsk (Thr359/Ser363)	Cell Signaling	1:1000
Phospho-S6 (Ser 240/244)	Cell Signaling	1:1000
Cyclin D1	Santa Cruz Biotechnologies	1:1000
Phospho-MEK (Ser 217/221)	Cell Signaling	1:1000
Ras (Ras10)	Millipore	1:10,000
MKP1	Santa Cruz Biotechnologies	1:1000
MKP2	Santa Cruz Biotechnologies	1:1000
MKP3	Santa Cruz Biotechnologies	1:1000
Spry2	Abcam	1:1000
Her2	Cell Signaling	1:1000
cKit	Santa Cruz Biotechnologies	1:1000

PDGFRα	Santa Cruz Biotechnologies	1:1000

Table M1.2: Antibodies for Western blots

and incubated with HRP-conjugated secondary antibodies for 45 minutes at room temperature. Signal detection was by chemiluminescence using X-ray film. Densitometry analysis was conducted using Adobe Photoshop.

Subcutaneous allografts

Cell lines were grown to confluence, trypsinized, washed in PBS and resuspended at 1 x 10^7 cells/ml in sterile PBS. Mice were shaved and cells were injected subcutaneously into the flanks of C57Bl6 and cathepsin B null mice, with cathepsin B null cells injected into the left flank and cathepsin B expressing cells into the right flank. Tumour growth was followed using callipers.

E64 survival study

Screening and ultrasound of mice was performed as has been previously described [43], and will be described in detail in chapter II. Mice were enrolled on study when tumours reach a mean diameter of 6-9 mm. E64 was prepared in saline as a 5mg/ml stock solution, Mice were dosed at 50mg/kg daily by intraperitoneal injection until endpoint. Endpoint included greater than 20% weight loss, development of ascites or obvious signs of ill health.

Statistical Analysis

Kaplan-Meier statistics for survival curves were conducted using the Gehan-Breslow-Wilcoxon test. Proliferation, cathepsin activity, phospho-ERK, necrosis and mean

vessel density data were analyzed by Mann-Whitney U test, and metastasis incidence data were evaluated by Fisher's exact test. Graphpad prism software was used to conduct statistical analysis.

RESULTS

Cathepsin B expression and cathepsin activity are increased during disease progression

To evaluate cathepsin B levels during the development of PDA, cathepsin B expression was assessed in mouse tissue. Cathepsin B in the normal pancreas was confined to punctate staining in the acini (Fig 1.1A, arrows), and low level expression in ducts (Fig 1.1A, arrowheads). In contrast, cathepsin B was highly elevated in PanINs, with the entire apical cytoplasm staining strongly positive (Fig 1.1B, arrowheads). It should be noted that staining in some PanINs was restricted to the perinuclear area of the cell (data not shown). In addition, some stromal cells also stained positively for cathepsin B (Fig 1.1B, arrows). Cathepsin B expression in PDA was strongly positive and distributed throughout the cytoplasm (Fig 1.1C). Tissue from a cathepsin B null mouse did not exhibit positivity, confirming the specificity of the stain (Fig 1.1D). *In vivo* cathepsin activity was increased in PanIN ($p=0.0040$) and tumour ($p=0.0159$) compared to normal pancreas (Fig 1.1E).

Cathepsin B expression in pancreatic cancer cell lines is mislocalized

A panel of pancreatic cancer cell lines derived from mice was evaluated for cathepsin B expression. Cathepsin B was expressed in all cell lines, as expected. Protein from a cathepsin B-null MEF line was used as a negative control (Fig 1.2A). Cathepsin B was secreted from these cell lines, and was detectable in conditioned medium (Fig 1.2A). In addition, enrichment of surface proteins by biotinylation followed by neutravidin pull-down showed that active cathepsin B is localized on the plasma membrane of tumour cell lines (red arrows, lanes 3). There was no cathepsin B in the

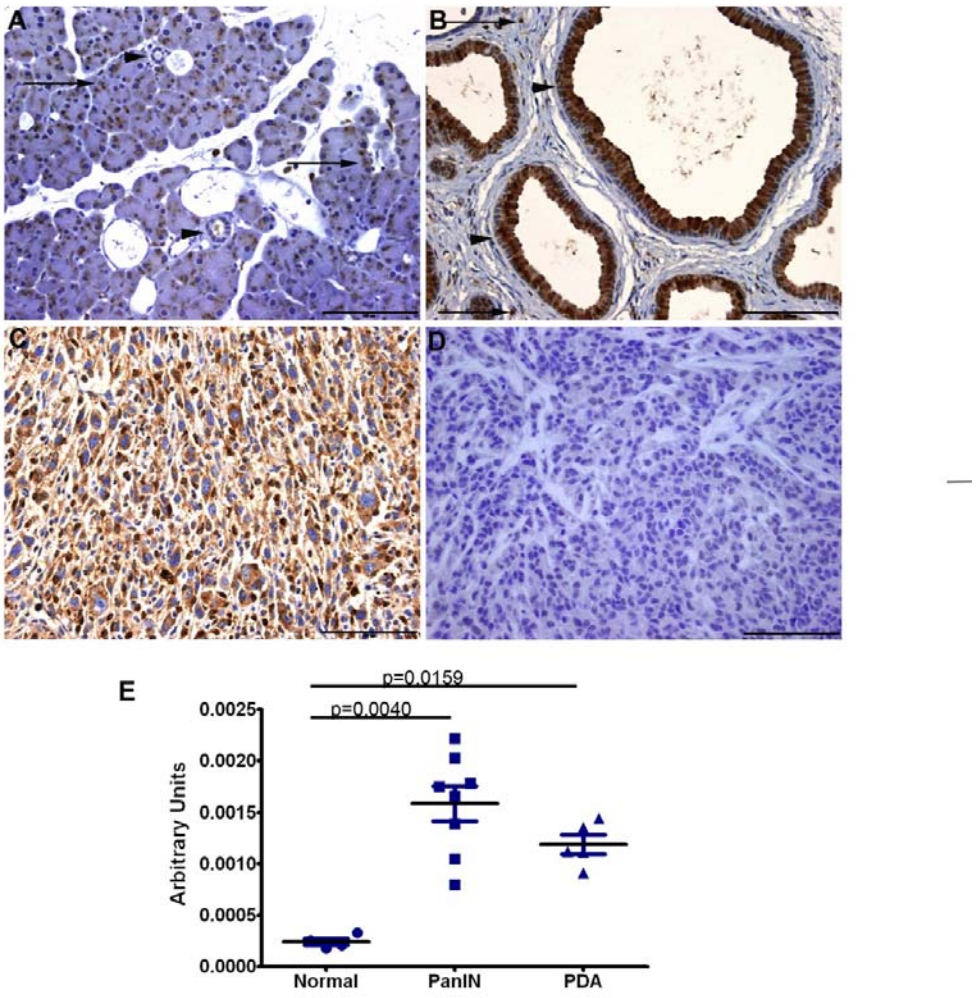

Figure 1.1: Increased cathepsin B expression during pancreatic cancer progression. Immunohistochemistry for cathepsin B shows that normal pancreatic tissue exhibits punctate staining in the acini (arrows) and low level staining in ducts (arrowheads) (A). Cathepsin B expression is greatly increased in PanINs (arrowheads). Positive staining is also seen in stromal cells (arrows) (B). Tumour cells are positive for cathepsin B (C). Cathepsin B null tissue is used as a negative control (D). (Scale bar = 100µm).Cathepsin activity is also increased *in vivo* (E). The Mann-Whitney test was used to determine differences in activity.

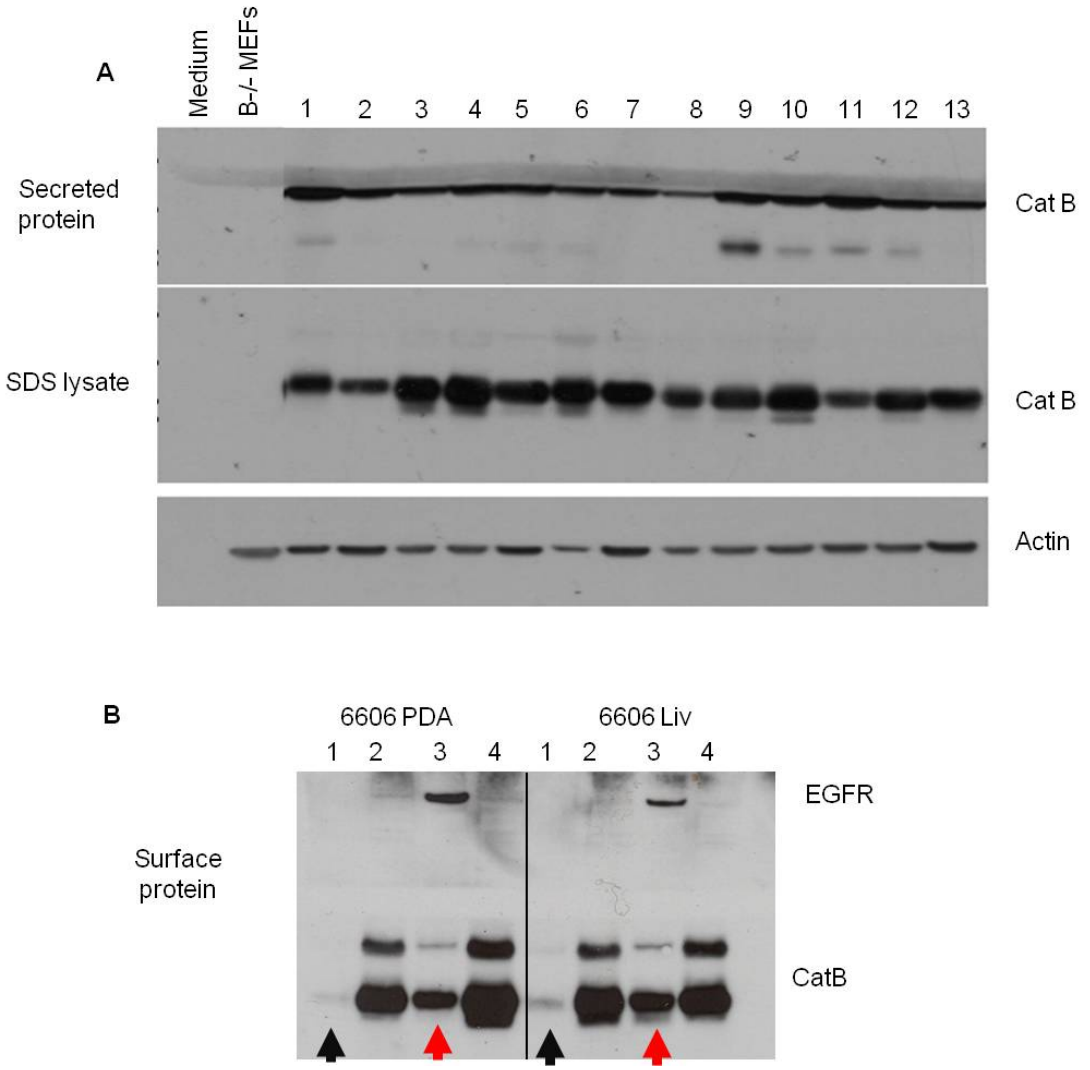

Figure 1.2: Cathepsin B is mislocalized in pancreatic cancer cell lines. Cathepsin B is universally expressed in lysates from a panel of PDA cell lines (A). In addition, it is also secreted into the medium, although secreted cathepsin B is not active (A). A cathepsin B null MEF line is used as a negative control (A). Surface biotinylation of tumour cell lines shows that active cathepsin B is present at the plasma membrane (B, lanes 3, red arrows). Cathepsin B is not present in the unbiotinylated controls (B, lanes 1, black arrows). EGFR is used as a positive control (B, lanes 3). Lanes 2 and 4 are input controls (B).

unbiotinylated control lanes, demonstrating the specificity of signal (black arrows, lanes 1) (Fig 1.2B).

Cathepsin B loss leads to decreased early PanIN burden and sustained decreased proliferation in PanINs

Cathepsin B null mice were used to evaluate the role of cathepsin B in the initiation of PDA [105]. These cathepsin B-deficient mice were crossed to mice harboring the *LSL-Kras^{G12D}* allele and mice harbouring a transgenic Pdx-1-Cre recombinase [6] to direct expression of oncogenic Kras to the pancreas. Pancreata from mice with the relevant genetic combinations were examined at different time points for disease burden including reactive acini and PanINs. Cathepsin B ablation did not prevent PanIN formation, and preneoplasms were morphologically similar regardless of cathepsin B status (data not shown). At two months, there was no significant difference in disease burden between pancreata from LSL-Kras^{G12D}; Pdx-1-Cre; Cathepsin B+/+ (KC;B+/+) and LSL-Kras^{G12D}; Pdx-1-Cre; Cathepsin B-/- (KC; B-/-) mice. The pancreatic lobules in KC;B+/+ mice were 54.42% (+/-6.715) normal and 31.23% (+/-4.279) reactive, consisting of acinar-to-ductal metaplasia. 14.35% (+/-4.279) of lobules had PanIN1s. There were no PanIN2s and PanIN3s at this time point. In the KC;B-/- cohort, the pancreas consisted of 69.16% (+/- 3.993) normal lobules. 21.98% (+/- 3.645) of lobules contained reactive areas, and 8.862% (+/- 2.721) of lobules carried PanIN1s. As with the KC;B+/+ cohort, there were no higher grade PanINs (Fig 1.3A).

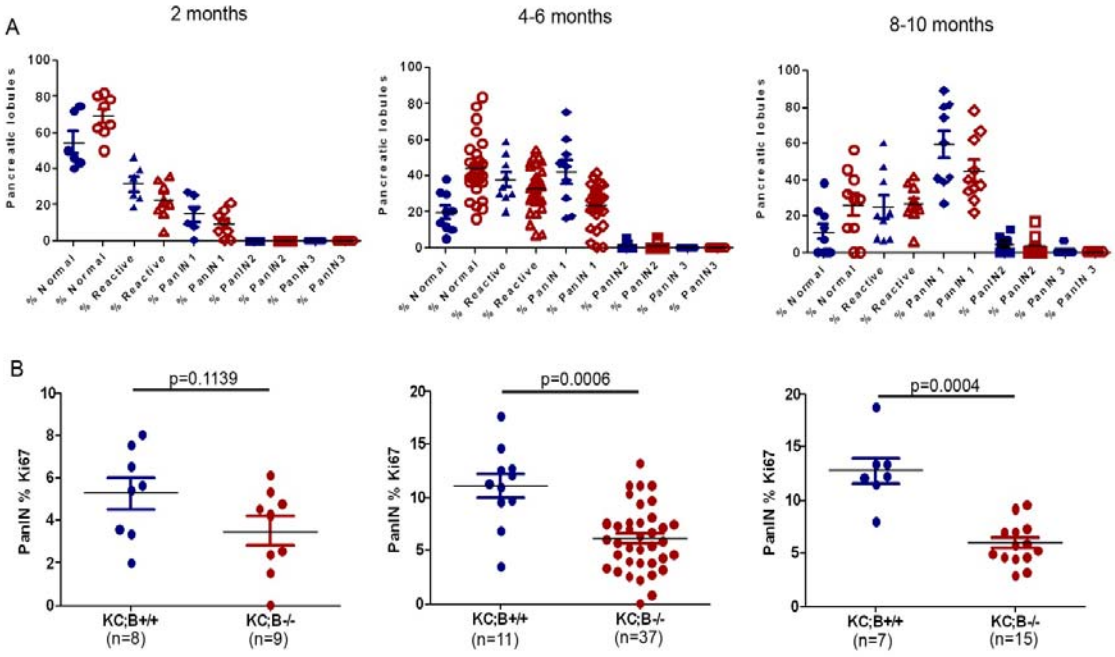

Figure 1.3: Loss of cathepsin B causes decreased early PanIN burden and decreased proliferation in PanINs. Analysis of disease burden reveals that at two months, cathepsin B loss does not affect reactive acini or PanIN load. At 4-6 months, pancreata from cathepsin B null mice have more normal lobules and decreased PanIN1-containing lobules. At 8-10 months, there is no difference between cathepsin B null and cathepsin B-expressing pancreata. (A). Quantification of proliferation in PanINs by Ki67 immunohistochemistry reveals that loss of cathepsin B causes a significant decrease in proliferation in 4-6 month old and 8-10 month old mice. At two months, there is a trend towards decreased proliferation, although this is not statistically significant (B). The Mann-Whitney test was used to analyze disease burden and proliferation data.

At 4-6 months, pancreata from the KC;B-/- cohort had a higher fraction of normal lobules (43.75%, +/-2.969) compared to the KC;B+/+ cohort (p=0.0002). In addition, there was a decrease in the number of PanIN 1-bearing lobules in the KC;B-/- cohort (23.33%, +/- 2.050) compared to the KC;B+/+ cohort (41.77%, +/- 6.519) (p=0.0178). There was no difference in reactive lobules or higher PanIN grades. At 8-10 months, there was no significant difference between the two cohorts in any of the disease grades analysed, although the KC;B-/- cohort tended towards decreased PanIN1 compared to the KC;B+/+ cohort (Fig 1.3A).

Cathepsin B loss led to decreased proliferation in PanINs. At two months, PanINs from KC;B-/- pancreata displayed a trend towards decreased proliferation (3.498 ± 1.998 mean percentage proliferation), though not statistically significant, compared to LSL-KC;B+/+ (5.267 ± 2.125) pancreata (Fig 1.3B). At 4-6 months, the difference in PanIN proliferation was statistically significant in KC;B-/- pancreata (6.095 ± 3.064) compared to KC;B+/+ (11.04 ± 3.756, p=0.0006) (Fig 1.3B). This effect on proliferation persisted at 8-10 months, with KC;B-/- mice (5.919 ± 1.940) exhibiting a >50% reduction in proliferation compared to KC;B+/+ (12.75 ± 3.201, p=0.0004) mice (Fig 1.3B). There was no difference in pancreatic apoptotic index between cohorts (data not shown).

Loss of cathepsin B prolongs survival in advanced models of pancreatic cancer

Following the initial observation of decreased proliferation in preinvasive lesions, the role of cathepsin B in pancreatic cancer progression was studied in mice. To accelerate the development of pancreatic cancer, the oncogenic $Kras^{G12D}$ allele was combined with a conditional point-mutant $Trp53^{R172H}$ allele, and a $Trp53^{flox/flox}$ allele,

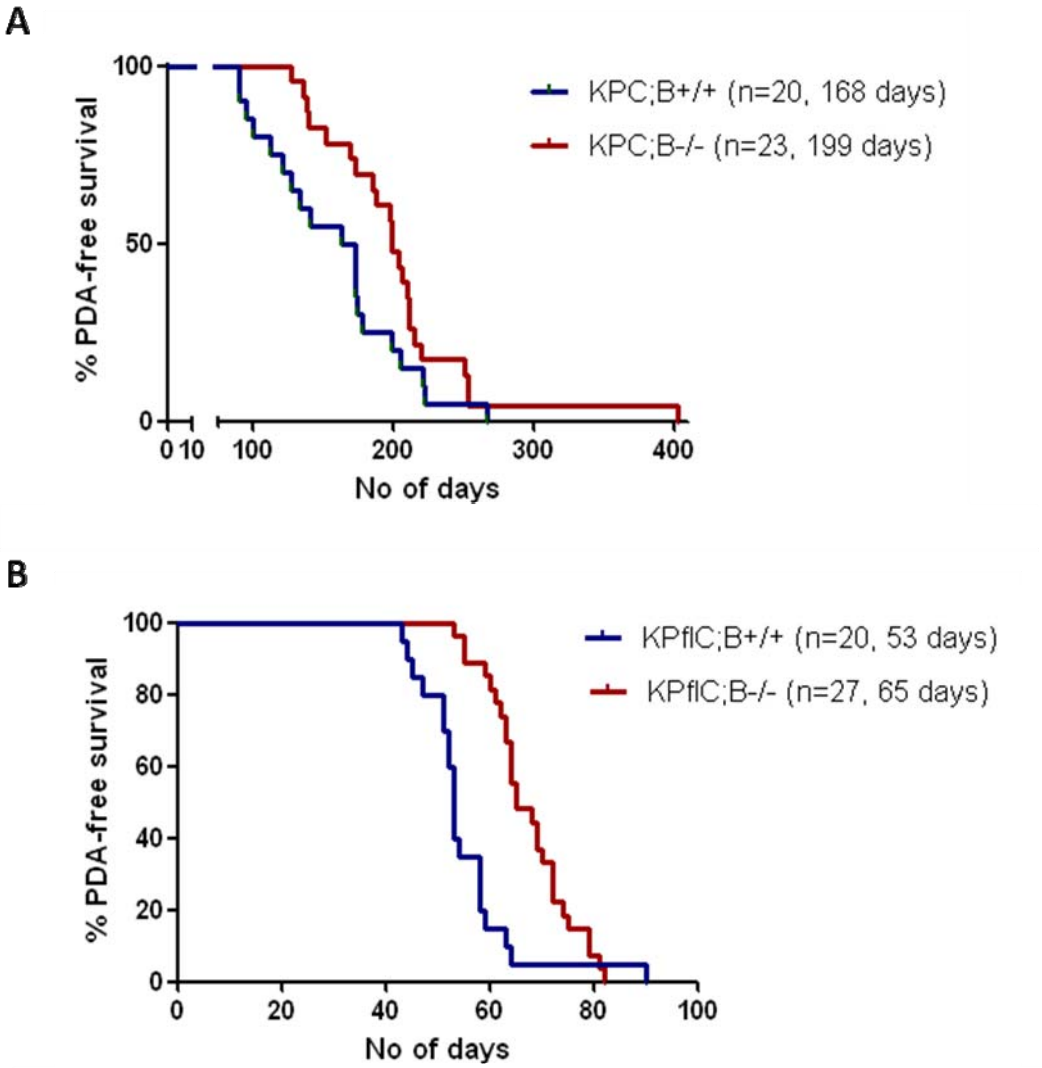

Figure 1.4: Cathepsin B loss extends survival of mice with PDA. KPC;B-/- mice have a median PDA-free survival of 199 days, a significant extension over KPC;B+/+ mice with a median of 168 days (p=0.0113) (A). Lack of cathepsin B also imparts a significant survival advantage in the context of *Trp53*$^{flox/flox}$ alleles, with a median survival of 65 days for KPflC;B-/- mice compared to 53 days for the KPflC;B+/+ cohort (p=<0.0001) (B). In both backgrounds, the earliest PDA-related morbidity in the cathepsin B cohorts was delayed, indicating that tumour onset may be delayed. Kaplan-Meier statistics were conducted using the Gehan-Breslow-Wilcoxon test.

as previously described [28, 104]. Once again, cathepsin B null mice were bred into these combinations of alleles and Pdx-1-cre was utilized to direct expression of the mutations to the pancreas to generate cohorts of mice with the various allelic combinations.

Kaplan-Meier statistics demonstrated that LSL-Kras^{G12D}; LSL-Trp53^{R172H}; Pdx-1-Cre; Cathepsin B-/- (KPC;B-/-) mice had a significantly increased PDA-free survival with a median of 199 days. In contrast, the median PDA-free survival of LSL-Kras^{G12D}; LSL-Trp53^{R172H}; Pdx-1-Cre; Cathepsin B+/+ (KPC;B+/+) was 168 days (p=0.0113). Cathepsin B loss delayed the onset of PDA, as the earliest case of PDA-related morbidity in the KPC;B-/- cohort was 127 days, compared to 90 days in the KPC;B+/+ cohort (Fig 1.4A). The survival advantage imparted by cathepsin B loss was also observed in LSL-Kras^{G12D}; Trp53$^{flox/flox}$; Pdx-1-Cre; Cathepsin B-/- (KPflC;B-/-) mice, with a median survival of 65 days, compared to 53 days in the LSL-Kras^{G12D}; Trp53$^{flox/flox}$; Pdx-1-Cre; Cathepsin B+/+ (KPflC;B+/+) mice (p=<0.0001) (Fig 1.4B).

Proliferation in tumours is decreased as a result of cathepsin B loss

Further analysis of cathepsin B loss on tumours was conducted in the context of the *Trp53*^{R172H} allele, as this model is of more physiological relevance. KPC;B-/- mice developed the expected features of PDA, including hemorrhagic ascites and liver and lung metastases. The morphology of PDA in the KPC;B-/- cohort was comparable to the KPC;B+/+ cohort, including histological patterns ranging from ductal (Fig 1.5A) to sarcomatoid (Fig 1.5B) and solid (Fig 1.5C).

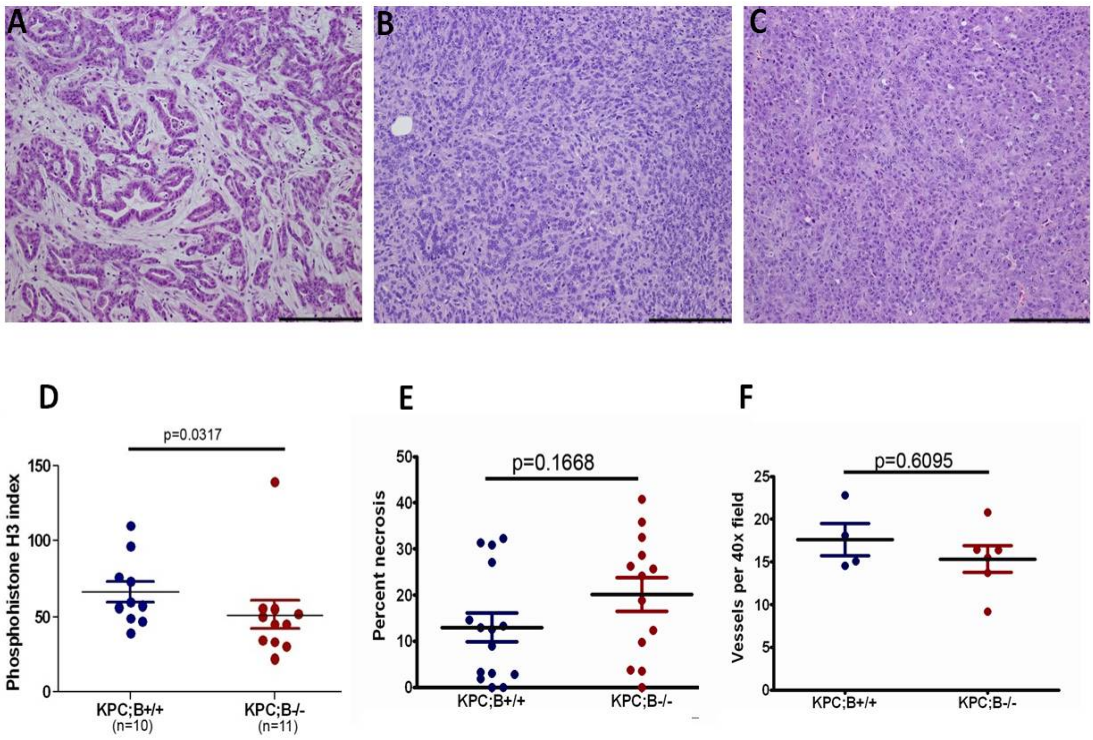

Figure 1.5: Cathepsin B null tumours exhibit decreased proliferation. Tumours in cathepsin B null mice exhibit mixed histology with ductal (A), sarcomatoid (B) and solid (C) features, similar to KPC tumours. (Scale bar = 200 μm). Proliferation measured by phospho-histone H3 is significantly decreased in null tumours compared to those that are wild-type for cathepsin B (p=0.0317) (D). Cathepsin B null tumours do not exhibit any differences in necrosis (E) or mean vessel density (F) compared to KPC tumours.

Proliferation in tumours, analysed by phospho-histone H3, revealed that the proliferative defect detected in preinvasive lesions was sustained in tumours. At end point, tumours in KPC;B-/- mice were significantly less proliferative (50.93 ± 31.20 phospho-histone H3 index), compared to KPC;B+/+ tumours (66.15 ± 22.61, p=0.0317) (Fig 1.5D). There were no significant differences in necrosis between the cohorts (Fig 1.5E). In addition, mean vessel density measured by CD31 immunohistochemistry was not significantly decreased in the KPC;B-/- tumours (Fig 1.5F).

Cathepsin B does not alter the stromal composition of diseased pancreata or tumours

The stromal compartment was assessed with Masson's trichrome stain to evaluate collagen deposition and probed with antibodies against alpha-smooth muscle actin to delineate activated myofibroblasts. No obvious stromal differences were evident between cohorts by either of these parameters. Trichrome staining was abundant in diseased areas and tumours irrespective of cathepsin B status (Fig 1.6). In diseased pancreata, alpha-smooth muscle actin staining was more robust around areas of acinar-ductal metaplasia (arrowheads) than PanINs (arrows) in both KC;B+/+ and KC;B-/- mice. There was also no difference in staining pattern in tumours from KPC;B+/+ and KPC;B-/- mice (Fig 1.6). This data suggests that the differences in cellular proliferation and PanIN content may be cell autonomous.

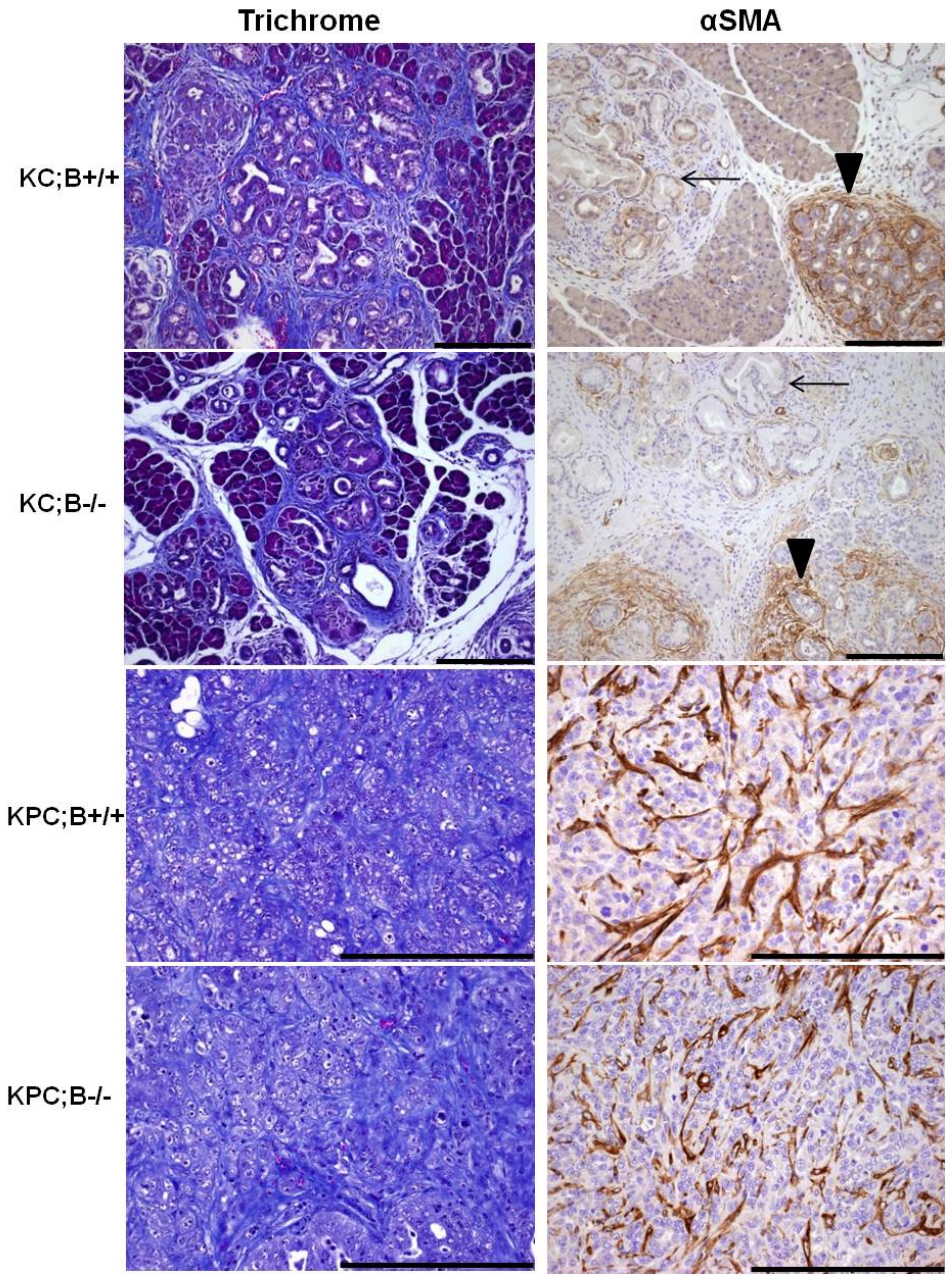

Figure 1.6: Cathepsin B loss does not affect stromal composition. Cathepsin B loss does not affect the deposition of desmoplastic fibres as measured by trichrome staining, in either PanIN pancreas or tumour. Activated fibroblasts, measured by alpha-smooth muscle actin are more abundant in areas of acinar-to-ductal metaplasia (arrowheads) than PanIN (arrows), irrespective of cathepsin B status. (Scalebar = 200μm).

Cathepsin B loss decreases the burden of liver metastasis

As cathepsin B has been previously implicated in metastasis [102, 98], a more comprehensive examination of the extent of liver and lung metastasis was conducted. Liver and lung metastases developed and were histologically similar in KPC;B+/+ and KPC;B-/- cohorts (Fig 1.7A and 1.7B, respectively). KPC;B-/- mice had a significant reduction in the number of liver metastases (1.421 ± 2.090), compared to KPC;B+/+ mice (4.000 ± 3.882, p=0.0359) (Fig 1.7C). The number of mice with liver metastases also decreased from 75% in the KPC;B+/+ cohort to 52.63% in the KPC;B-/- cohort, although this difference was not statistically significant (p=0.2928,

Fisher's exact test) (Table 1.1). A similar analysis of lung metastases revealed no change in metastatic burden (4.563 +/- 1.756 in the KPC;B+/+ cohort; 4.684 +/- 2.033 in the KPC;B-/- cohort, p=0.6616) (Fig 1.7D). Surprisingly, the incidence of lung metastasis increased in the cathepsin B null cohort (78.94%) compared to the KPC;B+/+ cohort (62.5%), although this increase was not significant (p=0.4543) (Table 1.1). There was no difference in the area of either liver (Fig 1.7E) or lung (Fig 1.7F) metastases between cohorts.

Genotype	Number of mice	Mice with liver metastases	Incidence of liver metastasis	Mice with lung metastases	Incidence of lung metastasis
KPC;B+/+	16	12	75%	10	62.5%
KPC;B-/-	19	10	52.63%	15	78.94%

Table 1.1: Incidence of liver and lung metastasis

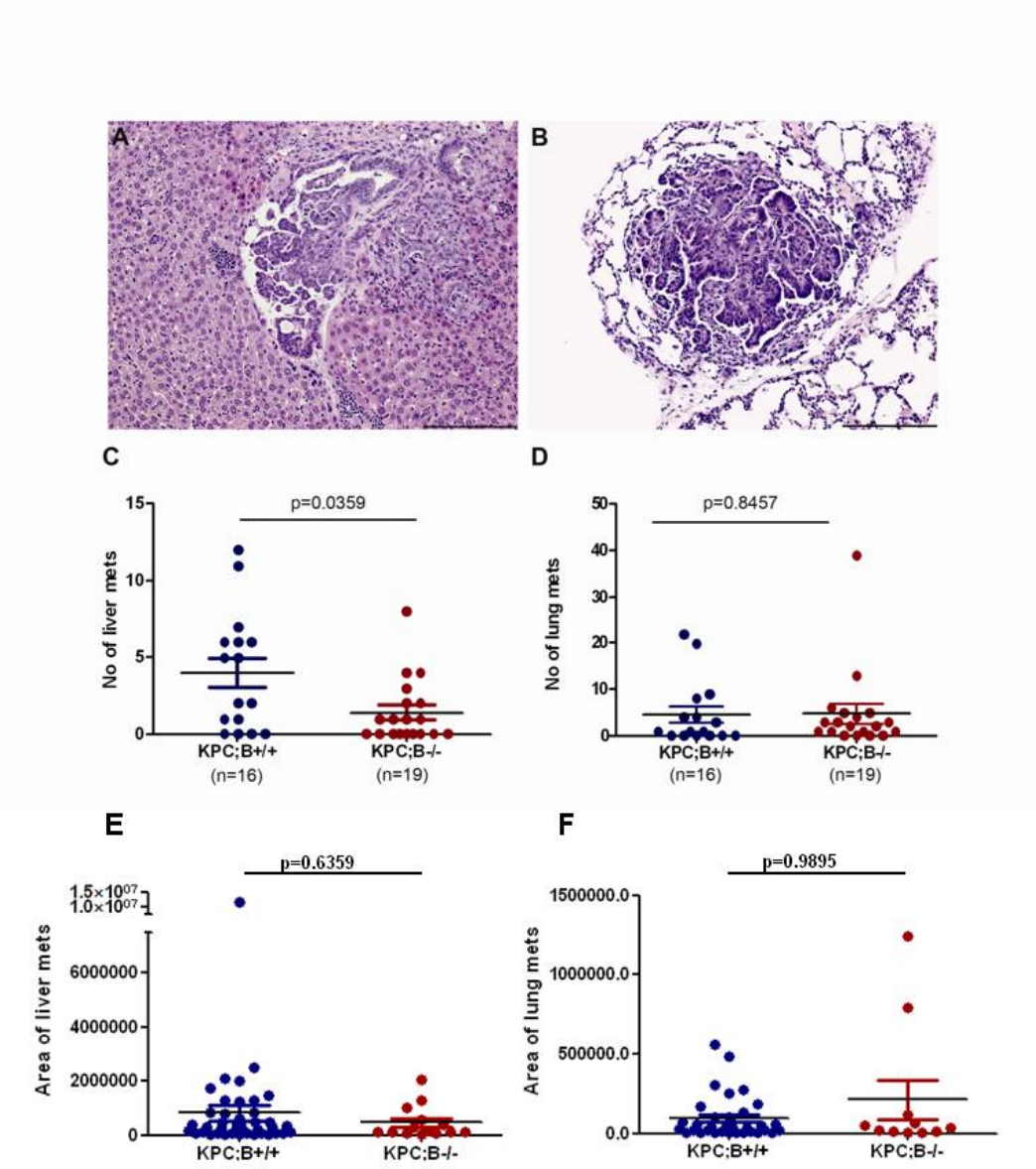

Figure 1.7: Decreased liver metastasis due to loss of cathepsin B

Histology of liver (A) and lung (B) metastases are similar in both cohorts. Although cathepsin B is not required for metastasis to the liver, the number of metastases per liver is decreased in the null animals (C). There is no significant change in the number of metastatic lung lesions (D). Cathepsin B status does not affect the area of either liver (E) or lung (F) metastases (Scale bar = 200μm).

Cathepsin B loss leads to increased active cathepsin L

To investigate the difference in metastasis to the liver and lung, the expression of alternate cathepsins was examined in metastatic lesions. Cathepsin L was found to be higher in lung metastases than in liver metastases in mice in both KPC;B+/+ and KPC;B-/- cohorts (Fig 1.8A), potentially indicating a role of this cathepsin in metastasis to the lung.

In addition, an analysis of *in vivo* cathepsin activity in cathepsin B-null mice demonstrated that there was no significant difference in activity compared to B+/+ mice in normal and PanIN pancreas and tumours, indicating compensation for cathepsin B activity (Fig 1.8B). Western blot analysis of tumour lysates showed that

KPC;B-/- tumours have more active cathepsin L than KPC;B+/+ tumours (Fig 1.8C, arrows). Total ERK is used as a loading control.

Loss of cathepsin B leads to decreased nuclear phospho-ERK *in vivo*

To elucidate the mechanism of decreased proliferation in the cathepsin B null background, tumour cell lines were derived from KPC;B-/- mice and transfected with recombinant cathepsin B to allow comparison of isogenic cell lines. Evaluation of cathepsin B expression in these cell lines (Fig 1.9, lanes 2,4,6) revealed the presence of intracellular cathepsin B at levels comparable to KPC;B+/+ cell lines (Fig 1.9, lanes 7,8). Cathepsin B in these reconstituted cell lines was also expressed at the plasma membrane and secreted into the medium (Fig 1.9). As expected, there was no cathepsin B expression in the parent KPC;B-/- lines (Fig 1.9, lanes 1,2,3).

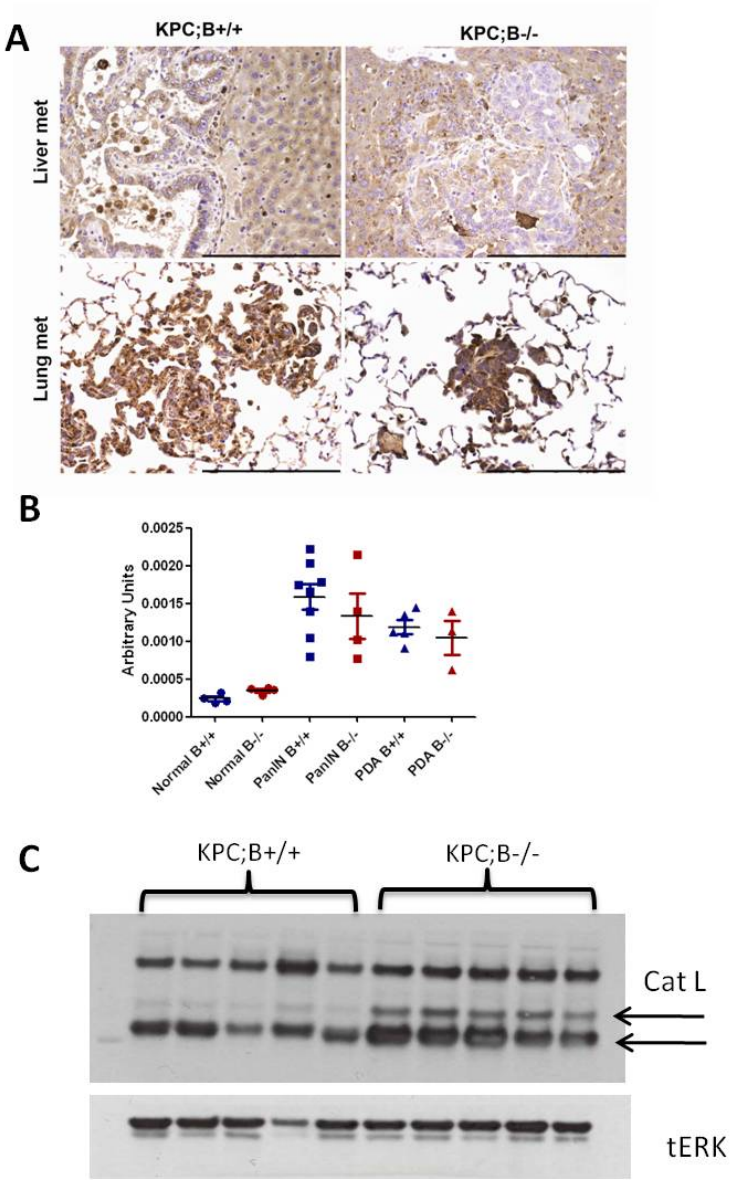

Figure 1.8: Cathepsin L expression and activity. Immunohistochemistry for cathepsin L shows that the levels of this cathepsin are increased in lung metastases compared to liver metastases in both cohorts (A). (Scale bar = 200µm).*In vivo* cathepsin activity does not decrease in cathepsin B null mice in normal, PanIN or PDA (B). Cathepsin B null tumours express higher levels of active cathepsin L (C, arrows), explaining the lack of diminished cathepsin activity. Total ERK is used as a loading control (C).

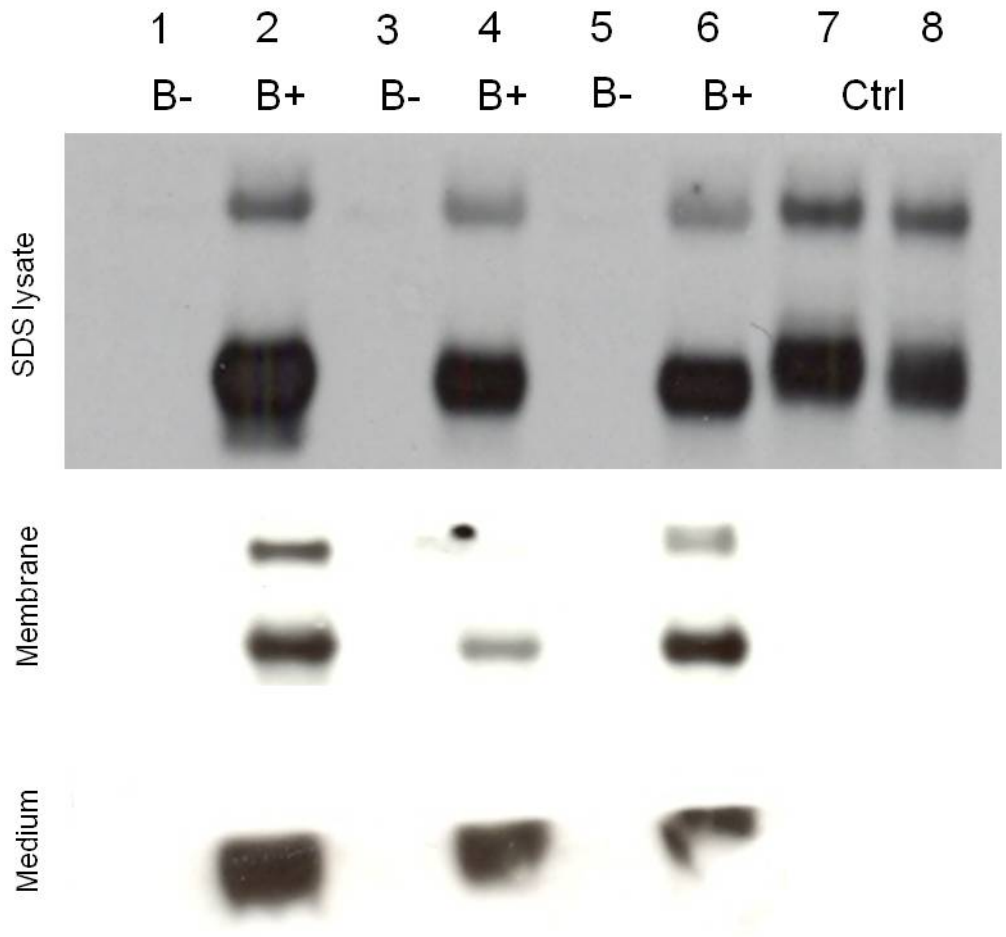

Figure 1.9: Reconstitution of cathepsin B in KPC;B-/- cell lines

Reconstitution of cathepsin B in null tumour cell lines results in comparable expression to tumour cell lines from KPC;B+/+ mice (A, 2,4,6 vs 7,8). As expected, cathepsin B is absent in the null cell lines (A, lanes 1,3,5). After reconstitution, recombinant cathepsin B is expressed on the plasma membrane in its active form. Inactive cathepsin B is secreted into the medium (A, 2,4,6).

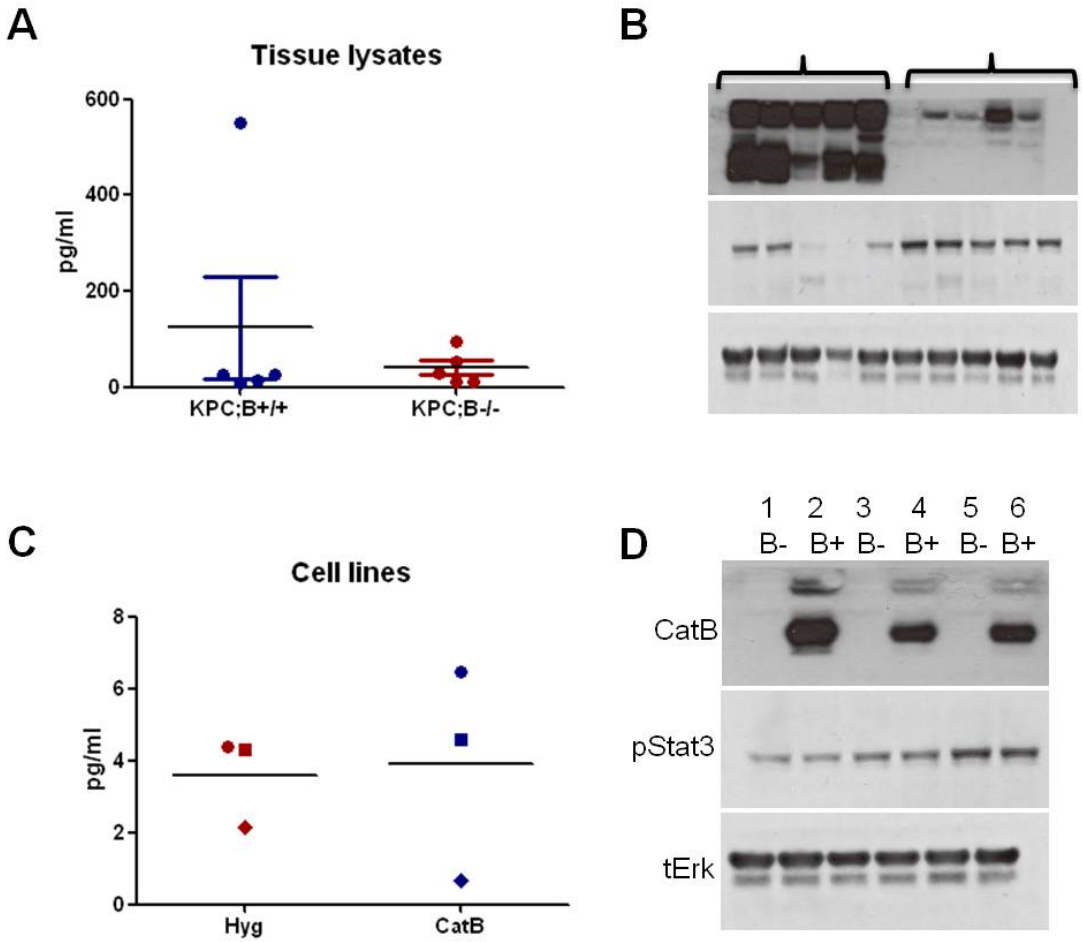

Figure 1.10: Cathepsin B loss does not affect interleukin-6 levels. Interleukin-6 ELISAs on tumour tissue reveals that cathepsin B loss does not affect IL-6 levels (A). Stat3 phosphorylation is not decreased in the cathepsin B null background (B). This data is consistent in cell lines, where reintroduction of cathepsin B into null cell lines does not affect IL-6 levels (C) or Stat3 phosphorylation (D 1vs2, 3vs4, and 5vs6). Total ERK is used as a loading control.

Since cathepsin B is known to be involved in the cleavage and processing of a number of cytokines and chemokines [108-110], antibody-based cytokine arrays were utilized to enumerate the differences in cytokine levels between KPC;B+/+ and KPC;B-/- tumours (Appendix 1). The protein which demonstrated the highest reduction was interleukin-6, a cytokine that is of interest in human PDA [111]. To confirm whether interleukin-6 is indeed down-regulated in a cathepsin B null background, ELISAs were carried out on tissue lysates from the same tumours used for the array analysis. The interleukin-6 ELISA showed that there was overall no difference between the tumours from the two cohorts, and only one outlying KPC;B+/+ sample with high expression levels was responsible for the array results (Fig 1.10A). Western blotting for Stat3, a known transducer of interleukin-6 signalling, confirmed that this pathway is not less active in KPC;B-/- tumours (Fig 1.10B). The interleukin-6 ELISA was also carried out on the cell lines reconstituted with cathepsin B and confirmed that there was no difference in interleukin-6 levels (Fig 1.10C) or Stat signalling (Fig 1.10D, lanes 1vs2, 3vs4 and 5vs6) in cell lines expressing cathepsin B. Total ERK is used as a loading control.

The cell lines were then analyzed for a number of signalling molecules and targets of the Ras pathway. No changes were seen in levels of phospho-Akt, phospho-Rsk, phospho-S6 ribosomal protein and cyclin D (Fig 1.11A, lanes 1vs2, 3vs4 and 5vs6). Cathepsin B expression, however, caused increased levels of phospho-ERK (Fig 1.11A, 1vs2, 3vs4 and 5vs6) in all three cell lines. To further investigate this finding, phospho-ERK immunohistochemistry was conducted on PanIN lesions from KC;B+/+ and KC;B-/- mice. Although the overall intensity of cytoplasmic phospho-

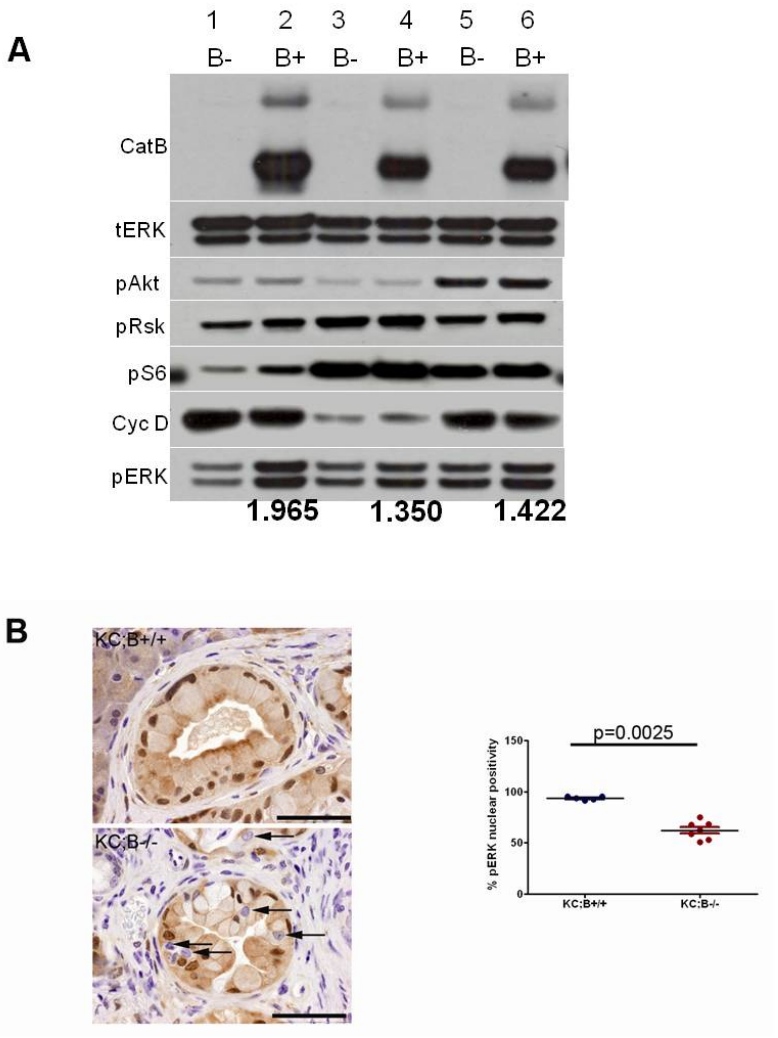

Figure 1.11: Cathepsin B affects phospho-ERK localization *in vivo*. Western blotting of cancer cell lines shows that cathepsin B expression leads to the upregulation of phospho-ERK in cancer cell lines (A, 1vs2, 3vs4, 5vs6). Phospho-ERK levels quantified by densitometry have been normalized to total ERK. Cathepsin B does not affect activation of other signalling molecules downstream of Ras including Akt, Rsk, S6 ribosomal protein and does not increase cyclin D1 levels (A). Localization of phospho-ERK in KC;B-/- PanINs was altered with a significant reduction in the number of phospho-ERK positive nuclei compared to KC;B+/+ PanINs (p=0.0025) (B, arrows). (Scale bar = 50μm).

ERK staining did not vary between the cohorts, differences in nuclear positivity were observed. PanIN lesions in KC;B+/+ pancreata exhibited a significantly higher percentage of phospho-ERK positive nuclei (93.48% +/- 1.787%) compared to KC;B-/- pancreata (62.26% +/- 8.740) (p=0.0025) (Fig 1.11B).

Modulation of phospho-ERK is not a result of altered MAP kinase signalling

Analysis of the cell lines revealed that the cathepsin B-induced increase in phospho-ERK was not due to Ras activation, as there was no consistent difference in Ras-GTP or phospho-MEK. There were no changes in phosphatases known to regulate MAP kinase signalling such as MKP1, MKP2, MKP3 and Sprouty2 (Fig 1.12A, 1vs2, 3vs4, 5vs6). Additionally, surface biotinylation of cell lines followed by neutravidin pull-down showed that there was no difference in levels of cell surface receptors such as Her2, EGFR, cKit and PDGFRα (Fig 1.12B, 1vs2, 3vs4 and 5vs6), further corroborating that the altered phospho-ERK was not simply due to modulation of MAP kinase signalling. Total ERK is used as an input control (Fig 1.12B).

Cathepsin B expression results in increased growth in soft agar

To evaluate the role of Cathepsin B expression *in vitro*, proliferation assays were conducted at 10% serum and 1% serum on plastic. Interestingly, there was no difference in proliferation at either condition (Fig 1.13A). Two of the cell lines with higher cathepsin B and phospho-ERK levels were selected for further studies. In soft agar assays, the cathepsin B-expressing cell lines formed larger colonies than lines lacking cathepsin B (Fig 1.13B).

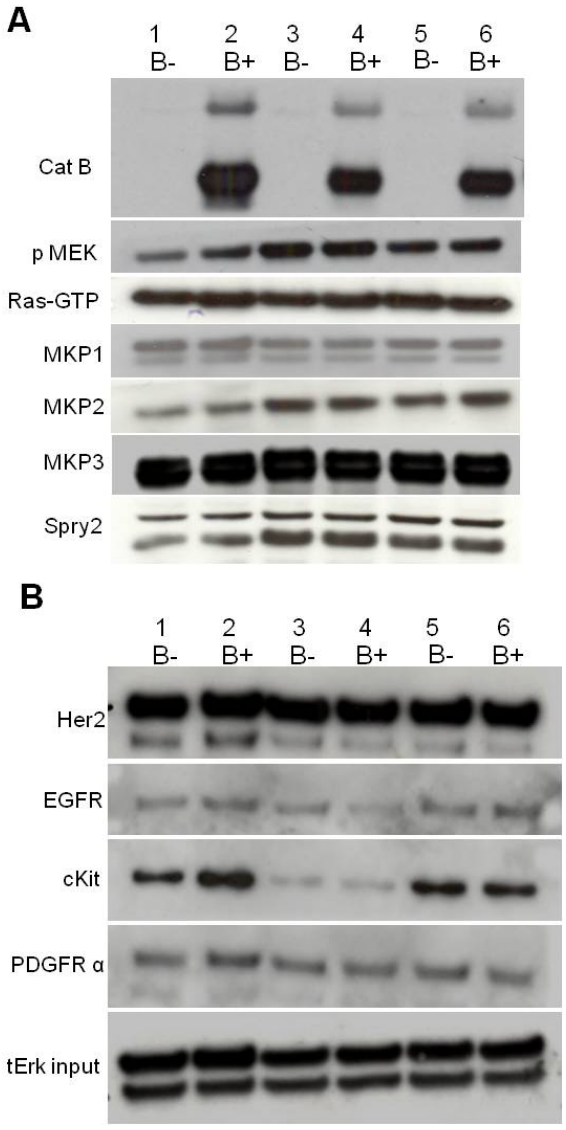

Figure 1.12: Increased phospho-ERK is not due to altered MAP kinase signalling. Cathepsin B expression does not affect levels of Ras-GTP or phospho-MEK. In addition, there are no changes in levels of phosphatases MKP1, MKP2, MKP3 and sprouty2 that are involved in modulation of MAP kinase signalling (A, lanes 1vs2, 3vs4, and 5vs6). Surface biotinylation of cancer cells reveals that levels of Her2, EGFR, cKit and PDGFRα are not altered at the plasma membrane (B). Total ERK is used as the input control (B).

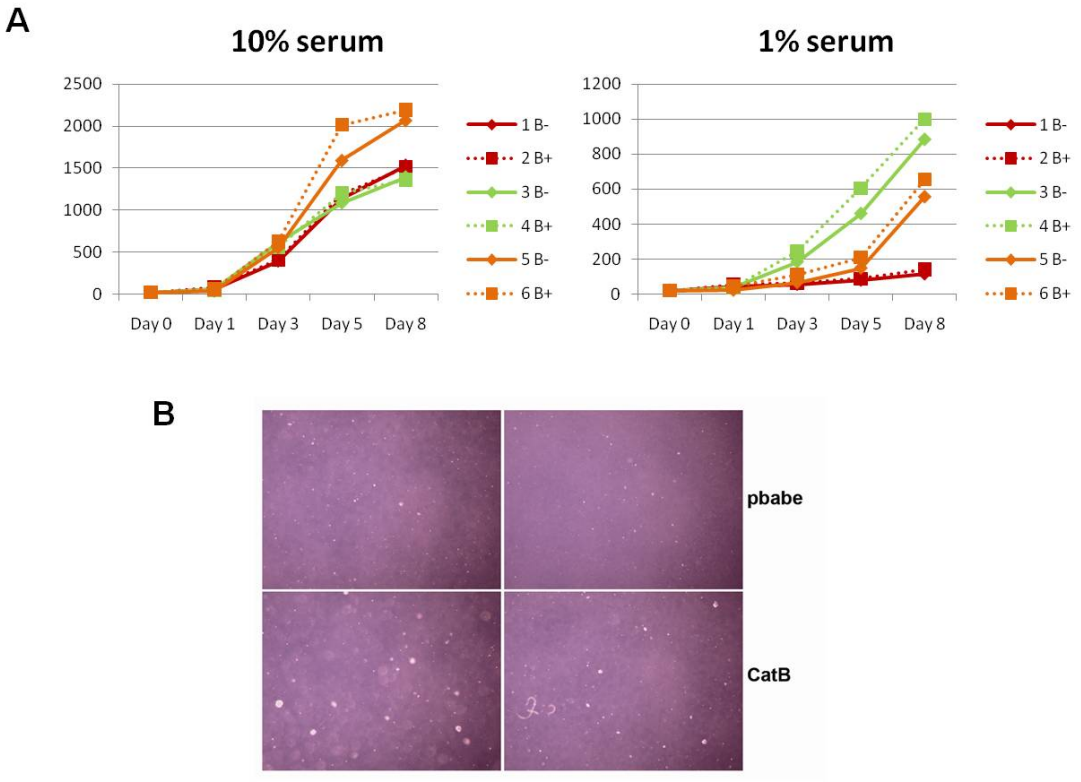

Figure 1.13: Cathepsin B increases colony growth in soft agar assays. Cathepsin B is not required for proliferation of adherent cells at either 10% or 1% serum (A). Representative images from two cell lines show that cathepsin B expression results in increased growth in soft agar assays (B).

Cathepsin B expression increases growth of subcutaneous allografts

To examine the role of cathepsin B on proliferation *in vivo*, and also to investigate whether cathepsin B has cell autonomous or non-cell autonomous roles in tumour growth, the cell lines were injected subcutaneously into wild-type (C57Bl6) and cathepsin B null mice to produce allografts. .

Cathepsin B-transfected cells formed larger tumours in both wild-type (0.2591 cm^3 +/- 0.165, p=0.0007) and cathepsin B null recipient mice (0.2432 cm^3 +/- 0.094, p=0.0041) compared to their null counterparts (0.09069 cm^3 +/- 0.081 in wild-type mice and 0.1300 cm^3 +/- 0.0779 in cathepsin B null mice) (Fig 1.14A, B). Analysis of proliferation by Ki67 showed that allografts formed by cathepsin B-expressing tumours have significantly increased proliferation in both backgrounds compared to tumours that lack cathepsin B expression (Fig 1.14C).

E64 in combination with gemcitabine does not improve survival compared to gemcitabine therapy

To investigate whether cathepsin B is a potential therapeutic target in PDA, the broad-spectrum cysteine protease inhibitor E64 was used as a therapeutic agent in mice bearing pancreatic tumours. E64 (50mgs/kg) was given daily to tumour-bearing mice intraperitoneally, either as a single agent or in combination with bi-weekly gemcitabine (100mgs/kg) till endpoint. The median survival on study of mice receiving E64 alone was 14 days, compared to 23 days for the combination arm (Fig 1.15A). As has been reported previously in this system, the median survival for untreated mice is 11 days, and 15 days for Gemcitabine alone (Fig 1.15B) [(43)].

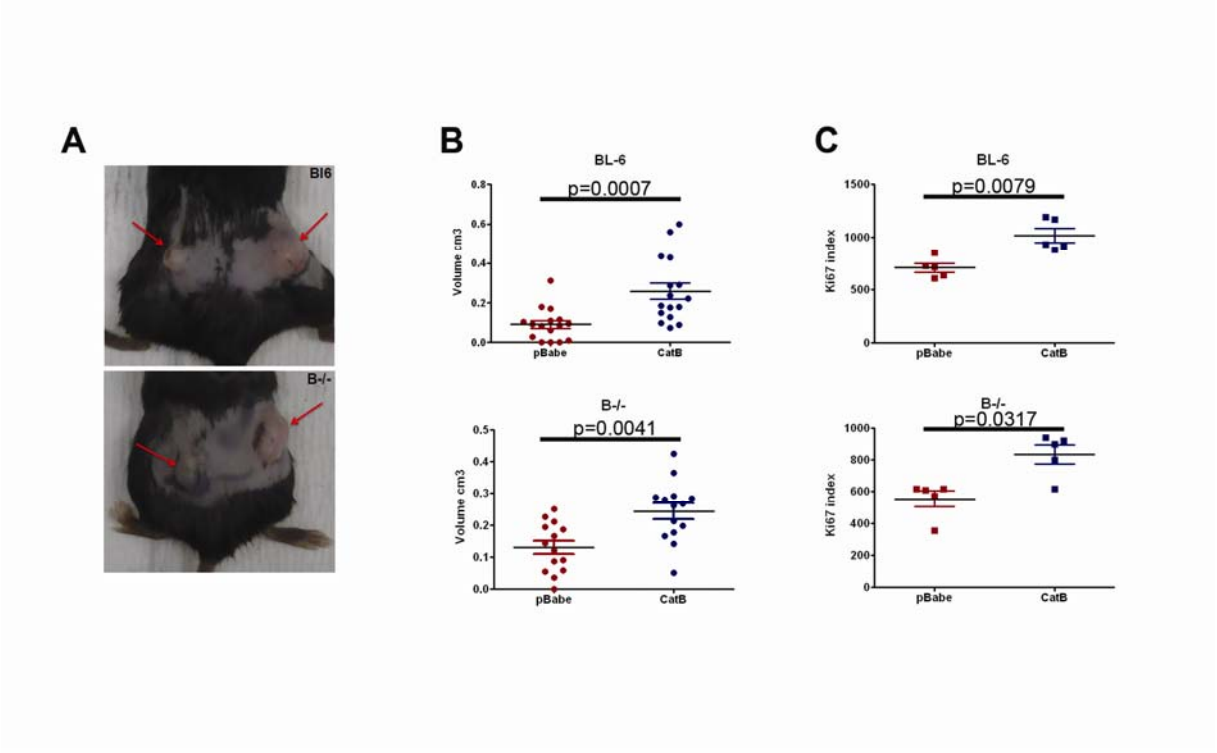

Figure 1.14: Lack of cathepsin B inhibits the growth of subcutaneous allografts. Tumour cells expressing cathepsin B (right flank) form larger subcutaneous tumours than cells lacking cathepsin B (left flank) in both wild-type and cathepsin B null recipient mice (A), with tumour volume at end point being significantly increased (B). This increased tumour size corresponds to increased proliferation as measured by the number of Ki67 positive cells per field (C).

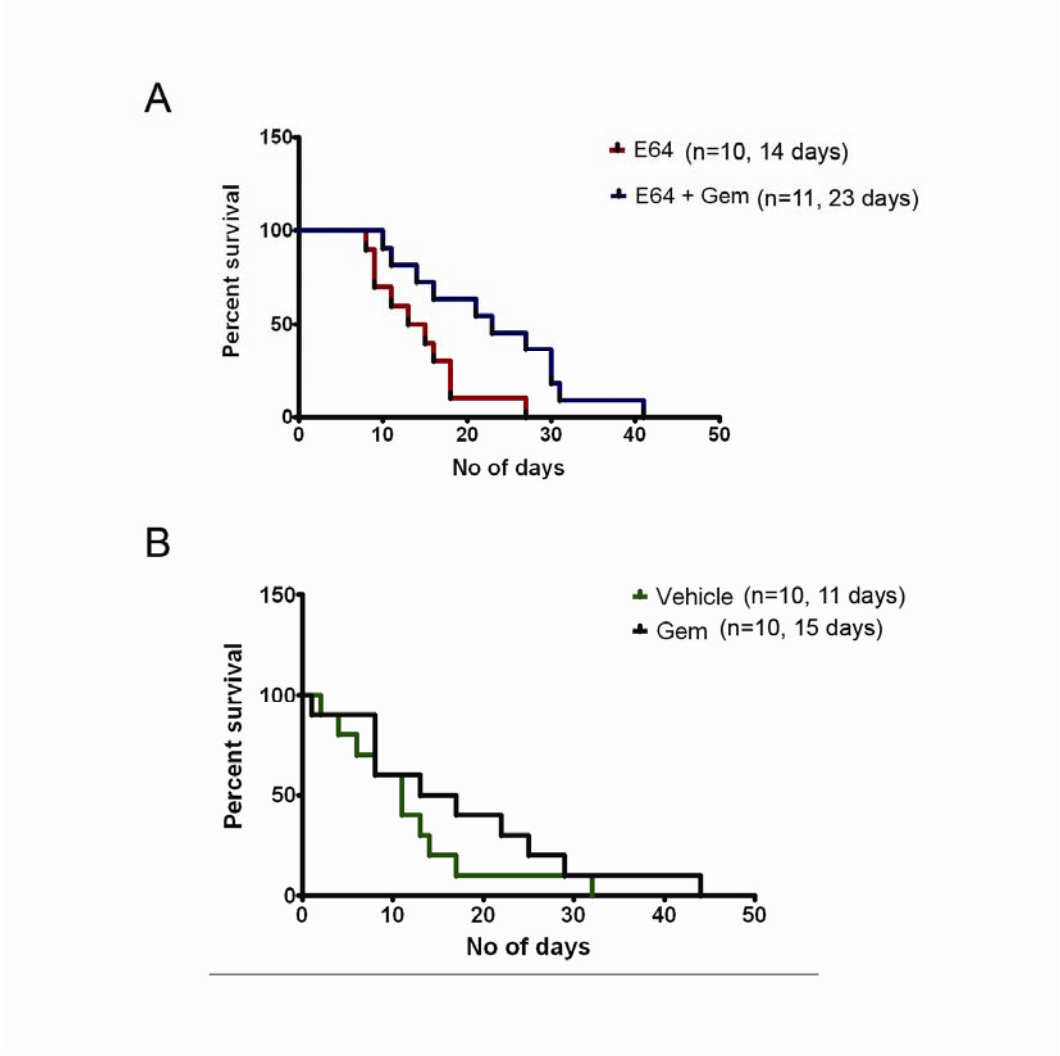

Figure 1.15: E64 in combination with Gemcitabine leads to a significant increase in survival. The median survival of mice receiving E64 in combination with gemcitabine is 23 days, a significant increase over E64 as a single agent (14 days) (A). Previously published data are provided as a reference for vehicle (11 days) and Gemcitabine (15 days) (B) [43]

The historical vehicle and gemcitabine control cohorts serve as a reference, as similar additional cohorts have been completed that corroborate the accuracy of the data (Tuveson, unpublished). Although E64 alone did not impart a survival benefit, the combination of E64 and gemcitabine provided a significant increase in survival compared to vehicle ($p=0.0137$) or E64 alone (0.0271). The combination treatment extended median survival on treatment by 53% compared to Gemcitabine alone, although this is not statistically significant ($p=0.1541$). This may be a result of augmentation of gemcitabine delivery to tumours, which remains to be investigated.

DISCUSSION

The cysteine cathepsin family of lysosomal proteases is of great interest due to their overexpression and mislocalization in a number of cancers [reviewed in 58]. In pancreatic cancer in particular, cathepsin B has been reported to be overexpressed in primary tumours and associated metastases in humans [112]. In addition, cathepsin B is also of interest in human PDA as a prognostic indicator of early recurrence after surgical resection [77, 113].

Following the initial observation that cathepsin B levels and overall cathepsin activity are increased in preinvasive and invasive pancreatic cancer in mice, and that mouse PDA cell lines have altered cathepsin B localization, this work delves into the role of cathepsin B in the initiation and progression of PDA. I have shown that cathepsin B loss causes a significant decrease in PanIN burden at an early time point, as well as sustained decreased proliferation in PanINs at early and late time points. In addition, loss of cathepsin B confers a significant survival advantage to mice with PDA in two accelerated models of pancreatic cancer. In both of the accelerated models, loss of cathepsin B delays onset of PDA. The survival benefit imparted by lack of cathepsin B is associated with decreased tumour proliferation, although the stromal and vascular compartments are not affected. Cathepsin B loss also corroborates with decreased liver metastases, and increased cathepsin L activity in tumours (Fig 1.16).

The observation that early morbidity is absent in cathepsin B null mice indicates that tumour development is retarded in the absence of cathepsin B. A major characteristic of PDA is the profound deposition of extracellular matrix consisting of numerous

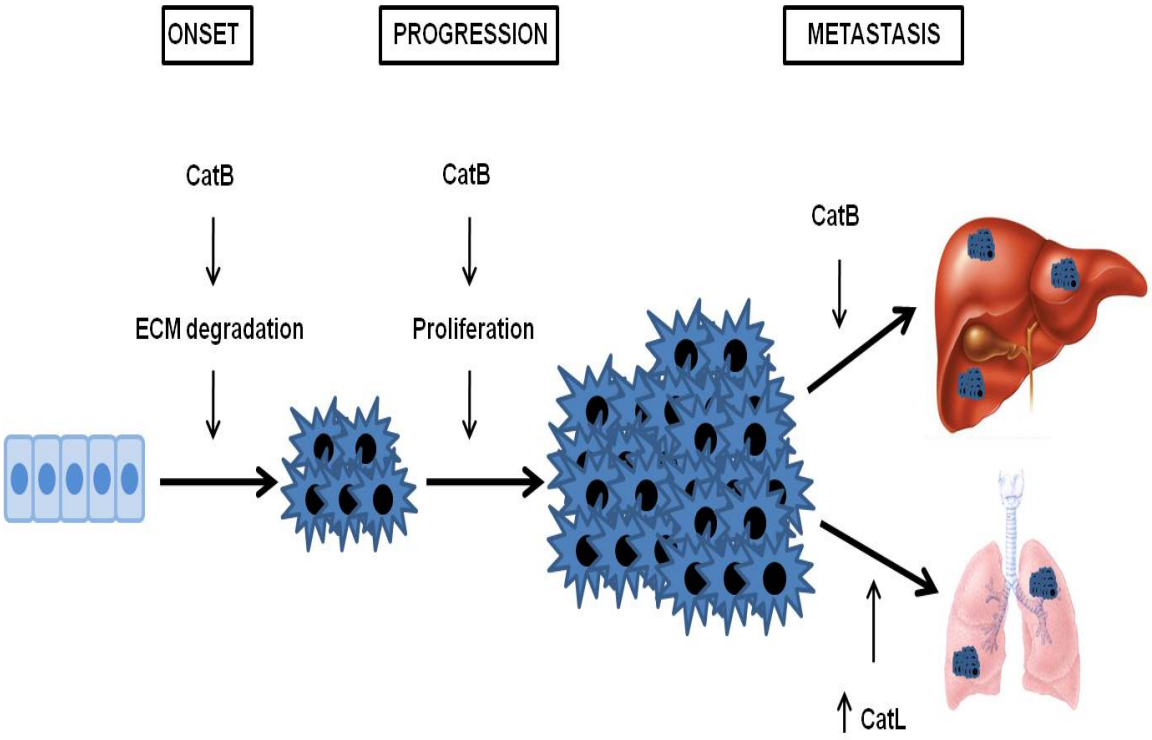

Figure 1.16: Schematic of cathepsin B involvement in the tumorigenic process. Cathepsin B may promote the progression from preinvasive disease to frank carcinoma by degrading extracellular matrix components. Cathepsin B influences proliferation and therefore promotes tumour progression. Although cathepsin B is not required for metastasis to the liver, establishment of metastatic lesions in the liver is more efficient in the presence of this protease. Cathepsin L is upregulated in lung metastases, and may therefore be important in site-specific metastasis to the lung.

components including collagens, laminin and fibronectin [reviewed in 22, 23]. The significance of cathepsin B in this setting is its ability to cleave collagen IV, laminin and fibronectin, as has been reported in normal and tumour tissue [114]. In addition, mislocalization of cathepsin B to the plasma membrane is reported to be induced by *Ras* oncogenes [91, 115, 116]. This may reflect the importance of cathepsin B in the degradation of the extracellular matrix and the progression from ductal carcinoma in situ to frank cancer, a highly probable scenario given that mouse PDA cell lines express active cathepsin B on their plasma membrane. Cathepsin B under cell culture conditions is secreted into medium as its inactive precursor, a phenotype that has been previously reported in other cell culture systems [53, 117]. Given that acidic extracellular pH is a common feature of tumours [reviewed in 118, 119], it is easy to envision a situation where the inactive cathepsin B is activated due to the extracellular milieu. Indeed, incubating culture medium with pepsin at acidic pH is sufficient to activate secreted procathepsin B [117, 90]. In this scenario, activation of cathepsin B may also be involved in promoting metastasis. Interestingly, active cathepsin B can also be secreted from cancer cells in response to acidic extracellular pH [93], and metastasis is promoted by low pH [120].

In our system, cathepsin B loss significantly decreases the burden of liver metastasis, with no change in metastatic burden in the lungs. In addition, there appears to be a trend towards decreased incidence of metastasis to the liver and, unexpectedly, increased evidence of metastasis to the lung. The finding that cathepsin L expression is increased in lung metastases compared to liver metastases suggests that different cathepsins may be responsible for site-specific metastasis. Interestingly, tissue from

cathepsin B null mice does not exhibit decreased *in vivo* cathepsin activity. This is explained by the presence of increased levels of active cathepsin L in the cathepsin B null tumours, which may account for the successful establishment of lung metastases. This is supported by evidence suggesting that proteases with different substrate specificities may variably affect metastasis to different distal sites [121, 122]. Moreover, crossing cathepsin B knockout mice into the MMTV-PyMT model of metastasizing breast cancer did not result in significantly reduced lung metastatic burden [102]. In this model, an alternate cystein cathepsin, cathepsin Z, partially compensates for the loss of cathepsin B [102]. Indeed cathepsin B/Z double knockouts show significantly reduced lung metastasis of the breast cancers [123]. Hence cathepsin B is part of a proteolytic network that affects metastasis.

The effect of cathepsin B loss on proliferation has been previously reported *in vivo* in other mouse models of cancer [97, 100]. Although the mechanism by which cathepsin B affects proliferation is not well understood, recently some mechanistic insight has been gained *in vitro* in cancer cell lines, albeit primarily in studies studying the cooperative effect of inhibition or silencing of multiple proteins. Concomitant knock-down of cathepsin B with the urokinase plasminogen activator receptor in glioma cell lines results in increased p27 expression and G0/G1 cell cycle arrest [124], and decreased phosphorylation of focal adhesion kinase and ERK [125] . Silencing of cathepsin B together with either matrix metalloprotease-9 or uPAR reduces colony growth and proliferation in glioma cells, in this case through integrin downregulation [126]. In hepatic stellate cells, inhibition of cathepsin B led to decreased Akt phosphorylation and an associated reduction in proliferation in response to platelet-derived growth factor [127]. Given that proliferation is consistently decreased at both

early and late stages of disease in our model in the setting of cathepsin B loss, this is a potential mechanism to explain the delayed tumour progression in these mice. This defect in proliferation does not appear to be a result of altered interleukin signalling in tumours and cell lines. The effect of cathepsin B loss on phospho-ERK both *in vitro* and *in vivo* is striking, and may explain the defect in proliferation. Although, cathepsin B inhibition has been previously reported to affect phosphorylation of various signalling molecules with corresponding decreases in proliferation [125, 127], this study is the first to report that cathepsin B affects the localization of phospho-ERK. The nuclear localization of phospho-ERK leads to the activation of transcription factors responsible for proliferation, and hence sequestration in the cytoplasm may prevent responses to mitogenic stimuli [reviewed in 128].

Since cathepsin B is expressed in both tumour and stromal cells, it may have non-cell autonomous roles as a result of paracrine signals between the different cell types. This conclusion is consistent with the finding that intravenous injection of cathepsin B expressing tumour cells into cathepsin B null mice results in lung metastases with decreased proliferation [100]. Recent supporting cell culture evidence has been reported where the use of cathepsin B-specific inhibitors has led to decreased proliferation of endothelial cells [129].The allograft experiments presented here strongly support a cell-autonomous role of cathepsin B in PDA, as cell lines expressing the protease proliferate more rapidly than cathepsin B-null cell lines irrespective of the background into which they are injected. The relative contributions of intracellular and extracellular cathepsin B in this setting remain to be clarified. These experiments do not exclude an additional non-cell autonomous role for cathepsin B, as the stromal response in allografts is rather limited compared to that seen in *in situ* tumours.

Cathepsins are under investigation as therapeutic targets in cancer. Previous studies conducted *in vivo* have shown promise in conjunction with chemotherapy [130], although bioavailability of the inhibitor may be problematic in specific cancer types [131]. In this system, inhibition of extracellular cathepsin B using a broad-spectrum cysteine protease inhibitor leads to an increase in survival when combined with gemcitabine, compared to treatment with the inhibitor alone. Although the improved survival in combination treatment was not statistically significant compared to Gemcitabine alone, the drug used here was not an optimal cathepsin inhibitor and the positive trend underlines the importance of understanding the specific contributions of different cathepsins in cancer. This work validates cathepsin B as a potential therapeutic target in pancreatic cancer, although caution must be exercised due to the successful establishment of lung metastases in the absence of cathepsin B. In this context, the use of a broad-spectrum cathepsin inhibitor may be more beneficial than targeting a single cathepsin enzyme.

CONCLUSIONS/FUTURE DIRECTIONS

In summary, cathepsin B is involved in the initiation and progression of pancreatic cancer, and loss of this protease provides a significant survival benefit. Cathepsin B loss results in decreased proliferation and metastasis to the liver, although cathepsin L activity is increased potentially permitting successful lung metastasis. Cathepsin B deficiency results in decreased phosphorylated ERK in cell lines, and decreased nuclear localization of phospho-ERK *in vivo*. Cathepsin B restoration improves anchorage-independent growth and growth of subcutaneous allografts in a cell autonomous manner.

Pancreatitis

Pancreatitis originates in the acinar cell compartment of the pancreas, and involves the intracellular activation of trypsinogen to active trypsin [reviewed in 132]. Cathepsin B can activate trypsinogen *in vitro*[133], and induced pancreatitis in mouse models results in the redistribution of cathepsin B in zymogen granule-containing sub-cellular fractions [134]. Importantly, cathepsin B null mice exhibit decrease trypsinogen activation and pancreatic damage in response to induced pancreatitis [105]. Since pancreatitis is a risk factor for pancreatic cancer, the importance of cathepsin B in induction of pancreatitis must be investigated, using the KC;B-/- mice. Induction of pancreatitis using established methods [135] in these mice will allow the examination of whether cathepsin B loss in the presence of oncogenic Kras mutations affects the course of disease. In addition, these experiments may address the question of whether progress from pancreatitis to preinvasive and ductal carcinoma is affected by the lack of cathepsin B.

Non-cell autonomous contribution of cathepsin B

The growth of cathepsin B-expressing tumour cells in allografts presented in this work supports a cell autonomous role for cathepsin B in pancreatic cancer. It does not, however, rule out any non-cell autonomous functions and these must be investigated in order to understand the various mechanisms by which cathepsin B affects tumorigenesis. Furthermore, cathepsin B from tumour-associated macrophages is known to promote tumour growth, angiogenesis and invasion *in vivo* [103]. The non cell autonomous effects of cathepsin B in pancreatic cancer tumorigenesis could be studied by bone marrow transplants to introduce cathepsin B null immune cells into KC;B+/+ mice, or alternately to reconstitute the immune system of KC;B-/- mice with cathepsin B-expressing cells. In addition, the effects of extracellular cathepsin B and its contribution to proliferation and metastasis can be studied *in vitro* and *in vivo* using non-cell permeable cathepsin B-specific inhibitors such as Ca074.

Cathepsin B and the localization of phospho-ERK

The finding that phospho-ERK localization is affected in cathepsin B null PanINs is an interesting observation, the mechanism for which remains to be elucidated. Nuclear phospho-ERK is required for proliferation [reviewed in 128], which can be affected by numerous signals. For instance, integrin-mediated adhesion and the resulting cytoskeletal organization are required for the nuclear translocation of ERK [136]. Other mechanisms regulating ERK nuclear localization are src kinase and Rho/ROCK activation, the importin machinery and Pea-15 [137-139]. Cathepsin B silencing results in downregulation of a number of integrins [126], and simultaneous downregulation of uPAR and cathepsin B modifies cytoskeletal dynamics by retarding cofilin

dephosphorylation [125]. Thus, cathepsin B loss might affect phospho-ERK localization by inhibiting integrin expression or altering cytoskeletal reorganization, directly and indirectly. Cathepsin B null cancer cell lines and MEFs can be used to explore alterations in integrin expression, and their relationship to nuclear phospho-ERK.

Cathepsins in metastasis

I have shown that cathepsin B loss diminishes the ability of tumour cells to metastasize to the liver, but has no impact on lung metastasis. Lung metastases express higher levels of cathepsin L than do liver metastases. In addition, cathepsin B null tumours tend to have higher levels of active cathepsin L. This data may indicate the importance of compensatory networks of protease activity, which has been previously shown in mouse models [123]. In order to study the contribution of cathepsin L to metastasis in a cathepsin B null background, short hairpin knockdown of cathepsin L may be carried out in tumour cell lines, followed by injection into cathepsin L null recipient mice, either by an intravenous or intrasplenic route. In addition, since cathepsin Z is thought to compensate for cathepsin B loss, this protease must also be analyzed in the cathepsin B null models of pancreatic carcinogenesis. Studying other cathepsins in this manner will not only delineate the functions of proteases in metastasis, but will also give a clearer indication of how cathepsin B loss is compensated for in tumours, which may explain why the absence of cathepsin B in PDA models does not have a greater impact on tumorigenesis.

CHAPTER II

FARNESYLTHIOSALICYLIC ACID AS A THERAPEUTIC AGENT IN PANCREATIC CANCER

INTRODUCTION

The Ras proteins

The first Ras proteins were identified in 1964 by Jennifer Harvey (H-Ras) and in 1970 by Werner Kirsten (K-Ras) from transforming retroviruses carrying host oncogenes that produced tumours in mice [140, 141]. Following this discovery, the human homologues of these oncogenes were identified in 1982, and the third Ras protein (N-Ras) was identified from neuroblastoma cells in 1983 [142-145].

The Ras proteins are small, ubiquitously-expressed guanosine nucleotide-bound GTPases. Ras proteins cycle between an inactive GDP-bound form and an active GTP-bound form. They are activated by multiple upstream signals including the binding of growth factors to receptors, G-protein signalling, activation of Janus kinases and calcium signalling (Fig I2.1). Activation through receptor tyrosine kinases results in the interaction of the adaptor protein Grb2 with the cytoplasmic tail of the receptor, thereby facilitating son-of-sevenless (SOS) recruitment to the membrane. SOS proteins are guanosine nucleotide exchange factors (GEFs) that activate Ras proteins by increasing the exchange of GDP for GTP [reviewed in 146-149].

Active GTP-bound Ras is a central signalling hub within the cell and activates a number of downstream pathways, and controls various aspects of cellular behaviour including proliferation, survival and cytoskeletal reorganization. The most intensively studied pathway downstream of ras is the mitogen-activated protein kinase (MAPK) pathway. Active ras contributes to the activation of Raf protein, downstream of which lie MEK and the extracellular signal-related kinases (ERKs). The phosphorylation of ERK results in the activation of the AP-1 transcription factor, comprising Jun and Fos

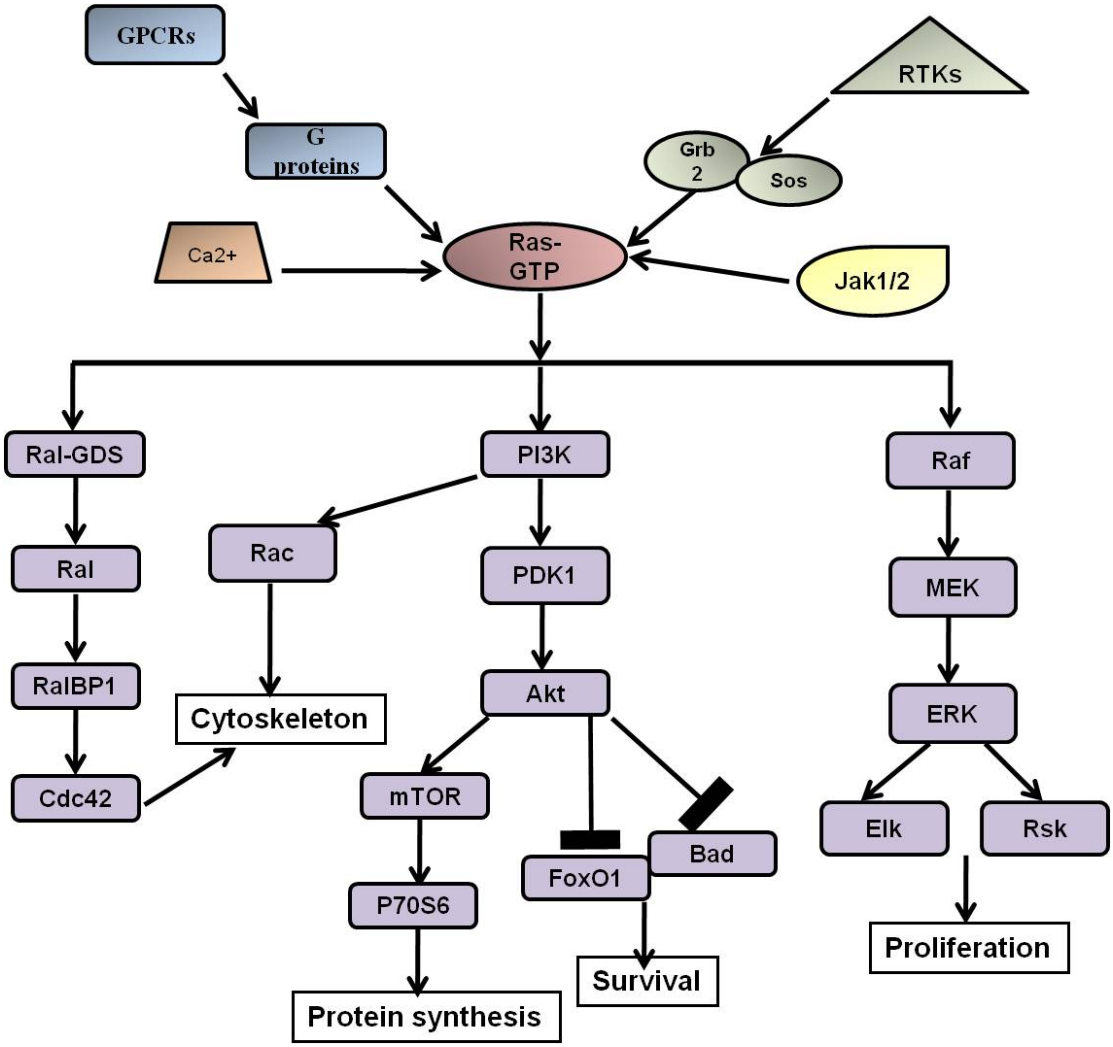

Fig I2.1 Ras signalling cascades. Ras is activated in response to upstream signals through numerous mechanisms such as receptor tyrosine kinases, G protein coupled receptors, Janus Kinases and calcium. Oncogenic Ras is intrinsically active and does not require these signals. Ras signals to numerous downstream pathways, three of which are represented in this image. Ras signalling stimulates processes such as proliferation, protein synthesis, survival and cytoskeletal reorganization.

heterodimers, which causes expression of cell-cycle regulatory proteins including the D-type cyclins [reviewed in 150, 151].

In addition to MAPK signalling, Ras also activates a number of other effector pathways. Ras directly interacts with type I phosphatidylinositol 3-kinases (PI3Ks), resulting in their activation and phosphorylation of downstream targets Akt and PDK1, with resulting effects on survival and protein synthesis respectively. Ras signalling also impinges upon cytoskeletal reorganization and through its activation of the Ras guanine nucleotide dissociation stimulator (RalGDS), and the subsequent activation of Cdc42 (Fig I2.1). Other ras effectors include phospholipase Cε and Rassf1 [reviewed in 152].

Although the three Ras proteins are closely related, with 85% amino acid sequence homology, and their functionality and effects *in vitro* are very similar, mouse models have delineated differences in their functions *in vivo*. H-Ras and N-Ras proteins are not required for normal mouse embryonic development, either alone or in combination [153, 154]. H-Ras deficiency however, results in impaired skin tumour formation in response to carcinogens and N-Ras deficient mice exhibit defective T-cell function and immune responses [155, 156]. K-ras, in contrast, is essential for embryonic development and knockout mice experience defective liver erythropoiesis and anaemia leading to gestational death [157], although this has been attributed to the Kras4B isoform, as Kras4A is not required for normal mouse development [158]. This data suggests that Ras proteins have certain non-overlapping functions and K-Ras deficiency in mouse tissues cannot be compensated.

Ras mutations in cancer

Ras mutations are the most frequent oncogenic event identified in cancer, with an overall frequency of about 30%. Of the ras proteins, K-ras is the most frequently mutated, being found in >90% of ductal pancreatic cancers, 45% of colorectal cancers and 35% of non-small cell lung cancers [152]. The mutations, mostly confined to codons 12, 13 and 61, decrease the intrinsic GTPase activity and result in hyperactivation of the protein and aberrant downstream signalling, and do not require upstream signals [143, 159, 160]. Ras mutations in cancer are associated with poor prognosis and outcome. Augmentation of ras signalling in cancer also occurs by other mechanisms such as by deletion of GAPs, mutational activation of growth factor receptors, and mutation or amplification of individual ras effectors [152].

Oncogene addiction

Oncogene addiction, a phrase coined by Bernard Weinstein, refers to the characteristic whereby cancer cells appear to be dependent on a single oncogenic event or signalling pathway to maintain their proliferation and survival, despite numerous other genetic alterations [161]. Experimental findings in human cell lines and mouse cancer models provide support for this phenomenon. Tumour dependency on oncogenes such as myc and ras has been well-studied, but experimental systems have also been used to demonstrate dependence upon other genes such as her2, Braf, EGFR, Met and Abl, as well as micro RNAs[reviewed in 162]. Oncogene addiction implies a cell autonomous response to oncogene inactivation. The genetic streamlining hypothesis proposes that natural selection and the inherent genomic instability in tumour cells results in the rewiring of signalling pathways with preference given to

oncogenic signalling. The benefit of this tumour characteristic is the relative insensitivity of normal tissues to the inactivation of oncogenes, making therapeutic approaches feasible without the overwhelming side effects often engendered by general chemotherapeutics [reviewed in 162].

Targeting ras in cancer

The localization of ras to the plasma membrane is essential for its activity, and therefore an obvious target for therapy was the post-translational modifications responsible for ras localization. Newly synthesized cytosolic ras is modified on its carboxyl terminus CAAX motif, where A is an aliphatic or aromatic residue and X is the terminal amino acid determining the specificity of the prenyl transferase. Farnesyl transferase (FTase) catalyses the addition of a 15-carbon isoprenoid chain from farnesyl pyrophosphate (FPP) onto the cysteine residue. This is followed by the release of the AAX residues, which is catalysed by ras converting enzyme (RCE1) by endoproteolytic digest. Finally, isoprenylcysteine carboxy methyl transferase (ICMT) methylates the isoprenylcysteine and this fully processed ras associates with the membrane. (Fig I2.2) [reviewed in 163].

Several strategies have been employed to inhibit ras farnesylation, the most common being the design of CAAX peptidomimetics that compete for binding to FTase and are therefore potent and selective inhibitors of FTase. A large number of farnesyltransferase inhibitors (FTIs) have been developed as potential anti-cancer therapies through high-throughput screening methodologies [164, 165]. These were shown to effectively inhibit Hras in cell culture. Evidence from mouse models also supported the use of FTIs in cancer therapy. In MMTV-Hras mice, for instance,

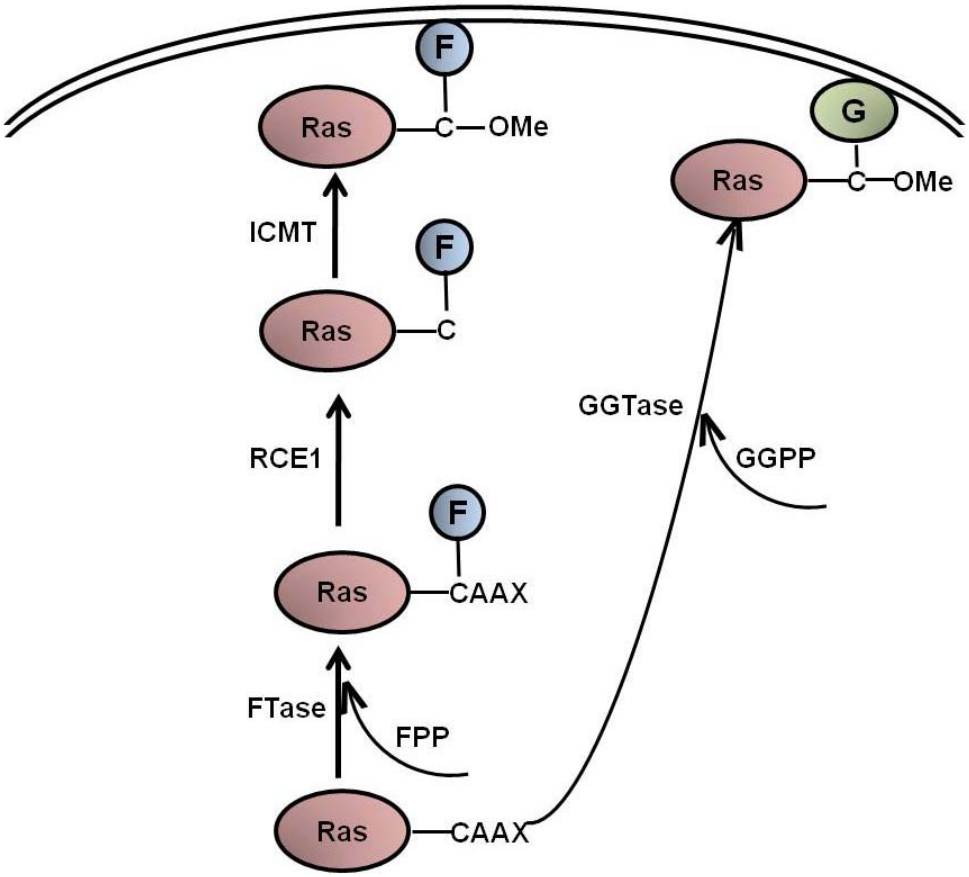

Fig I2.2 Processing of Ras proteins. Ras proteins undergo modifications with isoprenyl groups on their CAAX motif. Farnesyl transferase is responsible for the farnesylation of the CAAX motif, followed by the excision of –AAX by RCE1. ICMT then methylates the C- residue, and fully processed ras is able to associate with the membrane. Kras and Nras can undergo an alternate modification in the absence of farnesylation. Geranyl geranyl transferase is responsible for the addition of geranyl geranyl groups to the CAAX motif.

mammary carcinomas were efficiently reversed by FTI with very little associated toxicity [166]. Xenograft tumours of Calu-1 human lung adenocarcinoma responded well to FTIs, where tumour growth was blocked [167, 168]. Efficacy was also seen against intracranial glioblastoma in nude mice and in chemically-induced lung cancer mouse model [169-172].

The initial expectations for FTIs in cancer therapy were unfortunately not realized. The mechanism of action of FTIs remains unclear, and the successes seen in mouse models has not been recapitulated in human clinical trials. The main cause for this is that Kras, and to some extent Nras, can be alternatively prenylated. This prenylation is catalyzed by geranylgeranyl transferase I (GGTI), which uses geranylgeranyl pyrophosphate (GPP) as a substrate to add a 20-carbon geranylgeranyl group to the cysteine residue (Fig I2.2). Geranylgeranylation of Kras is only important under circumstances when farnesylation is blocked, and provides an alternate pathway for membrane localization, thus bypassing the inhibition of FTase. Attempts to inhibit Kras function by combining FTIs and GGTIs have been unsuccessful due to excessive toxicity associated with the combination [173].

Farnesylthiosalicylic acid

Ras membrane localization is mediated by interactions between the farnesyl moiety of ras and prenyl-binding pockets in proteins such as galectin-1 and galectin-3 [174, 175], which provides new possibilities for targeting ras. Farnesylthiosalicylic acid (FTS) is a small molecule rigid carboxylic acid derivative that mimics the farnesylated moiety of Ras (Fig I2.3A) [176]. Unlike the FTIs, FTS does not interfere with ras processing, rather it prevents the localization of fully-processed ras to the membrane by inhibiting

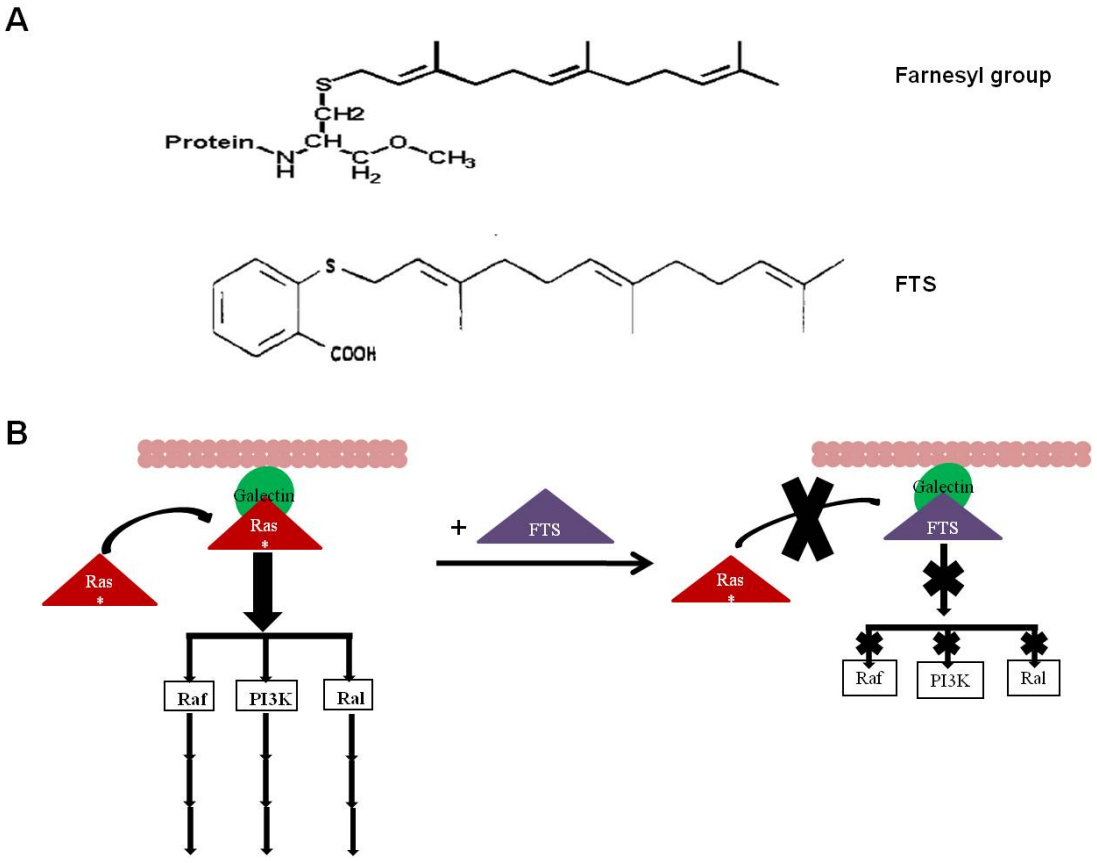

Fig I2.3 Mechanism of action of FTS. FTS is a small molecule mimetic of farnesyl groups (A). Active ras anchors to the membrane through proteins such as Galectins. Membrane-anchored ras is able to activate signalling cascades. FTS competes with Ras for galectin binding sites, thereby inhibiting the activation of downstream signals.

its interactions with galectin [174, 175, 177, 178]. It is readily taken up by cells, and appears to disrupt the association of ras with the cell membrane and to selectively inhibit ras-dependent cell growth [177, 178]. Treatment of ras-transformed rodent fibroblasts resulted in downregulation of MAP kinase signalling [179]. Glioblastoma cells treated with FTS exhibited decreased PI3kinase signalling and subsequent inhibition of cell migration by altering the rac-rho balance in the cells, and decreased hypoxia-inducible factor-1 alpha causing cessation of glycolysis and cell death [180, 181]. In neuroblastoma cell lines, the use of FTS resulted in attenuated MAPK and PI3K signalling, loss of MycN and inhibition of cell growth [182]. Experiments in xenograft models have supported the use of FTS as a therapeutic agent. The growth of ras-transformed rat-1 cells is inhibited by FTS in nude mice [183]. Panc-1 pancreatic cancer cells and melanoma cells carrying ras mutations both responded to FTS therapy [184-186].

FTS is also being tested in clinical trials in human patients. A first-in-man phase I clinical study indicated that FTS is well-tolerated in patients with solid tumours, and 29% of patients exhibited stable disease on treatment of >= 4 months, with a range of 4-23 months [187]. It is currently in trials for a number of different cancer types including non-small cell lung cancer, pancreatic and biliary tumours and solid and hematologic tumours.

MATERIALS AND METHODS

Mouse strains

The LSL-Kras^{G12D}, LSL-Trp53^{R172H} and Pdx-1-Cre strains of mice have been previously described [27, 28]. These strains of mice were interbred to ensure a mixed C57BL6/129Sv background for survival studies. Mice were housed and maintained, and experiments were conducted, in compliance with UK home office regulations.

Generation of experimental animals

LSL-Kras^{G12D}; Trp53^{R172H}; Pdx-1-Cre: LSL-Kras^{G12D}; Trp53^{R172H} mice were bred to Pdx-1-cre mice to generate KPC tumour mice used for survival and short-term studies.

Reagents

S-trans,trans-Farnesylthiosalicylic acid (FTS) was obtained from Concordia pharmaceuticals. Gemzar powder, produced by Eli Lilly was purchased. Carboxymethyl cellulose (CMC) was obtained from Sigma Aldrich. Alexa Fluor conjugated secondary antibodies for co-immunofluorescence were obtained from Invitrogen.

Imaging of pancreatic tumours

High resolution ultrasound (US) imaging of mice was carried out to identify and quantify pancreatic tumours, as described previously [43, 188]. Mice were anesthetized with isofluorane and the long hair was then shaved, followed by depilation using cream to remove any remaining hair. 3-4 mls of sterile saline was injected intraperitoneally to improve contrast. Imaging was performed using the Vevo770

system (Visual Sonics) with a 35MHz RMV Scan head. Three dimensional images for quantification of tumour volume were obtained by collecting serial images at 0.25mm intervals. Tumour reconstruction was carried out using Vevo 770 software by manually outlining the tumour in each 2-dimensional frame.

Study structure

KPC mice were enrolled on study when tumours measured 6-9 mm mean diameter by ultrasound. Mice enrolled on survival studies were imaged bi-weekly till endpoint. Mice enrolled on short-term studies did not receive further ultrasounds after enrolment. Endpoint is defined by a number of criteria including development of ascites, weight loss > 20%, severe cachexia or other obvious signs of ill health including extreme inactivity.

All studies included four treatment groups – vehicle, gemcitabine, FTS alone and FTS in combination with gemcitabine. Vehicle-treated mice were administered carboxymethylcellullose (CMC) daily by oral gavage. Mice on the gemcitabine arm received CMC daily and bi-weekly intraperitoneal injections of 100mg/kg gemcitabine. FTS was administered daily by oral gavage at 100mg/kg.

Drug formulation

The vehicle used for formulation of FTS is carboxymethyl cellulose (CMC). 0.5% CMC was prepared as previously described [(189)]. 0.5 gms CMC was dissolved in 50mls sterile water by stirring for approximately 4 hours, following which the solution was brought up to 100mls.

FTS was formulated at a concentration of 10mgs/ml by grinding in a mortar and pestle. CMC was gradually added, with constant grinding, to form a milky

suspension. The solution was poured out of the mortar and pestle, and they were rinsed with CMC to extract any remaining FTS. FTS in this preparation is stable at 4°C for a month. Before administration, the drug was brought to room temperature along with constant stirring to resuspend any settled drug.

Gemcitabine stock of 5mg/ml was prepared by dissolving Gemzar (48% difluoro-deoxycytidine) in sterile normal saline. Gemcitabine goes into solution rapidly and was prepared fresh immediately before use every time.

Immunohistochemistry

Immunohistochemistry was carried out on tissue using the same protocol as described in chapter I. The antibodies used were phospho-histone H3, alpha smooth muscle actin, Ki67 and phospho-ERK that are listed in table M1.1

Co-immunofluroescence

Tissue sections were deparaffinised in xylene and rehydrated through a graded alcohol series into 1X PBS as for immunohistochemistry. Antigen retrieval was mediated by boiling 10mM citrate buffer, pH6.0 and the slides were cooled. Slides were blocked with 10% serum + 1% BSA in TBST for 1 hour at room temperature. Slides were then incubated overnight at 4°C with a mixture of 1:100 diluted Ki67 antibody (Neomarkers) and 1:100 dilution of alpha smooth muscle actin antibody (Abcam). Sections were washed with TBST and were incubated with 1:500 dilutions of the relevant alexa fluor conjugated secondary antibodies at room temperature for one hour. The slides were then washed with TBST and mounted in Prolong gold anti-fade reagent with DAPI (Invitrogen). Slides were imaged using the Nikon Eclipse 90i microscope with the D-Eclipse C1 Si confocal system.

FTS pharmacokinetic analysis

Plasma samples for FTS pharmacology were obtained as follows – blood was collected by terminal cardiac puncture into tubes containing lithium-heparin. Samples were spun at 6000g for 10 minutes, plasma was aliquoted and snap frozen in liquid nitrogen. Tissue samples were snap frozen in liquid nitrogen.

The protocol for FTS pharmacokinetic analysis has been previously published [190]. Prior to extraction, frozen samples were thawed in a water bath at ambient temperature. Tissue homogenates were prepared at a concentration of 200 mg/mL in PBS and further diluted 1:5 or 1:10 in human plasma prior to extraction. Mouse plasma was diluted 1:10 in human plasma prior to extraction. Sample preparation involved a liquid-liquid extraction by the addition of 0.5 mL of plasma or tissue homogenate with 5 mL of methyl t-butyl ether containing 20 ng/mL of the internal standard S-trans,trans-5-fluoro-farnesylthiosalicylic acid (5-F-FTS). Chromatographic separation was achieved on a Waters X-Terra C(18) (50 mm x 2.1 mm i.d., 3.5 μm) analytical column using a mobile phase consisting of acetonitrile containing formic acid (0.1%, v/v)/ammonium acetate (10 mM) (80:20, v/v) using isocratic flow at 0.2 mL/min for 5 minutes. FTS and the internal standard were monitored by a Micromass Quattro LC triple-quadrupole MS detector using an electrospray probe operating in negative ionization mode. Linear calibration curves were generated over the range of 1-1000 ng/mL for plasma or 30-60000 ng/g for tissue homogenates. Samples that were diluted 1:10 (v/v) with plasma were accurately quantitated allowing for dilution of samples that were > 1000 ng/mL. The accuracy and within- and between-day precisions were within the acceptance criteria for bioanalytical assays.

Ras-GTP assays from tissue

Tissue harvested for Ras-GTP assays was snap frozen immediately in liquid nitrogen. Before lysis for the assay, the tissue fragments were ground to a fine powder using a liquid nitrogen-cooled mortar and pestle. The powdered tissue was lysed in ice-cold Mg2+ lysis buffer (25mM Hepes pH 7.5, 150 mM NaCl, 1% Igepal CA-630, 10mM $MgCl_2$ and 2% glycerol). The remainder of the Ras-GTP assay was conducted as described in chapter I.

Western blotting from tissue

Tissue samples from tumours were snap-frozen in liquid nitrogen immediately after harvesting. Tissue samples were lysed in SDS lysis buffer with protease and phosphatase inhibitors.

The procedure for western blotting is described in detail in chapter I. The antibodies used are listed in table M1.2. Additional antibodies used are listed in Table M2.1

Antibody	Source	Dilution
Kras (F234)	Santa Cruz Biotechnologies	1:1000
Akt	Cell Signaling	1:1000
Survivin	Cell Signaling	1:1000
Bip	Cell Signaling	1:1000
p21	Santa Cruz Biotechnologies	1:1000

Table M2.1 Antibodies for westerns

Quantification of proliferation

Tumour proliferation was quantified using phospho histone H3 immunohistochemistry. The number of positive and negative nuclei were enumerated in 5 20X fields, and proliferation was presented as a percentage of the total number of cells. Proliferation of stromal cells was quantified as a percentage of alpha smooth muscle cells staining for Ki67.

Statistical analysis

Graphpad prism software was used for statistical analysis. The Log-Rank (Mantel-Cox) test was used for analysis of survival curves. Proliferation and metastatic burden were analyzed using the Mann-Whitney test. Metastatic incidence was calculated by the Chi square test.

RESULTS

Detection of tumours by high-resolution ultrasound

For therapeutic studies, mice harboring the conditional *LSL-Kras^{G12D}* and *LSL-Trp53^{R172H}* alleles are bred to Pdx-1-Cre mice to direct expression of these alleles to the pancreas. LSL-Kras^{G12D}; LSL-Trp53^{R172H}; Pdx-1-Cre (KPC) mice develop pancreatic cancer with a 100% penetrance, and have a median survival of 5.6 months [28], although with variable latency. High-resolution ultrasound is a non-invasive imaging technique that allows the accurate measurement of tumour size to standardize enrolment of mice onto therapeutic studies [43, 188].

Starting at two months of age, mice are examined by palpation to detect pancreatic tumours. Palpation is a simple non-invasive method of pre-screening that reduces the number of ultrasound scans required. Once a palpable mass is detected, the mice are subjected to a pre-screening ultrasound. Mice with tumours <6 mm in mean diameter are followed by weekly ultrasound. Mice with pancreatic tumours between 6-9 mm mean diameter are suitable for therapeutic intervention. Short-term studies do not require follow-up ultrasounds, but mice on survival studies are scanned bi-weekly till end-point (Fig 2.1A).

Ultrasound images give information not only about size, but also about tumour location and characteristics. In Fig 2.1B, a pancreatic tumour is seen between a loop of intestine and an area of diseased pancreas. Both tumour and diseased pancreas have cystic areas.

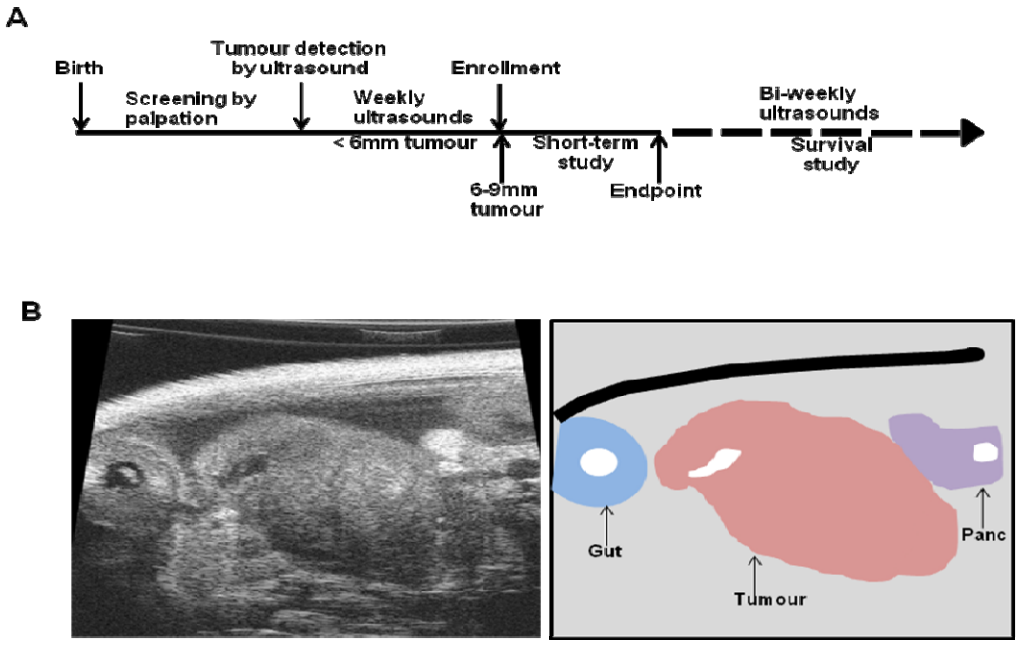

Fig 2.1 Use of high-resolution ultrasound to image pancreatic tumours The schematic represents the method used to identify mice with PDA. Mice are pre-screened by palpation from the age of two months onwards. Once a palpable mass is detected, an initial ultrasound is conducted to confirm the presence of a tumour. Mice with detectable tumours of < 6mm mean diameter are screened weekly to follow tumour growth. Mice bearing tumours between 6-9 mm are enrolled on study. Short term intervention does not involve further ultrasounds. Any animals enrolled onto a survival study will receive bi-weekly ultrasounds during the course of treatment (A). A sample ultrasound image showing a pancreatic tumour in the abdomen (B). The depiction on the right is a representation of the ultrasound image. The tumour is in the centre of the image (pink), with a cyst within the tumour represented in white. To the right is an area of diseased pancreas (purple), also with a cyst (white). The blue area on the left is a cross-section through the intestine with the lumen visible (B).

Farnesylthiosalicylic acid in combination with gemcitabine improves survival of tumour-bearing KPC mice

Since farnesylthiosalicylic acid (FTS) inhibits Ras *in vitro* and in xenograft models [177-179, 186, 189], the efficacy of this molecule as a pancreatic cancer therapy was tested in KPC mice. FTS was administered daily at a dosage of 100mg/kg by oral gavage. Gemcitabine was administered by intraperitoneal injection twice weekly at 100mg/kg (Fig 2.2A). Additionally, bi-weekly ultrasounds were carried out for survival studies (Fig 2.2A), but not for short-term intervention (Fig 2.2B).

The combination of FTS and gemcitabine leads to a significant extension in median survival (29 days), compared to vehicle-treated animals (12 days, p=0.0175). Gemcitabine monotherapy did not improve survival, with mice surviving a median of 13 days (p=0.3218). Single-agent FTS also did not have a beneficial effect on median survival, with mice living 15 days (p=0.0175) (Fig 2.3, Table 2.1). The combination therapy was not significantly different from gemcitabine alone (p= 0.2461). It should be noted, however, that there was a nearly 50% increase in survival on the combination therapy compared to gemcitabine alone, that therefore merits further investigation.

GROUP	COHORT SIZE	MEDIAN SURVIVAL IN DAYS	p value compared to vehicle
Vehicle	11	12	
Gem	11	13	0.3218
FTS	11	15	0.8901
FTS + Gem	16	29	0.0175

Table 2.1 Analysis of median survival

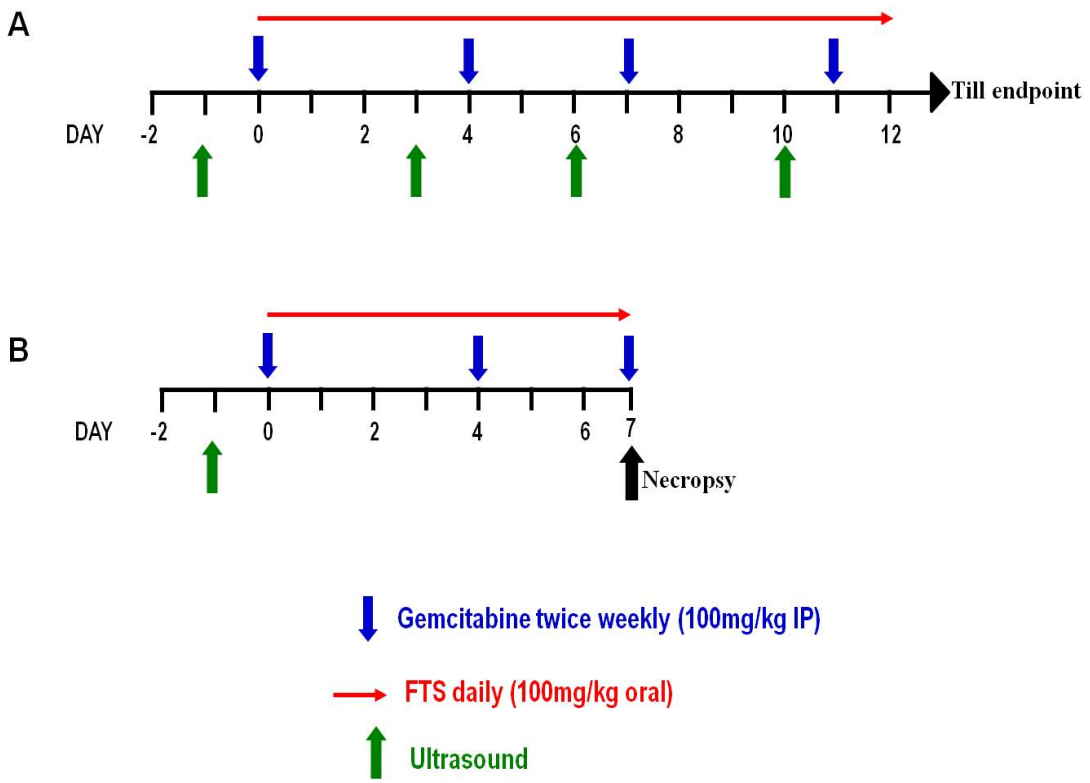

Fig 2.2 FTS study structure. Mice on long-term intervention are subject to the protocol outlined in (A). Mice are enrolled on study following identification of tumours between 6-9 mm mean diameter (Day -1). FTS is dosed at 100mg/kg daily by oral gavage. Gemcitabine is dosed by intraperitoneal injection at 100mg/kg twice weekly. Tumour growth is followed by twice weekly ultrasounds until endpoint. For short-term studies (B), the same enrolment criteria and dosing scheme are followed. However, follow-up ultrasounds are not carried out during the course of treatment, and mice are euthanized on Day 7 (B).

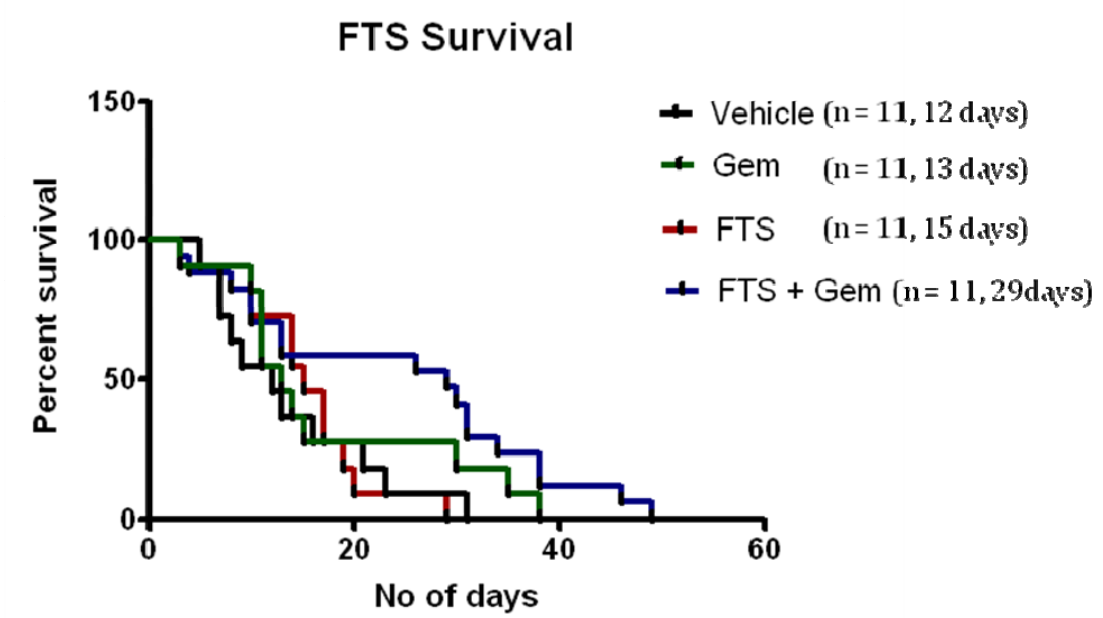

Fig 2.3 FTS in combination with gemcitabine extends survival The cohort treated with the combination of FTS and Gemcitabine has a median survival on study of 29 days, a significant extension over vehicle-treated mice (11 days, p=0.0175). Gemcitabine by itself does not extend survival compared to vehicle (13 days, p=0.3218). FTS as a single agent does not affect survival (15 days, p=0.8901). Although the increase in survival of the combination arm is not statistically significant compared to gemcitabine (p=0.2461), it should be noted that the combination results in an almost doubling of median survival.

Tumour kinetics are delayed by combination therapy

In order to address whether FTS affects tumour growth, ultrasound images were quantified. Three-dimensional images were used to generate volumetric measurements by outlining the tumours on sequential two-dimensional frames. The initial tumour volumes on enrolment were not different between the four treatment groups (Fig 2.4A), confirming that results were not biased.

KPC tumour growth in untreated mice is very rapid, as seen by the traces of individual tumours (Fig 2.4B). Gemcitabine overall did not affect tumour kinetics, with only responders to treatment showing a slight decrease in growth rates. FTS as a single agent had no effect on tumour growth. Tumours in mice that received the combination of FTS and gemcitabine grew slower than tumours in any of the other three groups (Fig 2.4B).

FTS does not affect tumour histology

Previous therapeutic work in KPC mice has shown that tumour histology after treatment can provide information on the mechanism of action of the drug [(43)]. Despite the increase in survival and the reduction in tumour kinetics, the combination therapy did not have any obvious noticeable effects on tumour histology. Tumours at end point displayed mixed ductal (Fig 2.5A), sarcomatoid (Fig 2.5B) and solid characteristics, with deposition of extracellular matrix and abundant stroma (Fig 2.5C). FTS also did not prevent the development of liver metastases (Fig 2.5D). An analysis of lung metastasis could not be carried out, as lung tissue was harvested for pharmacokinetic analysis.

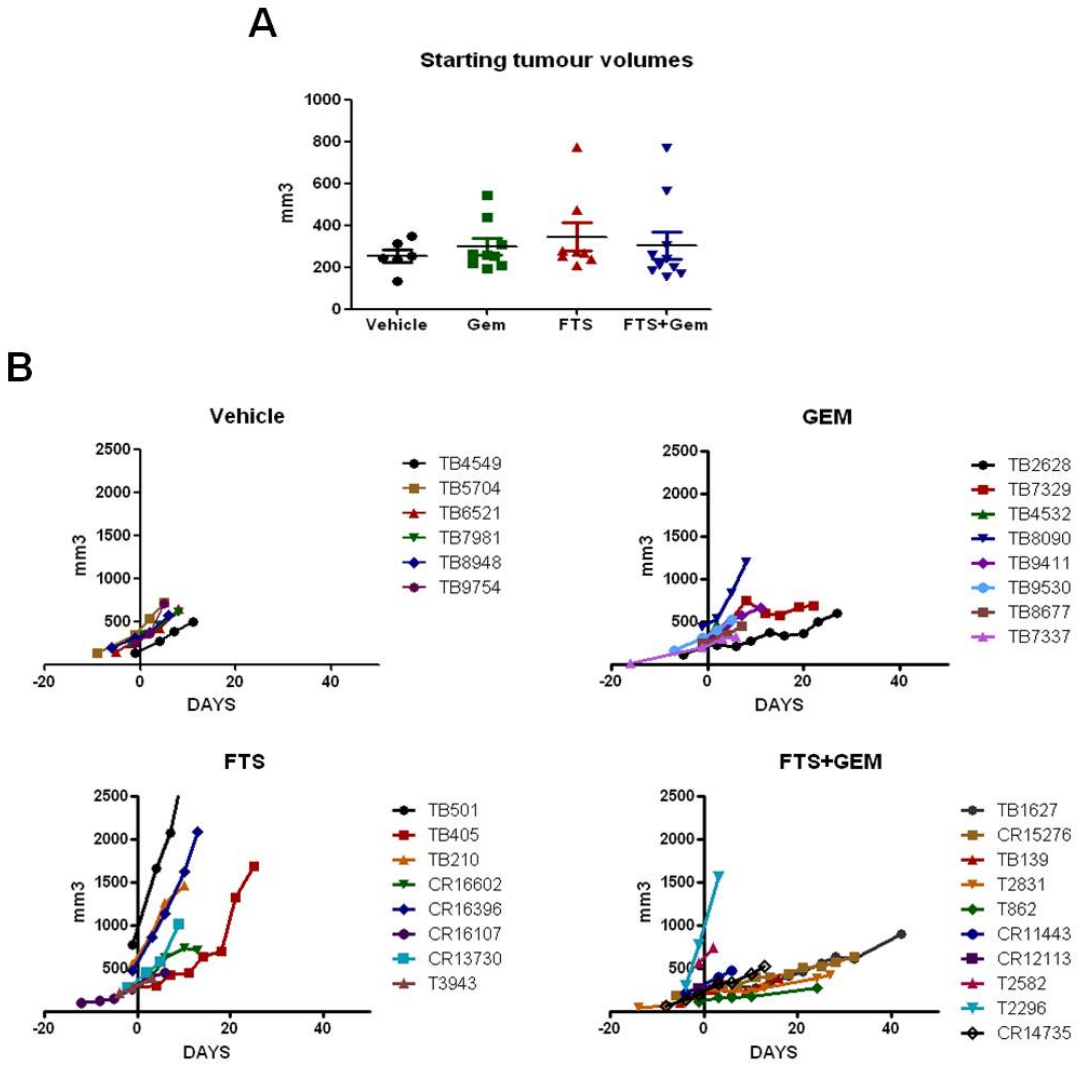

Fig 2.4 Combination treatment decreases tumour growth. Initial tumour volumes are equal across the four cohorts, indicating that the effects of treatment are not biased (A). Analysis of tumour growth by volumetric ultrasound measurements shows that single agent FTS does not affect tumour kinetics compared to vehicle. Gemcitabine as a single agent affects tumour growth in a fraction of responders, as expected. The combination of FTS and gemcitabine, however, reduces the growth rate of the majority of tumours. Each trace represents an individual animal (B).

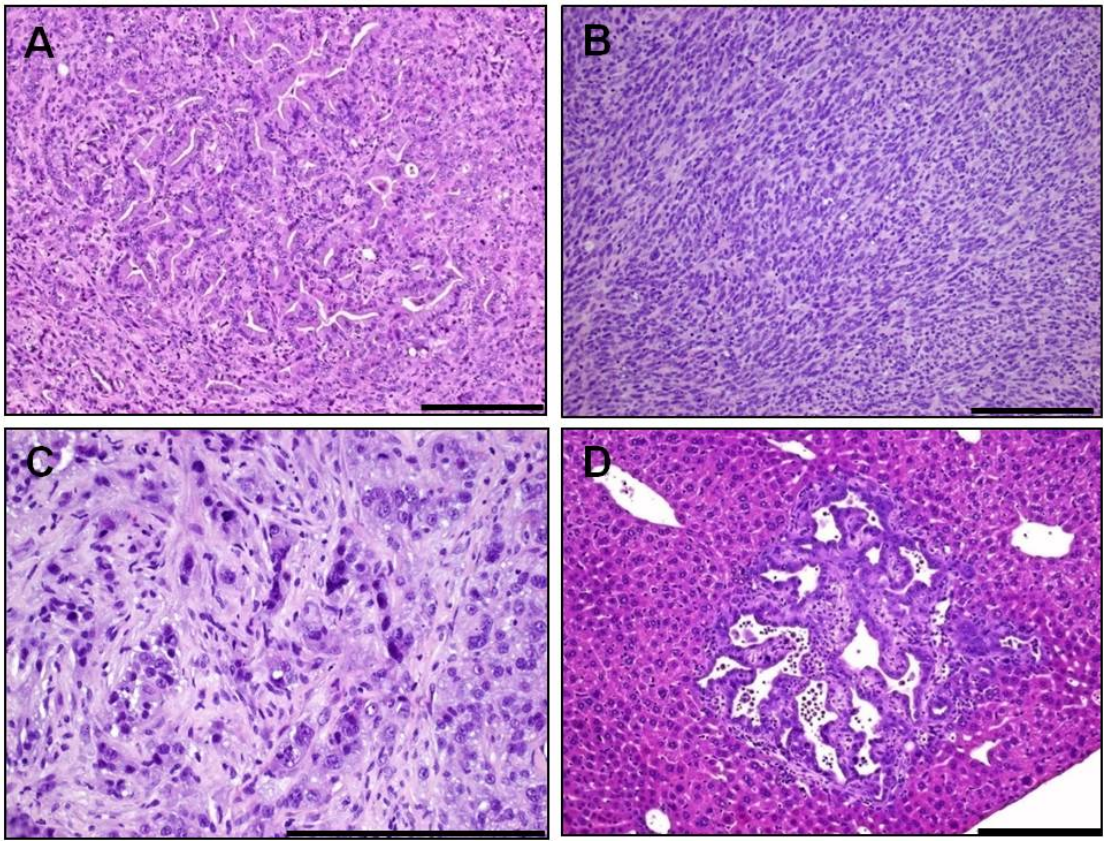

Fig 2.5 FTS does not affect tumour histology FTS-treated tumours exhibit ductal (A) and sarcomatoid (B) morphologies. Tumour stromal content did not appear to be affected (C). FTS treatment did not completely prevent the formation of liver metastases (D).

Proliferation is decreased in tumours by combination treatment

Since tumour growth is affected by combination treatment, proliferation in tumours was measured by phospho-histone H3 immunohistochemistry. Combination treatment results in a lowered rate of tumour proliferation (1.058% +/- 0.2170), a significant decrease compared to vehicle (5.167% +/- 1.834, p=0.0357). FTS monotherapy does not alter proliferation with a rate of 4.19% +/- 1.798 (p=0.8571). Gemcitabine by itself lowered proliferation slightly, although this was not significantly different (2.775% +/- 1.161, p=0.1143) (Fig 2.6A).

Stromal proliferation was also analyzed by co-immunofluorescence for alpha-smooth muscle actin and Ki67. There was no difference in the proliferation of activated myofibroblasts in response to treatment. Stromal proliferation in the combination-treated tumours was 5.17% +/- 1.712, compared to vehicle which was 7.713 +/- 1.711 (p=0.1143). Neither gemcitabine (7.123 +/- 0.9429, p=0.8857) more FTS (12.44% +/- 2.4, p=0.0571) as single agents affected proliferation in alpha-smooth muscle actin positive cells, although FTS alone appeared to induce a slight increase (Fig 2.6B).

To determine whether increased apoptosis might be involved in decreasing tumour growth, tumours were stained for cleaved caspase 3. There was no change in apoptosis in any of the treatment groups, with the tumours overall having a very low level of apoptosis (representative images, Fig 2.6C).

FTS is detectable in plasma and tumour tissue at end-point

It has been previously reported that pancreatic tumours in the KPC model are poorly perfused and display decreased delivery of the chemotherapeutic agent gemcitabine

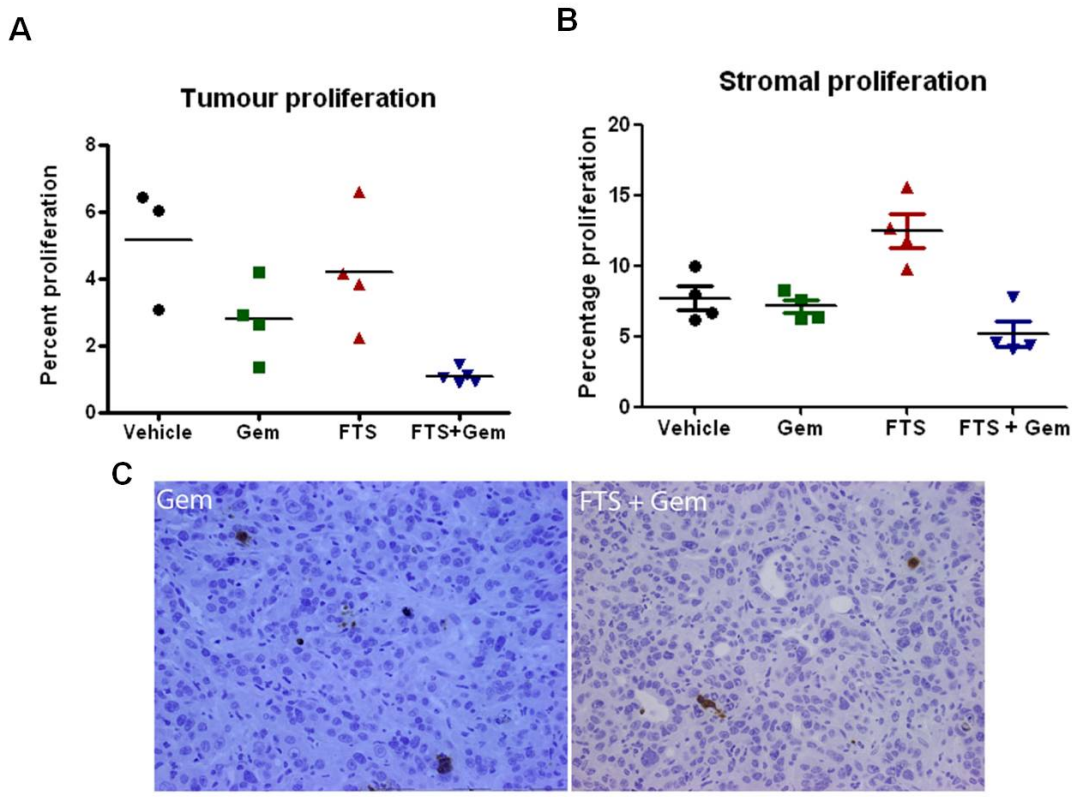

Fig 2.6 Treatment of KPC tumours with a combination of FTS and gemcitabine decreases tumour proliferation. Phosphohistone H3 analysis reveals that gemcitabine does not significantly affect proliferation compared to vehicle (p=0.1143), and neither does FTS as a single agent (p=0.8571). FTS when combined with gemcitabine leads to a significant decrease in proliferation compared to vehicle (p=0.0357) and gemcitabine (p=0.0317) (A). Proliferation of stromal fibroblasts is not affected in any of the treatment arms (B). Cleaved caspase 3 immunohistochemistry reveals that the combination treatment does not induce apoptosis compared to gemcitabine (C).

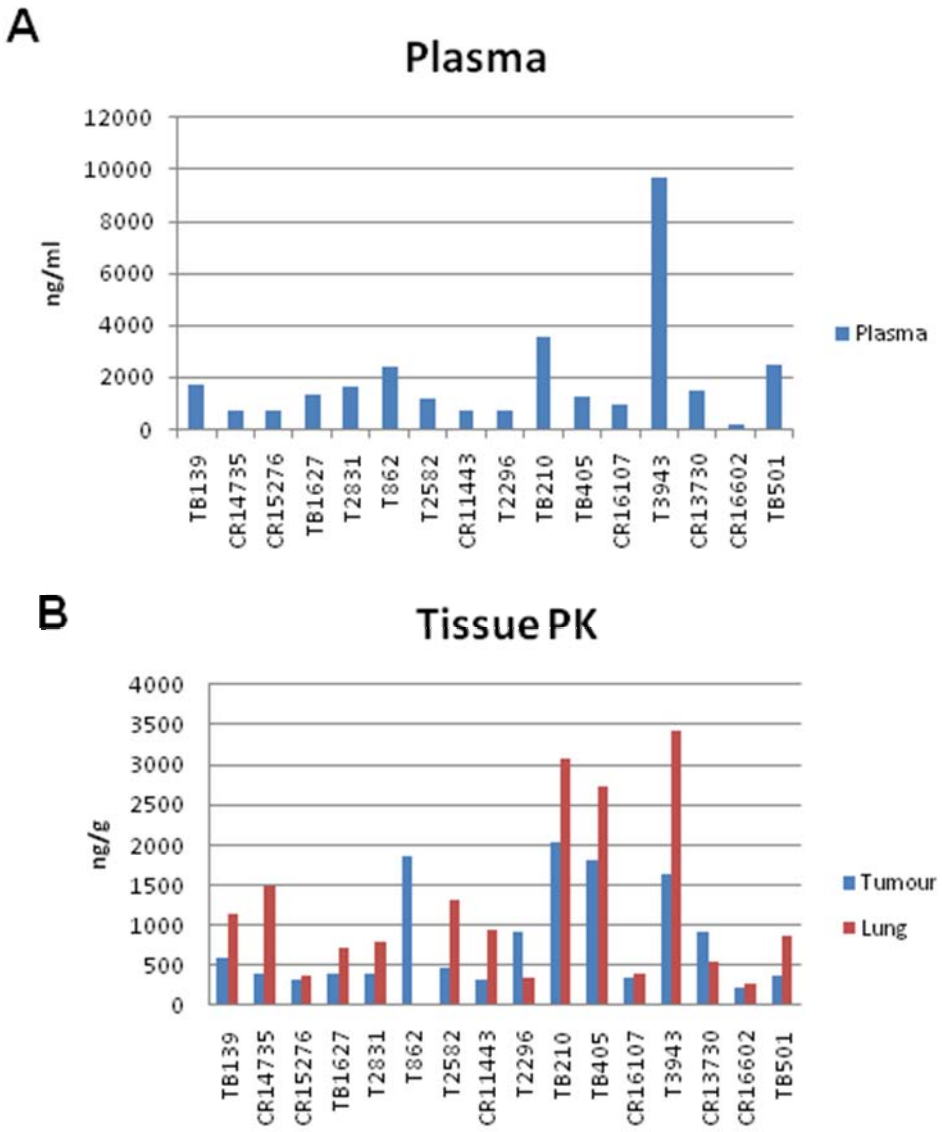

Fig 2.7 FTS is successfully delivered to pancreatic tumours. Pharmacokinetic analysis of FTS reveals that drug levels in plasma (A) and tissue (B) are variable. FTS was detected in all tumour samples processed, at comparable levels to drug found in the lungs, which is used as a reference (B).

[43]. In order to confirm that FTS was delivered to tumours successfully, pharmacokinetic analysis was conducted on plasma and tissue samples from treated mice. In all mice studied, FTS was detected in plasma as expected (Fig 2.7A). FTS was also present in measurable levels in all tumours analysed, although at varying levels from tumour to tumour (Fig 2.7B). The same variability in FTS levels was seen in lung tissue, which was used as a reference (Fig 2.7B, Table 2.2). The reason for this variability is unknown, but FTS levels do not correspond to survival.

ANIMAL ID	Plasma FTS (ng/mL)	Tumour FTS (ng/g)	Lung FTS (ng/g)
TB139	1692.4	596.1	1128.9
CR14735	698.9	391.2	1486.2
CR15276	752.1	322.2	381
TB1627	1310.1	401.7	712.2
T2831	1635.2	394.5	799.2
T862	2413.5	1851.6	31070.7
T2582	1153.4	459	1306.8
CR11443	691.2	324.3	954
T2296	740.1	912	343.8
TB210	3565.3	2027.4	3078.3
TB405	1244.5	1811.1	2722.8
CR16107	935.3	346.8	389.1
T3943	9653.3	1640.7	3423.3
CR13730	1466.2	924	549.3
CR16602	173.4	220.2	279.3

TB501	2456.6	373.2	858.6

Table 2.2 Pharmacokinetic analysis of FTS levels in plasma, tumour and lung tissue.

FTS does not appear to modulate Ras signalling in KPC tumours

Since FTS is described as an anti-Ras therapy, tumours at end-point were examined for Ras activity and signalling to determine whether this was the mechanism for decreased tumour growth and proliferation. Western blots were performed on tumours from all four treatment groups. There was no difference in levels of total Ras-GTP or of active Kras upon treatment with FTS. FTS also did not affect levels of either Kras alone or total Ras in tumours. In addition, there was no difference in phospho-Akt in treated tumours. FTS did not diminish levels of phospho-ERK in end-point tumours. On the contrary, three combination-treated tumours had high levels of phospho-ERK, although this was not seen in the FTS alone group (Fig 2.8). Total ERK was used as the loading control.

Immunohistochemistry for phospho-ERK confirmed that this downstream target of Ras signalling was not altered. Tumours in all four groups at end point had robust phospho-ERK signal in tumour cells (Fig 2.9).

Further analysis on tumours also showed that FTS treatment did not affect other signalling molecules and targets downstream of Ras including phosphorylated S6 ribosomal protein, p38 MAP kinase and cyclin D1 (Fig 2.10). There was also no alteration in levels of both Bip and survivin, although FTS has been shown to down-regulate both of these proteins [191, 192] (Fig 2.10).

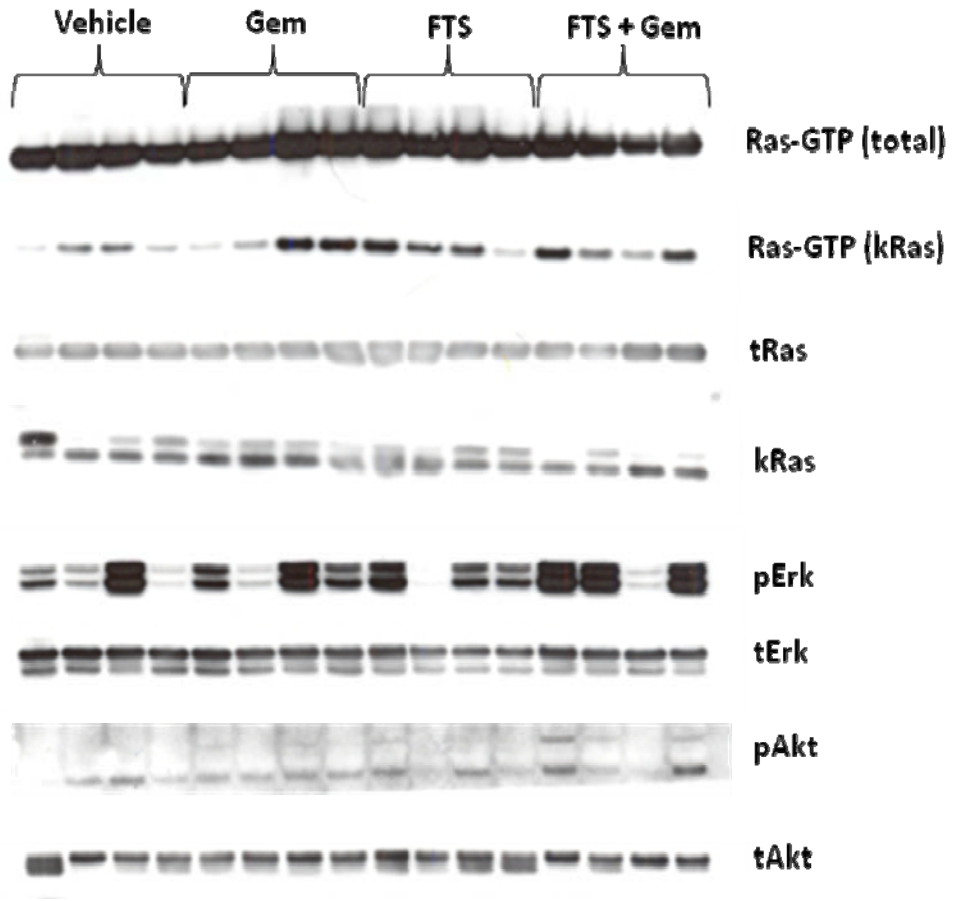

Fig 2.8 FTS does not appear to modulate Ras signalling. Analysis of end-point samples from long-term intervention studies reveals that FTS does not alter levels of active Ras or total Ras compared to vehicle and gemcitabine-treated tumours. In addition, there is no inhibitory effect of FTS treatment on levels of phospho-ERK or phospho-Akt. Total ERK is used as a loading control.

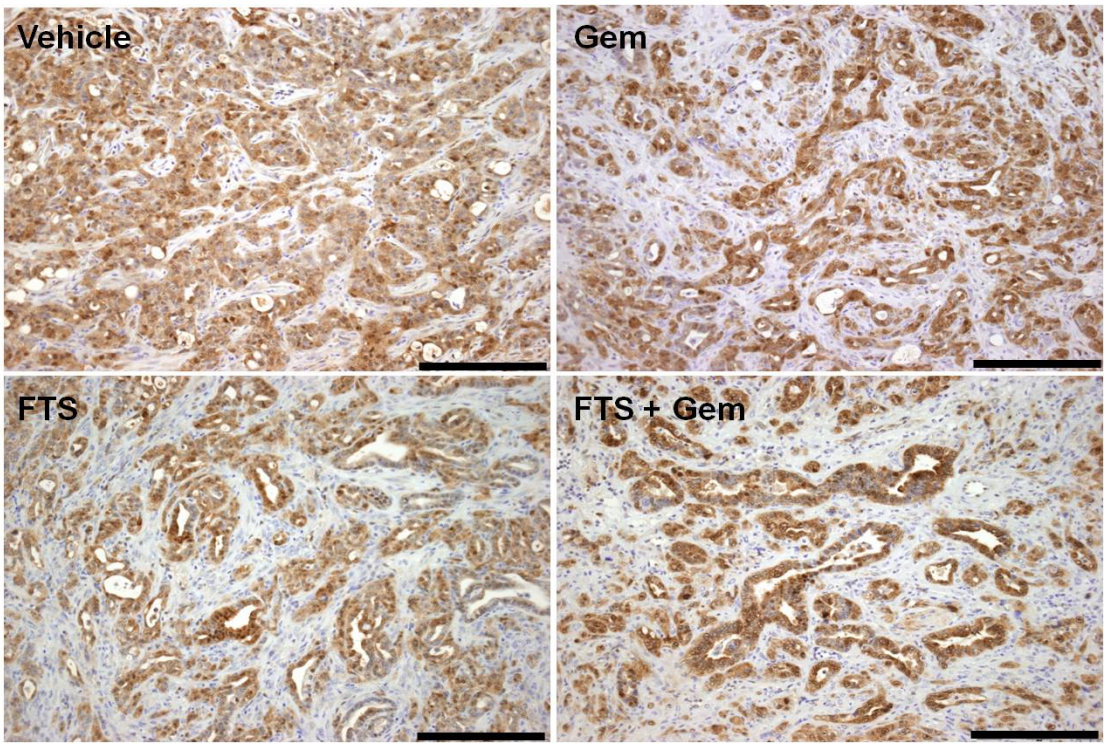

Fig 2.9 Phospho-ERK levels *in vivo* are not altered by FTS treatment. Immunohistochemical analysis of phospho-ERK at end-point reveals that FTS treatment, either by itself or in combination with gemcitabine, does not lower levels of phospho-ERK in comparison with vehicle or gemcitabine. (Scale bar = 200μm).

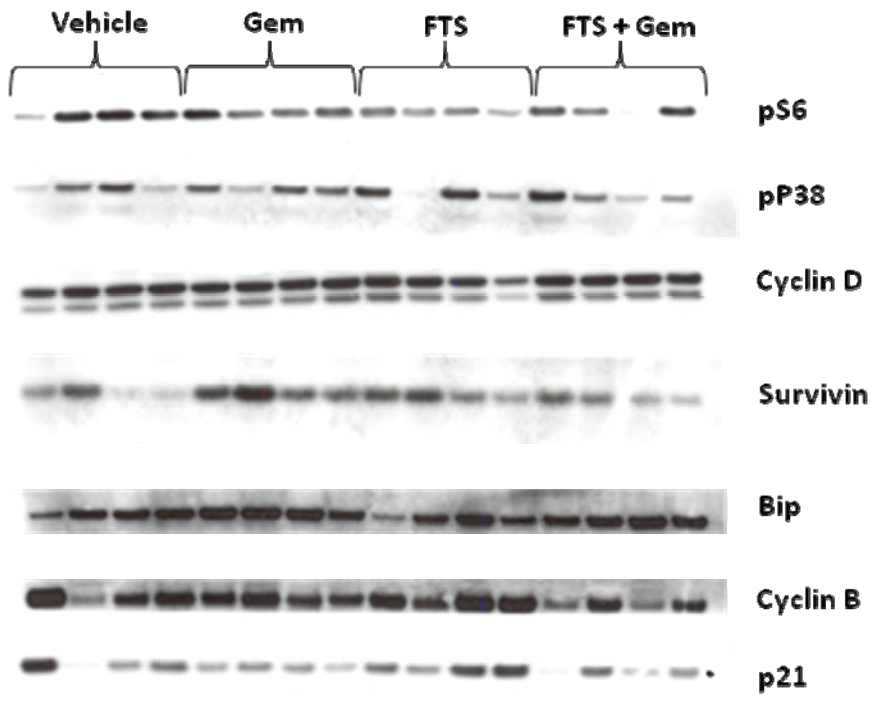

Fig 2.10 FTS does not affect signalling at end-point. Further examination of tumours at end point reveals that there is no decrease in phosphorylation of S6 ribosomal protein or p38 MAP kinase, and no alteration in levels of Cyclin D1, cyclin B, survivin and Bip.

There is no modulation of Ras signalling by short-term intervention

End-point tumours, which have been subjected to longer periods of FTS exposure, might lack alterations to Ras signalling due to escape mechanisms or feedback loops. In order to determine whether Ras signalling is indeed affected in pancreatic tumours, a short-term analysis was performed by treating KPC tumour-bearing mice with FTS for 7 days. The tumours were then subjected to a similar analysis as those at end-point.

At this short timepoint, there was no modulation of either Ras levels, or signalling modules downstream of Ras including phosphorylation of ERK, Akt, S6, p38 and Rsk. There was also no difference in levels of cyclin D1, survivin and Bip (Fig 2.11), confirming that FTS in the KPC model of pancreatic cancer does not affect Ras signalling, or previous known targets of the inhibitor. These results were also recapitulated in patient-specific xenografts, which have been previously described [31]. Tissue samples of patient-specific xenografts treated with FTS were obtained and were analysed for effects on Ras signalling. There were no changes in Ras-GTP, phospho-ERK or phospho-Akt (Fig 2.12).

FTS affects liver metastatic burden

In order to examine the effect of FTS treatment on metastasis, the burden of liver metastasis was quantified by counting the number of metastatic lesions in the livers of mice in the different treatment groups. The combination of FTS and gemcitabine led to a significant decrease in the number of metastases per mouse (0.454 +/- 0.5222) compared to vehicle-treated mice (5.875 +/- 5.693, p=0.0045). Neither gemcitabine (10.67 +/- 20.35, p=0.6978) nor FTS alone (4.909 +/- 10.79, p=0.1068) had this effect

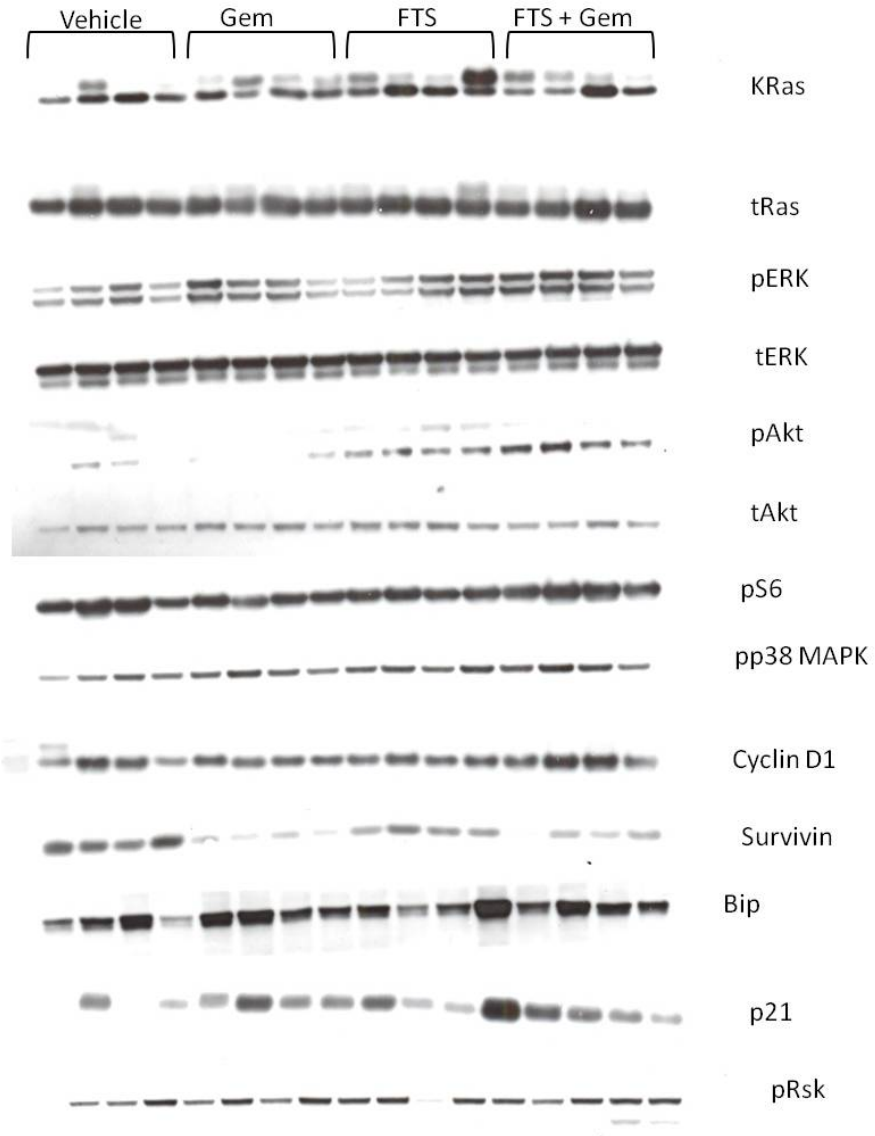

Fig 2.11 Short-term analysis of FTS treatment on signalling in tumours. Treatment of tumours for 7 days confirms that FTS does not inhibit Ras signaling in pancreatic tumours. There are no changes in levels of Ras, or in phosphorylation of molecules downstream of Ras such as ERK, Akt, S6, Rsk and p38 MAP kinase. FTS treatment also does not affect the expression of cyclin D1, survivin or Bip.

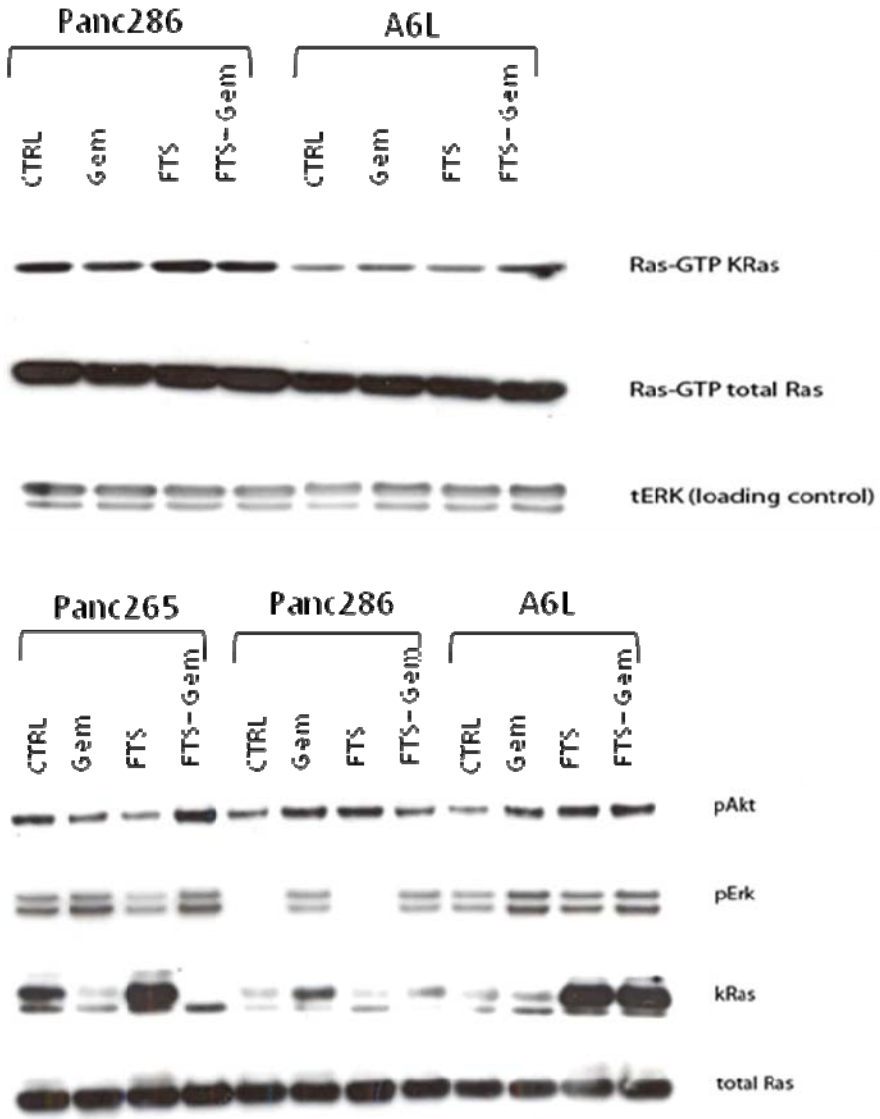

Fig 2.12 FTS does not alter Ras signalling in patient-specific xenograft tumours. There are no changes in ras activity or levels or phosphorylation of ERK or Akt in response to FTS, either as a single agent or in combination with gemcitabine, in patient-specific xenografts.

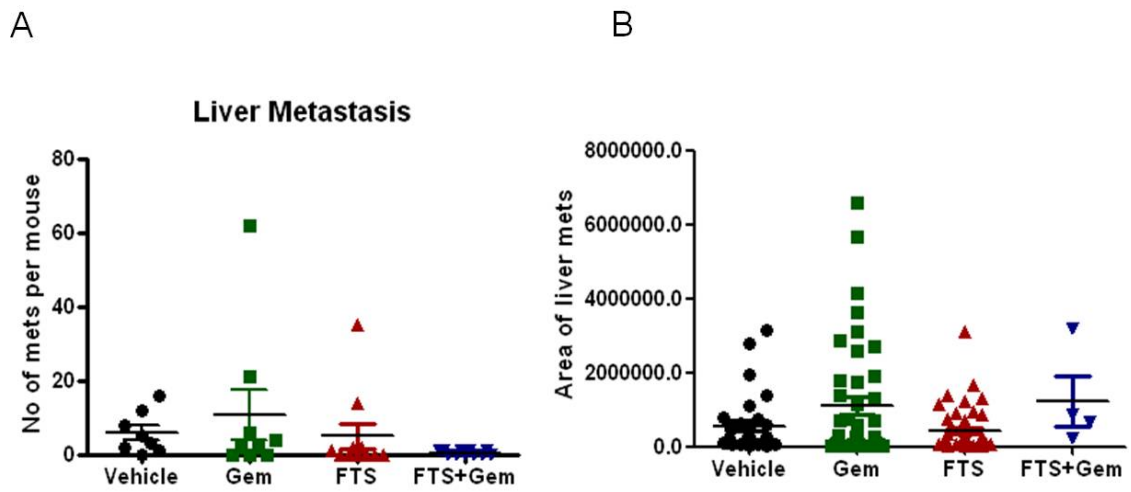

Fig 2.13 FTS combination treatment decreases the burden of liver metastasis. Although treatment with FTS does not prevent liver metastasis, FTS in combination with gemcitabine significantly decreases the burden of liver metastases compared to vehicle-treated animals (p=0.0045). Gemcitabine (p=0.6978) and FTS (p=0.1068) as single agents do not inhibit liver metastasic burden (A). There was no significant difference between any of the groups in the size of metastases to the liver (B).

(Fig 2.13A). There was no significant difference between any of the treatment arms with regards to tumour size (Fig 2.13B).

FTS, whether alone or in combination with gemcitabine, significantly decreased the incidence of liver metastasis with only 45.45% of mice developing metastases to the liver compared to 87.5% of vehicle-treated mice (Table 2.3, p=0.0141). Gemcitabine alone decreased the incidence of metastasis to 67.67%, although this was not statistically significant (p=0.3619).

Genotype	Number of mice	Mice with liver metastases	Incidence of liver metastasis
Vehicle	8	7	87.5%
Gemcitabine	9	6	67.67%
FTS	11	5	45.45%
FTS + Gem	11	5	45.45%

Table 2.3 Incidence of liver metastasis

FTS does not decrease phospho-ERK in liver metastases

Pharmacokinetic analysis of liver tissue revealed that the liver accumulated 15-30 times more FTS than tumour tissue (Fig 2.14A). Due to this large difference, liver metastases were examined to determine whether phospho-ERK was decreased in response to FTS. Immunohistochemistry revealed that there was no difference in phospho-ERK in liver metastasis after FTS treatment (Fig 2.14B), further corroborating that the response of pancreatic tumours to FTS is not a result of altered Ras signalling.

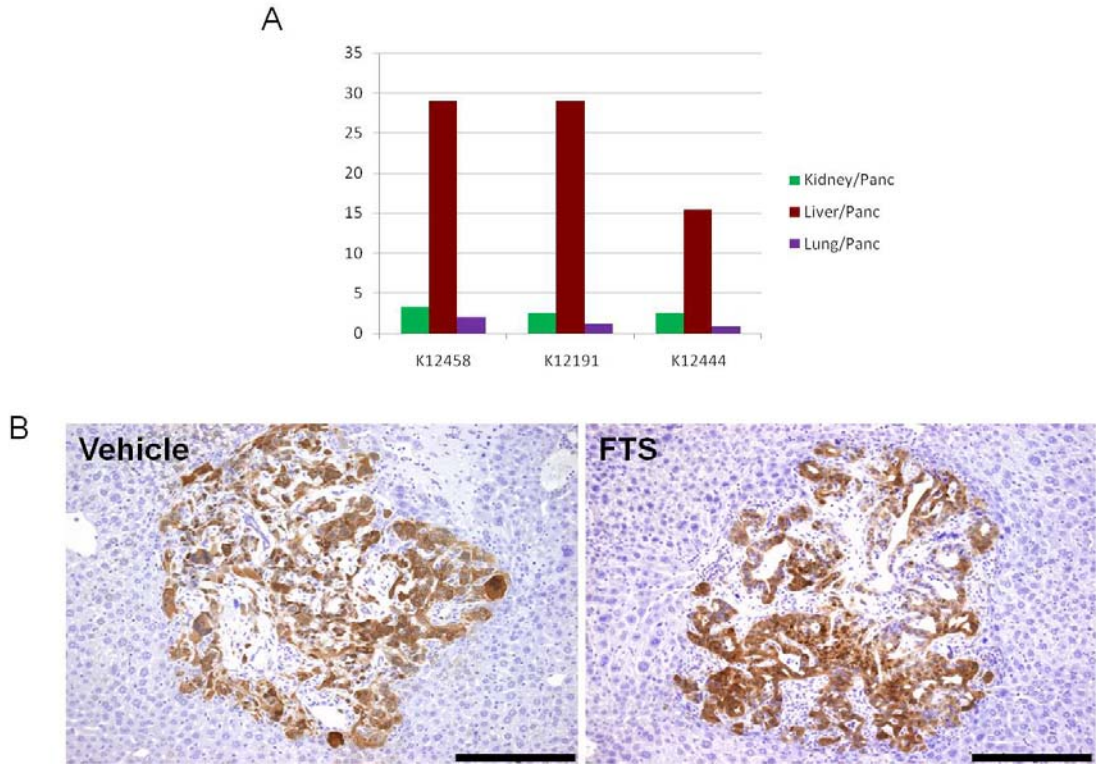

Fig 2.14 Phospho-ERK levels in liver metastases are not affected by FTS treatment. Pharmacokinetic analysis of the liver reveals that liver tissue accumulates 15-30 times more FTS than pancreatic tumour tissue (A). Despite this increase in drug levels, phospho-ERK is not changed in liver metastases from FTS-treated mice compared to vehicle-treated mice (B).

DISCUSSION

FTS is a derivative of farnesylated rigid carboxylic acids. It mimics the farnesylated moiety of Ras by binding to adaptor proteins such as galectin in the plasma membrane. In this manner, FTS prevents active Ras from anchoring to the membrane, leading to its degradation and the inhibition of downstream signalling [177-179, 189]. *In vitro* experiments demonstrated that FTS selectively inhibited Ras-dependent cell growth, transformation and survival [178, 180, 185, 191, 193, 194]. Additionally, FTS inhibited growth in xenograft models of neurofibromatosis, breast cancer, melanoma, Merkel cell carcinoma and pancreatic cancer [186, 195-198].

FTS was tested in the KPC mouse model of pancreatic cancer to evaluate its efficacy as a therapeutic agent in this disease. FTS as a monotherapy did not have an effect on survival, but in combination with gemcitabine led to a substantial increase in median survival. This effect was associated with delayed tumour kinetics and decreased proliferation in tumours. In addition, combination therapy decreased the burden of liver metastasis, and treatment with FTS decreased the incidence of liver metastasis both as single agent and combination treatment. Despite these effects, FTS in this mouse model did not appear to decrease ras activity or modulate ras signalling in either end-point analyses or short-term intervention studies in primary tumours and liver metastases.

A simple explanation for the effect of FTS in the KPC model of pancreatic cancer may be the augmentation of gemcitabine delivery, thereby improving survival. This phenomenon has been previously reported in this model in combination therapy [43].

Although FTS is reported to be a ras inhibitor, evidence from the literature also suggests that it has other molecular targets. In MCF-7 cells, for instance, FTS inhibits

mTOR with minimal effects on MAPkinase signalling [199], a result that is recapitulated in MEFs where FTS inhibits S6kinase activation by mTOR and decreases mTOR levels [200]. The effects of FTS on mTOR signalling appear to be due to the dissociation of the mTOR-raptor complex [201]. FTS may also be able to independently influence p53 function, although this requires further investigation [202]. In addition, as it mimics farnesylated moieties, FTS may have the potential to inhibit other farnesylated proteins which include protein tyrosine phosphatases, inositol polyphosphate phosphatases and phospholipase A2 among others [203-205]. Other proteins which have carboxyl terminal CAAX that might make them candidates for farnesylation include bone morphogenetic proteins, transforming growth factor-beta precursors and serine-threonine kinase 11, which have potential roles in regulation of growth [163]. Alternatively, the feedback loops that regulate signalling downstream of ras such as the MAP kinase phosphatases and dual-specificity phosphatases may be altered, to compensate for decreased ras activation.

The galectins are a group of carbohydrate binding proteins that exhibit diverse biological activities. They have a number of extracellular and intracellular functions. They are capable of cross-linking cell surface glycoproteins and transducing signalling events across the plasma membrane. More importantly, and perhaps more relevant to FTS, are their intracellular functions which include regulation of pre-mRNA splicing, cell growth, apoptosis and cell cycle progression. These functions involve protein-protein interactions, although the binding sites in galectin have yet to be identified [206-209]. It is conceivable, however, that the binding of FTS to galectins may interfere with their intracellular functions by preventing such protein-protein interactions, and may be responsible for the effects that FTS engenders in pancreatic

tumours. Alternatively, galectins might be upregulated in tumours in response to FTS treatment, to compensate for the competitive inhibition of active ras proteins. Indeed, galectin-3 is known to serve as a scaffold that augments ras activation, and a dominant-negative galectin-3 abrogates signalling down the MAP kinase cascade [210].

CONCLUSIONS/FUTURE DIRECTIONS

In summary, FTS treatment in combination with gemcitabine extends survival in tumour-bearing mice, with a corresponding decrease in tumour kinetics, proliferation and liver metastasis. The mechanism of action of FTS in pancreatic cancer does not appear to be clear-cut as there is no change in levels of ras protein or ras activity, as would be expected if ras was unable to localize to the membrane in response to therapy. Furthermore, there is no alteration in signalling modules downstream of ras, further corroborating the lack of ras modulation and indicating that FTS may influence survival in the KPC model of pancreatic cancer through a mechanism other than ras inhibition.

Compensation

In response to treatment, tumours are capable of altering gene expression patterns to compensate for inhibition by therapeutic agents. The proteins in the MAP kinase family, including ERK, SAPK and Jnk, are regulated by a number of phosphatases such as the MAP kinase phosphatases and dual specificity phosphatases [(reviewed in 211)]. It is possible that these phosphatases are altered upon treatment with FTS as an early response to changes in signalling downstream of ras. Tumour samples and cell lines treated with FTS must be examined for changes in these proteins, which might indicate a response to therapy and restoration of signalling. An alternative method of compensation would be the upregulation of the galectins. Overexpression of galectins would overcome competitive inhibition by FTS, and ras would be able to localize to the membrane and activate downstream signalling.

FTS and proliferation

Since FTS in combination with gemcitabine slows tumour kinetics, and proliferation is decreased without a change in apoptosis, the mechanism by which FTS affects proliferation should be examined. This can be performed *in vitro* using tumour cell lines. Cell cycle analyses should be conducted to determine whether FTS treatment results in alteration of cell cycle profiles. In addition, various cell cycle regulators should be compared post treatment with FTS. These experiments will also permit the investigation of differential effects on cells of gemcitabine and FTS alone and in combination.

FTS and gemcitabine

Although pharmacokinetics demonstrates that FTS can be measured in tumour tissue, it has not yet been determined whether the intracellular drug concentrations are sufficient to inhibit oncogenic ras. Most *in vitro* studies of FTS biochemistry have been conducted using micromolar concentrations of drug in cell culture systems. FTS in tumour tissue does not accumulate to such high concentrations, and the presence of desmoplasia and other cell types may interfere with the ability of the drug to reach the target cell population. The effect of lower concentrations of FTS on ras signalling may be determined in cell culture to determine whether the lack of ras modulation in pancreatic tumours is simply due to insufficient drug concentrations.

The survival benefit imparted by FTS in combination with gemcitabine may be due to improved delivery of the chemotherapeutic agent to pancreatic tumours. This is a phenomenon that has been previously reported in this model [(43)]. The levels of gemcitabine should be determined in FTS-treated tumours to determine whether

increased gemcitabine levels may account for the decreased proliferation seen in tumours.

Other targets of FTS

As has been previously discussed, FTS is thought to have other targets than ras, including p53 and mTOR [199-202]. Tumour samples must be analyzed to determine whether FTS has additional targets in cells. Gene expression profiles have been previously used to generate signatures of treated cells which are indicative of specific responses to therapy [212]. Such expression profiles carried out in FTS-treated pancreatic tumours may give an indication of targets that are being affected. Tumour cells must be isolated from tumours by laser capture microdissection in order to eliminate contamination from the microenvironment. A similarly useful approach would be a proteomic or phospho-proteomic analysis to elucidate alterations in protein profiles or signalling modules.

REFERENCES

1. Jemal, A. et al. Cancer statistics, 2009. *CA Cancer J Clin* 59, 225-49 (2009).

2. Warshaw, A.L. & Fernandez-del Castillo, C. Pancreatic carcinoma. *N Engl J Med* 326, 455-65 (1992).

3. Stolzenberg-Solomon, R.Z. et al. Insulin, glucose, insulin resistance, and pancreatic cancer in male smokers. *JAMA* 294, 2872-8 (2005).

4. Berrington de Gonzalez, A., Sweetland, S. & Spencer, E. A meta-analysis of obesity and the risk of pancreatic cancer. *Br J Cancer* 89, 519-23 (2003).

5. Everhart, J. & Wright, D. Diabetes mellitus as a risk factor for pancreatic cancer. A meta-analysis. *JAMA* 273, 1605-9 (1995).

6. Fuchs, C.S. et al. A prospective study of cigarette smoking and the risk of pancreatic cancer. *Arch Intern Med* 156, 2255-60 (1996).

7. Michaud, D.S. et al. Physical activity, obesity, height, and the risk of pancreatic cancer. *JAMA* 286, 921-9 (2001).

8. Gapstur, S.M. et al. Abnormal glucose metabolism and pancreatic cancer mortality. *JAMA* 283, 2552-8 (2000).

9. Jaffee, E.M., Hruban, R.H., Canto, M. & Kern, S.E. Focus on pancreas cancer. *Cancer Cell* 2, 25-8 (2002).

10. Petersen, G.M. & Hruban, R.H. Familial pancreatic cancer: where are we in 2003? *J Natl Cancer Inst* 95, 180-1 (2003).

11. Schenk, M. et al. Familial risk of pancreatic cancer. *J Natl Cancer Inst* 93, 640-4 (2001).

12. Nair, R.J., Lawler, L. & Miller, M.R. Chronic pancreatitis. *Am Fam Physician* 76, 1679-88 (2007).

13. Etemad, B. & Whitcomb, D.C. Chronic pancreatitis: diagnosis, classification, and new genetic developments. *Gastroenterology* 120, 682-707 (2001).

14. Lowenfels, A.B. et al. Hereditary pancreatitis and the risk of pancreatic cancer. International Hereditary Pancreatitis Study Group. *J Natl Cancer Inst* 89, 442-6 (1997).

15. McWilliams, R.R. et al. Cystic fibrosis transmembrane conductance regulator (CFTR) gene mutations and risk for pancreatic adenocarcinoma. *Cancer* 116, 203-9.

16. Shimosegawa, T., Kume, K. & Satoh, K. Chronic pancreatitis and pancreatic cancer: prediction and mechanism. *Clin Gastroenterol Hepatol* 7, S23-8 (2009).

17. Lohr, M., Maisonneuve, P. & Lowenfels, A.B. K-Ras mutations and benign pancreatic disease. *Int J Pancreatol* 27, 93-103 (2000).

18. Hruban, R.H., Iacobuzio-Donahue, C., Wilentz, R.E., Goggins, M. & Kern, S.E. Molecular pathology of pancreatic cancer. *Cancer J* 7, 251-8 (2001).

19. Heinemann, V. & Boeck, S. Perioperative management of pancreatic cancer. *Ann Oncol* 19 Suppl 7, vii273-8 (2008).

20. Stathis, A. & Moore, M.J. Advanced pancreatic carcinoma: current treatment and future challenges. *Nat Rev Clin Oncol*.

21. Hruban, R.H. & Adsay, N.V. Molecular classification of neoplasms of the pancreas. *Hum Pathol* 40, 612-23 (2009).

22. Lohr, M. et al. Human ductal adenocarcinomas of the pancreas express extracellular matrix proteins. *Br J Cancer* 69, 144-51 (1994).

23. Adler, G. Has the biology and treatment of pancreatic diseases evolved? *Best Pract Res Clin Gastroenterol* 18 Suppl, 83-90 (2004).

24. Hezel, A.F., Kimmelman, A.C., Stanger, B.Z., Bardeesy, N. & Depinho, R.A. Genetics and biology of pancreatic ductal adenocarcinoma. *Genes Dev* 20, 1218-49 (2006).

25. Hruban, R.H. et al. Pancreatic intraepithelial neoplasia: a new nomenclature and classification system for pancreatic duct lesions. *Am J Surg Pathol* 25, 579-86 (2001).

26. Hruban, R.H. et al. An illustrated consensus on the classification of pancreatic intraepithelial neoplasia and intraductal papillary mucinous neoplasms. *Am J Surg Pathol* 28, 977-87 (2004).

27. Hingorani, S.R. et al. Preinvasive and invasive ductal pancreatic cancer and its early detection in the mouse. *Cancer Cell* 4, 437-50 (2003).

28. Hingorani, S.R. et al. Trp53R172H and KrasG12D cooperate to promote chromosomal instability and widely metastatic pancreatic ductal adenocarcinoma in mice. *Cancer Cell* 7, 469-83 (2005).

29. Aguirre, A.J. et al. Activated Kras and Ink4a/Arf deficiency cooperate to produce metastatic pancreatic ductal adenocarcinoma. *Genes Dev* 17, 3112-26 (2003).

30. Izeradjene, K. et al. Kras(G12D) and Smad4/Dpc4 haploinsufficiency cooperate to induce mucinous cystic neoplasms and invasive adenocarcinoma of the pancreas. *Cancer Cell* 11, 229-43 (2007).

31. Rubio-Viqueira, B. et al. An in vivo platform for translational drug development in pancreatic cancer. *Clin Cancer Res* 12, 4652-61 (2006).

32. Shu, Q. et al. Direct orthotopic transplantation of fresh surgical specimen preserves CD133+ tumor cells in clinically relevant mouse models of medulloblastoma and glioma. *Stem Cells* 26, 1414-24 (2008).

33. Boehm, T., Folkman, J., Browder, T. & O'Reilly, M.S. Antiangiogenic therapy of experimental cancer does not induce acquired drug resistance. *Nature* 390, 404-7 (1997).

34. Sarraf, P. et al. Differentiation and reversal of malignant changes in colon cancer through PPARgamma. *Nat Med* 4, 1046-52 (1998).

35. Twombly, R. First clinical trials of endostatin yield lukewarm results. *J Natl Cancer Inst* 94, 1520-1 (2002).

36. Kulke, M.H. et al. A phase II study of troglitazone, an activator of the PPARgamma receptor, in patients with chemotherapy-resistant metastatic colorectal cancer. *Cancer J* 8, 395-9 (2002).

37. Frese, K.K. & Tuveson, D.A. Maximizing mouse cancer models. *Nat Rev Cancer* 7, 645-58 (2007).

38. Dunn, G.P., Old, L.J. & Schreiber, R.D. The three Es of cancer immunoediting. *Annu Rev Immunol* 22, 329-60 (2004).

39. de Visser, K.E., Eichten, A. & Coussens, L.M. Paradoxical roles of the immune system during cancer development. *Nat Rev Cancer* 6, 24-37 (2006).

40. Bocci, G. et al. Antiangiogenic versus cytotoxic therapeutic approaches to human pancreas cancer: an experimental study with a vascular endothelial growth factor receptor-2 tyrosine kinase inhibitor and gemcitabine. *Eur J Pharmacol* 498, 9-18 (2004).

41. Jia, L., Zhang, M.H., Yuan, S.Z. & Huang, W.G. Antiangiogenic therapy for human pancreatic carcinoma xenografts in nude mice. *World J Gastroenterol* 11, 447-50 (2005).

42. Vantyghem, S.A. et al. Dietary genistein reduces metastasis in a postsurgical orthotopic breast cancer model. *Cancer Res* 65, 3396-403 (2005).

43. Olive, K.P. et al. Inhibition of Hedgehog signaling enhances delivery of chemotherapy in a mouse model of pancreatic cancer. *Science* 324, 1457-61 (2009).

44. Faca, V.M. et al. A mouse to human search for plasma proteome changes associated with pancreatic tumor development. *PLoS Med* 5, e123 (2008).

45. Ji, H. et al. The impact of human EGFR kinase domain mutations on lung tumorigenesis and in vivo sensitivity to EGFR-targeted therapies. *Cancer Cell* 9, 485-95 (2006).

46. Politi, K. et al. Lung adenocarcinomas induced in mice by mutant EGF receptors found in human lung cancers respond to a tyrosine kinase inhibitor or to down-regulation of the receptors. *Genes Dev* 20, 1496-510 (2006).

47. Rottenberg, S. et al. Selective induction of chemotherapy resistance of mammary tumors in a conditional mouse model for hereditary breast cancer. *Proc Natl Acad Sci U S A* 104, 12117-22 (2007).

48. Rottenberg, S. & Jonkers, J. Modeling therapy resistance in genetically engineered mouse cancer models. *Drug Resist Updat* 11, 51-60 (2008).

49. Turk, B., Turk, D. & Turk, V. Lysosomal cysteine proteases: more than scavengers. *Biochim Biophys Acta* 1477, 98-111 (2000).

50. Turk, B. et al. Apoptotic pathways: involvement of lysosomal proteases. *Biol Chem* 383, 1035-44 (2002).

51. Friedrichs, B. et al. Thyroid functions of mouse cathepsins B, K, and L. *J Clin Invest* 111, 1733-45 (2003).

52. Conus, S. & Simon, H.U. Cathepsins and their involvement in immune responses. *Swiss Med Wkly* 140, w13042.

53. Hanewinkel, H., Glossl, J. & Kresse, H. Biosynthesis of cathepsin B in cultured normal and I-cell fibroblasts. *J Biol Chem* 262, 12351-5 (1987).

54. Cuozzo, J.W., Tao, K., Wu, Q.L., Young, W. & Sahagian, G.G. Lysine-based structure in the proregion of procathepsin L is the recognition site for mannose phosphorylation. *J Biol Chem* 270, 15611-9 (1995).

55. Tao, K., Stearns, N.A., Dong, J., Wu, Q.L. & Sahagian, G.G. The proregion of cathepsin L is required for proper folding, stability, and ER exit. *Arch Biochem Biophys* 311, 19-27 (1994).

56. Kominami, E., Tsukahara, T., Hara, K. & Katunuma, N. Biosyntheses and processing of lysosomal cysteine proteinases in rat macrophages. *FEBS Lett* 231, 225-8 (1988).

57. Nishimura, Y., Kawabata, T. & Kato, K. Identification of latent procathepsins B and L in microsomal lumen: characterization of enzymatic activation and proteolytic processing in vitro. *Arch Biochem Biophys* 261, 64-71 (1988).

58. Mohamed, M.M. & Sloane, B.F. Cysteine cathepsins: multifunctional enzymes in cancer. *Nat Rev Cancer* 6, 764-75 (2006).

59. Roth, W. et al. Cathepsin L deficiency as molecular defect of furless: hyperproliferation of keratinocytes and pertubation of hair follicle cycling. *FASEB J* 14, 2075-86 (2000).

60. Stypmann, J. et al. Dilated cardiomyopathy in mice deficient for the lysosomal cysteine peptidase cathepsin L. *Proc Natl Acad Sci U S A* 99, 6234-9 (2002).

61. Reinheckel, T., Deussing, J., Roth, W. & Peters, C. Towards specific functions of lysosomal cysteine peptidases: phenotypes of mice deficient for cathepsin B or cathepsin L. *Biol Chem* 382, 735-41 (2001).

62. Felbor, U. et al. Neuronal loss and brain atrophy in mice lacking cathepsins B and L. *Proc Natl Acad Sci U S A* 99, 7883-8 (2002).

63. Chapman, H.A., Riese, R.J. & Shi, G.P. Emerging roles for cysteine proteases in human biology. *Annu Rev Physiol* 59, 63-88 (1997).

64. Kirschke, H., Barrett, A.J. & Rawlings, N.D. Proteinases 1: lysosomal cysteine proteinases. *Protein Profile* 2, 1581-643 (1995).

65. Gong, Q., Chan, S.J., Bajkowski, A.S., Steiner, D.F. & Frankfater, A. Characterization of the cathepsin B gene and multiple mRNAs in human tissues: evidence for alternative splicing of cathepsin B pre-mRNA. *DNA Cell Biol* 12, 299-309 (1993).

66. Musil, D. et al. The refined 2.15 A X-ray crystal structure of human liver cathepsin B: the structural basis for its specificity. *EMBO J* 10, 2321-30 (1991).

67. McGrath, M.E. The lysosomal cysteine proteases. *Annu Rev Biophys Biomol Struct* 28, 181-204 (1999).

68. Fox, T., de Miguel, E., Mort, J.S. & Storer, A.C. Potent slow-binding inhibition of cathepsin B by its propeptide. *Biochemistry* 31, 12571-6 (1992).

69. Pungercar, J.R. et al. Autocatalytic processing of procathepsin B is triggered by proenzyme activity. *FEBS J* 276, 660-8 (2009).

70. Quraishi, O. et al. The occluding loop in cathepsin B defines the pH dependence of inhibition by its propeptide. *Biochemistry* 38, 5017-23 (1999).

71. Rozman, J., Stojan, J., Kuhelj, R., Turk, V. & Turk, B. Autocatalytic processing of recombinant human procathepsin B is a bimolecular process. *FEBS Lett* 459, 358-62 (1999).

72. Chan, A.T. et al. Cathepsin B Expression and Survival in Colon Cancer: Implications for Molecular Detection of Neoplasia. *Cancer Epidemiol Biomarkers Prev*.

73. Devetzi, M. et al. Cathepsin B protein levels in endometrial cancer: Potential value as a tumour biomarker. *Gynecol Oncol* 112, 531-6 (2009).

74. Cordes, C. et al. Simultaneous expression of Cathepsins B and K in pulmonary adenocarcinomas and squamous cell carcinomas predicts poor recurrence-free and overall survival. *Lung Cancer* 64, 79-85 (2009).

75. Colin, C. et al. High expression of cathepsin B and plasminogen activator inhibitor type-1 are strong predictors of survival in glioblastomas. *Acta Neuropathol* 118, 745-54 (2009).

76. Strojnik, T., Kavalar, R., Trinkaus, M. & Lah, T.T. Cathepsin L in glioma progression: comparison with cathepsin B. *Cancer Detect Prev* 29, 448-55 (2005).

77. Niedergethmann, M. et al. Prognostic impact of cysteine proteases cathepsin B and cathepsin L in pancreatic adenocarcinoma. *Pancreas* 29, 204-11 (2004).

78. Vigneswaran, N. et al. Variable expression of cathepsin B and D correlates with highly invasive and metastatic phenotype of oral cancer. *Hum Pathol* 31, 931-7 (2000).

79. Kos, J. et al. Cathepsins B, H, and L and their inhibitors stefin A and cystatin C in sera of melanoma patients. *Clin Cancer Res* 3, 1815-22 (1997).

80. Hughes, S.J. et al. A novel amplicon at 8p22-23 results in overexpression of cathepsin B in esophageal adenocarcinoma. *Proc Natl Acad Sci U S A* 95, 12410-5 (1998).

81. Lin, L. et al. A minimal critical region of the 8p22-23 amplicon in esophageal adenocarcinomas defined using sequence tagged site-amplification mapping and quantitative polymerase chain reaction includes the GATA-4 gene. *Cancer Res* 60, 1341-7 (2000).

82. Yan, S. & Sloane, B.F. Molecular regulation of human cathepsin B: implication in pathologies. *Biol Chem* 384, 845-54 (2003).

83. Berquin, I.M., Cao, L., Fong, D. & Sloane, B.F. Identification of two new exons and multiple transcription start points in the 5'-untranslated region of the human cathepsin-B-encoding gene. *Gene* 159, 143-9 (1995).

84. Hizel, C. et al. Evaluation of the 5' spliced form of human cathepsin B mRNA in colorectal mucosa and tumors. *Oncol Rep* 5, 31-4 (1998).

85. Zwicky, R., Muntener, K., Csucs, G., Goldring, M.B. & Baici, A. Exploring the role of 5' alternative splicing and of the 3'-untranslated region of cathepsin B mRNA. *Biol Chem* 384, 1007-18 (2003).

86. Yan, S., Berquin, I.M., Troen, B.R. & Sloane, B.F. Transcription of human cathepsin B is mediated by Sp1 and Ets family factors in glioma. *DNA Cell Biol* 19, 79-91 (2000).

87. Konduri, S. et al. Elevated levels of cathepsin B in human glioblastoma cell lines. *Int J Oncol* 19, 519-24 (2001).

88. Berquin, I.M. et al. Differentiating agents regulate cathepsin B gene expression in HL-60 cells. *J Leukoc Biol* 66, 609-16 (1999).

89. Mai, J., Finley, R.L., Jr., Waisman, D.M. & Sloane, B.F. Human procathepsin B interacts with the annexin II tetramer on the surface of tumor cells. *J Biol Chem* 275, 12806-12 (2000).

90. Cavallo-Medved, D., Mai, J., Dosescu, J., Sameni, M. & Sloane, B.F. Caveolin-1 mediates the expression and localization of cathepsin B, pro-urokinase plasminogen activator and their cell-surface receptors in human colorectal carcinoma cells. *J Cell Sci* 118, 1493-503 (2005).

91. Cavallo-Medved, D. et al. Mutant K-ras regulates cathepsin B localization on the surface of human colorectal carcinoma cells. *Neoplasia* 5, 507-19 (2003).

92. Koblinski, J.E. et al. Interaction of human breast fibroblasts with collagen I increases secretion of procathepsin B. *J Biol Chem* 277, 32220-7 (2002).

93. Rozhin, J., Sameni, M., Ziegler, G. & Sloane, B.F. Pericellular pH affects distribution and secretion of cathepsin B in malignant cells. *Cancer Res* 54, 6517-25 (1994).

94. Stahl, A. & Mueller, B.M. The urokinase-type plasminogen activator receptor, a GPI-linked protein, is localized in caveolae. *J Cell Biol* 129, 335-44 (1995).

95. Annabi, B. et al. Localization of membrane-type 1 matrix metalloproteinase in caveolae membrane domains. *Biochem J* 353, 547-53 (2001).

96. Puyraimond, A., Fridman, R., Lemesle, M., Arbeille, B. & Menashi, S. MMP-2 colocalizes with caveolae on the surface of endothelial cells. *Exp Cell Res* 262, 28-36 (2001).

97. Gocheva, V. et al. Distinct roles for cysteine cathepsin genes in multistage tumorigenesis. *Genes Dev* 20, 543-56 (2006).

98. Joyce, J.A. et al. Cathepsin cysteine proteases are effectors of invasive growth and angiogenesis during multistage tumorigenesis. *Cancer Cell* 5, 443-53 (2004).

99. Sevenich, L. et al. Transgenic expression of human cathepsin B promotes progression and metastasis of polyoma-middle-T-induced breast cancer in mice. *Oncogene*.

100. Vasiljeva, O. et al. Reduced tumour cell proliferation and delayed development of high-grade mammary carcinomas in cathepsin B-deficient mice. *Oncogene* 27, 4191-9 (2008).

101. Gounaris, E. et al. Live imaging of cysteine-cathepsin activity reveals dynamics of focal inflammation, angiogenesis, and polyp growth. *PLoS One* 3, e2916 (2008).

102. Vasiljeva, O. et al. Tumor cell-derived and macrophage-derived cathepsin B promotes progression and lung metastasis of mammary cancer. *Cancer Res* 66, 5242-50 (2006).

103. Gocheva, V. et al. IL-4 induces cathepsin protease activity in tumor-associated macrophages to promote cancer growth and invasion. *Genes Dev* 24, 241-55.

104. Marino, S., Vooijs, M., van Der Gulden, H., Jonkers, J. & Berns, A. Induction of medulloblastomas in p53-null mutant mice by somatic inactivation of Rb in the external granular layer cells of the cerebellum. *Genes Dev* 14, 994-1004 (2000).

105. Halangk, W. et al. Role of cathepsin B in intracellular trypsinogen activation and the onset of acute pancreatitis. *J Clin Invest* 106, 773-81 (2000).

106. Schreiber, F.S. et al. Successful growth and characterization of mouse pancreatic ductal cells: functional properties of the Ki-RAS(G12V) oncogene. *Gastroenterology* 127, 250-60 (2004).

107. Ebert, D.H., Kopecky-Bromberg, S.A. & Dermody, T.S. Cathepsin B Is Inhibited in Mutant Cells Selected during Persistent Reovirus Infection. *J Biol Chem* 279, 3837-51 (2004).

108. Hasan, L. et al. Function of liver activation-regulated chemokine/CC chemokine ligand 20 is differently affected by cathepsin B and cathepsin D processing. *J Immunol* 176, 6512-22 (2006).

109. Canbay, A. et al. Cathepsin B inactivation attenuates hepatic injury and fibrosis during cholestasis. *J Clin Invest* 112, 152-9 (2003).

110. Ha, S.D. et al. Cathepsin B is involved in the trafficking of TNF-alpha-containing vesicles to the plasma membrane in macrophages. *J Immunol* 181, 690-7 (2008).

111. Talar-Wojnarowska, R. et al. Clinical significance of interleukin-6 (IL-6) gene polymorphism and IL-6 serum level in pancreatic adenocarcinoma and chronic pancreatitis. *Dig Dis Sci* 54, 683-9 (2009).

112. Ohta, T. et al. Pancreatic trypsinogen and cathepsin B in human pancreatic carcinomas and associated metastatic lesions. *Br J Cancer* 69, 152-6 (1994).

113. Niedergethmann, M. et al. Angiogenesis and cathepsin expression are prognostic factors in pancreatic adenocarcinoma after curative resection. *Int J Pancreatol* 28, 31-9 (2000).

114. Buck, M.R., Karustis, D.G., Day, N.A., Honn, K.V. & Sloane, B.F. Degradation of extracellular-matrix proteins by human cathepsin B from normal and tumour tissues. *Biochem J* 282 (Pt 1), 273-8 (1992).

115. Fearon, E.R. & Vogelstein, B. A genetic model for colorectal tumorigenesis. *Cell* 61, 759-67 (1990).

116. Sloane, B.F. et al. Membrane association of cathepsin B can be induced by transfection of human breast epithelial cells with c-Ha-ras oncogene. *J Cell Sci* 107 (Pt 2), 373-84 (1994).

117. Mach, L., Stuwe, K., Hagen, A., Ballaun, C. & Glossl, J. Proteolytic processing and glycosylation of cathepsin B. The role of the primary structure of the latent precursor and of the carbohydrate moiety for cell-type-specific molecular forms of the enzyme. *Biochem J* 282 (Pt 2), 577-82 (1992).

118. Cardone, R.A., Casavola, V. & Reshkin, S.J. The role of disturbed pH dynamics and the Na+/H+ exchanger in metastasis. *Nat Rev Cancer* 5, 786-95 (2005).

119. Stubbs, M., McSheehy, P.M., Griffiths, J.R. & Bashford, C.L. Causes and consequences of tumour acidity and implications for treatment. *Mol Med Today* 6, 15-9 (2000).

120. Rofstad, E.K., Mathiesen, B., Kindem, K. & Galappathi, K. Acidic extracellular pH promotes experimental metastasis of human melanoma cells in athymic nude mice. *Cancer Res* 66, 6699-707 (2006).

121. Brodt, P., Reich, R., Moroz, L.A. & Chambers, A.F. Differences in the repertoires of basement membrane degrading enzymes in two carcinoma sublines with distinct patterns of site-selective metastasis. *Biochim Biophys Acta* 1139, 77-83 (1992).

122. Navab, R., Mort, J.S. & Brodt, P. Inhibition of carcinoma cell invasion and liver metastases formation by the cysteine proteinase inhibitor E-64. *Clin Exp Metastasis* 15, 121-9 (1997).

123. Sevenich, L. et al. Synergistic antitumor effects of combined cathepsin B and cathepsin Z deficiencies on breast cancer progression and metastasis in mice. *Proc Natl Acad Sci U S A* 107, 2497-502.

124. Gopinath, S. et al. Co-depletion of cathepsin B and uPAR induces G0/G1 arrest in glioma via FOXO3a mediated p27 upregulation. *PLoS One* 5, e11668.

125. Gondi, C.S. et al. RNAi-mediated inhibition of cathepsin B and uPAR leads to decreased cell invasion, angiogenesis and tumor growth in gliomas. *Oncogene* 23, 8486-96 (2004).

126. Veeravalli, K.K. et al. MMP-9, uPAR and cathepsin B silencing downregulate integrins in human glioma xenograft cells in vitro and in vivo in nude mice. *PLoS One* 5, e11583.

127. Moles, A., Tarrats, N., Fernandez-Checa, J.C. & Mari, M. Cathepsins B and D drive hepatic stellate cell proliferation and promote their fibrogenic potential. *Hepatology* 49, 1297-307 (2009).

128. Mebratu, Y. & Tesfaigzi, Y. How ERK1/2 activation controls cell proliferation and cell death: Is subcellular localization the answer? *Cell Cycle* 8, 1168-75 (2009).

129. Kenig, S., Alonso, M.B., Mueller, M.M. & Lah, T.T. Glioblastoma and endothelial cells cross-talk, mediated by SDF-1, enhances tumour invasion and endothelial proliferation by increasing expression of cathepsins B, S, and MMP-9. *Cancer Lett* (2009).

130. Bell-McGuinn, K.M., Garfall, A.L., Bogyo, M., Hanahan, D. & Joyce, J.A. Inhibition of cysteine cathepsin protease activity enhances chemotherapy regimens by decreasing tumor growth and invasiveness in a mouse model of multistage cancer. *Cancer Res* 67, 7378-85 (2007).

131. Schurigt, U. et al. Trial of the cysteine cathepsin inhibitor JPM-OEt on early and advanced mammary cancer stages in the MMTV-PyMT-transgenic mouse model. *Biol Chem* 389, 1067-74 (2008).

132. Lerch, M.M. & Halangk, W. Human pancreatitis and the role of cathepsin B. *Gut* 55, 1228-30 (2006).

133. Figarella, C., Miszczuk-Jamska, B. & Barrett, A.J. Possible lysosomal activation of pancreatic zymogens. Activation of both human trypsinogens by cathepsin B and spontaneous acid. Activation of human trypsinogen 1. *Biol Chem Hoppe Seyler* 369 Suppl, 293-8 (1988).

134. Saluja, A. et al. Subcellular redistribution of lysosomal enzymes during caerulein-induced pancreatitis. *Am J Physiol* 253, G508-16 (1987).

135. Lugea, A. et al. Pancreas recovery following cerulein-induced pancreatitis is impaired in plasminogen-deficient mice. *Gastroenterology* 131, 885-99 (2006).

136. Aplin, A.E., Stewart, S.A., Assoian, R.K. & Juliano, R.L. Integrin-mediated adhesion regulates ERK nuclear translocation and phosphorylation of Elk-1. *J Cell Biol* 153, 273-82 (2001).

137. Zhao, M., Discipio, R.G., Wimmer, A.G. & Schraufstatter, I.U. Regulation of CXCR4-mediated nuclear translocation of extracellular signal-related kinases 1 and 2. *Mol Pharmacol* 69, 66-75 (2006).

138. Formstecher, E. et al. PEA-15 mediates cytoplasmic sequestration of ERK MAP kinase. *Dev Cell* 1, 239-50 (2001).

139. Smith, E.R. et al. Nuclear entry of activated MAPK is restricted in primary ovarian and mammary epithelial cells. *PLoS One* 5, e9295.

140. Kirsten, W.H., Schauf, V. & McCoy, J. Properties of a murine sarcoma virus. *Bibl Haematol*, 246-9 (1970).

141. Harvey, J.J. An Unidentified Virus Which Causes the Rapid Production of Tumours in Mice. *Nature* 204, 1104-5 (1964).

142. Cooper, G.M. Cellular transforming genes. *Science* 217, 801-6 (1982).

143. Parada, L.F., Tabin, C.J., Shih, C. & Weinberg, R.A. Human EJ bladder carcinoma oncogene is homologue of Harvey sarcoma virus ras gene. *Nature* 297, 474-8 (1982).

144. Hall, A., Marshall, C.J., Spurr, N.K. & Weiss, R.A. Identification of transforming gene in two human sarcoma cell lines as a new member of the ras gene family located on chromosome 1. *Nature* 303, 396-400 (1983).

145. Taparowsky, E., Shimizu, K., Goldfarb, M. & Wigler, M. Structure and activation of the human N-ras gene. *Cell* 34, 581-6 (1983).

146. Reuther, G.W. & Der, C.J. The Ras branch of small GTPases: Ras family members don't fall far from the tree. *Curr Opin Cell Biol* 12, 157-65 (2000).

147. Daub, H., Weiss, F.U., Wallasch, C. & Ullrich, A. Role of transactivation of the EGF receptor in signalling by G-protein-coupled receptors. *Nature* 379, 557-60 (1996).

148. Cullen, P.J. & Lockyer, P.J. Integration of calcium and Ras signalling. *Nat Rev Mol Cell Biol* 3, 339-48 (2002).

149. Takai, Y., Sasaki, T. & Matozaki, T. Small GTP-binding proteins. *Physiol Rev* 81, 153-208 (2001).

150. Yordy, J.S. & Muise-Helmericks, R.C. Signal transduction and the Ets family of transcription factors. *Oncogene* 19, 6503-13 (2000).

151. Pruitt, K. & Der, C.J. Ras and Rho regulation of the cell cycle and oncogenesis. *Cancer Lett* 171, 1-10 (2001).

152. Downward, J. Targeting RAS signalling pathways in cancer therapy. *Nat Rev Cancer* 3, 11-22 (2003).

153. Esteban, L.M. et al. Targeted genomic disruption of H-ras and N-ras, individually or in combination, reveals the dispensability of both loci for mouse growth and development. *Mol Cell Biol* 21, 1444-52 (2001).

154. Umanoff, H., Edelmann, W., Pellicer, A. & Kucherlapati, R. The murine N-ras gene is not essential for growth and development. *Proc Natl Acad Sci U S A* 92, 1709-13 (1995).

155. Ise, K. et al. Targeted deletion of the H-ras gene decreases tumor formation in mouse skin carcinogenesis. *Oncogene* 19, 2951-6 (2000).

156. Perez de Castro, I. et al. Mice deficient for N-ras: impaired antiviral immune response and T-cell function. *Cancer Res* 63, 1615-22 (2003).

157. Johnson, L. et al. K-ras is an essential gene in the mouse with partial functional overlap with N-ras. *Genes Dev* 11, 2468-81 (1997).

158. Plowman, S.J. et al. While K-ras is essential for mouse development, expression of the K-ras 4A splice variant is dispensable. *Mol Cell Biol* 23, 9245-50 (2003).

159. Reddy, E.P., Reynolds, R.K., Santos, E. & Barbacid, M. A point mutation is responsible for the acquisition of transforming properties by the T24 human bladder carcinoma oncogene. *Nature* 300, 149-52 (1982).

160. Bos, J.L. ras oncogenes in human cancer: a review. *Cancer Res* 49, 4682-9 (1989).

161. Weinstein, I.B. Cancer. Addiction to oncogenes--the Achilles heal of cancer. *Science* 297, 63-4 (2002).

162. Sharma, S.V. & Settleman, J. Oncogene addiction: setting the stage for molecularly targeted cancer therapy. *Genes Dev* 21, 3214-31 (2007).

163. Sebti, S.M. & Der, C.J. Opinion: Searching for the elusive targets of farnesyltransferase inhibitors. *Nat Rev Cancer* 3, 945-51 (2003).

164. Sebti, S.M. & Hamilton, A.D. Farnesyltransferase and geranylgeranyltransferase I inhibitors and cancer therapy: lessons from mechanism and bench-to-bedside translational studies. *Oncogene* 19, 6584-93 (2000).

165. Cox, A.D. & Der, C.J. Farnesyltransferase inhibitors: promises and realities. *Curr Opin Pharmacol* 2, 388-93 (2002).

166. Kohl, N.E. et al. Inhibition of farnesyltransferase induces regression of mammary and salivary carcinomas in ras transgenic mice. *Nat Med* 1, 792-7 (1995).

167. Sun, J. et al. Antitumor efficacy of a novel class of non-thiol-containing peptidomimetic inhibitors of farnesyltransferase and geranylgeranyltransferase I: combination therapy with the cytotoxic agents cisplatin, Taxol, and gemcitabine. *Cancer Res* 59, 4919-26 (1999).

168. Lerner, E.C. et al. Ras CAAX peptidomimetic FTI-277 selectively blocks oncogenic Ras signaling by inducing cytoplasmic accumulation of inactive Ras-Raf complexes. *J Biol Chem* 270, 26802-6 (1995).

169. Bredel, M., Pollack, I.F., Freund, J.M., Hamilton, A.D. & Sebti, S.M. Inhibition of Ras and related G-proteins as a therapeutic strategy for blocking malignant glioma growth. *Neurosurgery* 43, 124-31; discussion 131-2 (1998).

170. Pollack, I.F., Bredel, M., Erff, M., Hamilton, A.D. & Sebti, S.M. Inhibition of Ras and related guanosine triphosphate-dependent proteins as a therapeutic strategy for blocking malignant glioma growth: II--preclinical studies in a nude mouse model. *Neurosurgery* 45, 1208-14; discussion 1214-5 (1999).

171. Lantry, L.E. et al. Effect of farnesyltransferase inhibitor FTI-276 on established lung adenomas from A/J mice induced by 4-(methylnitrosamino)-1-(3-pyridyl)-1-butanone. *Carcinogenesis* 21, 113-6 (2000).

172. Zhang, Z. et al. Farnesyltransferase inhibitors are potent lung cancer chemopreventive agents in A/J mice with a dominant-negative p53 and/or heterozygous deletion of Ink4a/Arf. *Oncogene* 22, 6257-65 (2003).

173. Lobell, R.B. et al. Evaluation of farnesyl:protein transferase and geranylgeranyl:protein transferase inhibitor combinations in preclinical models. *Cancer Res* 61, 8758-68 (2001).

174. Elad-Sfadia, G., Haklai, R., Ballan, E., Gabius, H.J. & Kloog, Y. Galectin-1 augments Ras activation and diverts Ras signals to Raf-1 at the expense of phosphoinositide 3-kinase. *J Biol Chem* 277, 37169-75 (2002).

175. Elad-Sfadia, G., Haklai, R., Balan, E. & Kloog, Y. Galectin-3 augments K-Ras activation and triggers a Ras signal that attenuates ERK but not phosphoinositide 3-kinase activity. *J Biol Chem* 279, 34922-30 (2004).

176. Marciano, D. et al. Farnesyl derivatives of rigid carboxylic acids-inhibitors of ras-dependent cell growth. *J Med Chem* 38, 1267-72 (1995).

177. Elad, G. et al. Targeting of K-Ras 4B by S-trans,trans-farnesyl thiosalicylic acid. *Biochim Biophys Acta* 1452, 228-42 (1999).

178. Marom, M. et al. Selective inhibition of Ras-dependent cell growth by farnesylthiosalisylic acid. *J Biol Chem* 270, 22263-70 (1995).

179. Gana-Weisz, M. et al. The Ras antagonist S-farnesylthiosalicylic acid induces inhibition of MAPK activation. *Biochem Biophys Res Commun* 239, 900-4 (1997).

180. Goldberg, L. & Kloog, Y. A Ras inhibitor tilts the balance between Rac and Rho and blocks phosphatidylinositol 3-kinase-dependent glioblastoma cell migration. *Cancer Res* 66, 11709-17 (2006).

181. Blum, R., Jacob-Hirsch, J., Amariglio, N., Rechavi, G. & Kloog, Y. Ras inhibition in glioblastoma down-regulates hypoxia-inducible factor-1alpha, causing glycolysis shutdown and cell death. *Cancer Res* 65, 999-1006 (2005).

182. Yaari, S. et al. Disruption of cooperation between Ras and MycN in human neuroblastoma cells promotes growth arrest. *Clin Cancer Res* 11, 4321-30 (2005).

183. Egozi, Y., Weisz, B., Gana-Weisz, M., Ben-Baruch, G. & Kloog, Y. Growth inhibition of ras-dependent tumors in nude mice by a potent ras-dislodging antagonist. *Int J Cancer* 80, 911-8 (1999).

184. Jansen, B. et al. Novel Ras antagonist blocks human melanoma growth. *Proc Natl Acad Sci U S A* 96, 14019-24 (1999).

185. Weisz, B. et al. A new functional Ras antagonist inhibits human pancreatic tumor growth in nude mice. *Oncogene* 18, 2579-88 (1999).

186. Haklai, R., Elad-Sfadia, G., Egozi, Y. & Kloog, Y. Orally administered FTS (salirasib) inhibits human pancreatic tumor growth in nude mice. *Cancer Chemother Pharmacol* 61, 89-96 (2008).

187. Tsimberidou, A.M. et al. Phase 1 first-in-human clinical study of S-trans, trans-farnesylthiosalicylic acid (salirasib) in patients with solid tumors. *Cancer Chemother Pharmacol* (2009).

188. Cook, N., Olive, K.P., Frese, K. & Tuveson, D.A. K-Ras-driven pancreatic cancer mouse model for anticancer inhibitor analyses. *Methods Enzymol* 439, 73-85 (2008).

189. Rotblat, B., Ehrlich, M., Haklai, R. & Kloog, Y. The Ras inhibitor farnesylthiosalicylic acid (Salirasib) disrupts the spatiotemporal localization of active Ras: a potential treatment for cancer. *Methods Enzymol* 439, 467-89 (2008).

190. Zhao, M. et al. Determination of salirasib (S-trans,trans-farnesylthiosalicylic acid) in human plasma using liquid chromatography-tandem mass spectrometry. *J Chromatogr B Analyt Technol Biomed Life Sci* 869, 142-5 (2008).

191. Yaari-Stark, S. et al. Ras inhibits endoplasmic reticulum stress in human cancer cells with amplified Myc. *Int J Cancer* 126, 2268-81.

192. Blum, R., Jacob-Hirsch, J., Rechavi, G. & Kloog, Y. Suppression of survivin expression in glioblastoma cells by the Ras inhibitor farnesylthiosalicylic acid promotes caspase-dependent apoptosis. *Mol Cancer Ther* 5, 2337-47 (2006).

193. Zundelevich, A., Elad-Sfadia, G., Haklai, R. & Kloog, Y. Suppression of lung cancer tumor growth in a nude mouse model by the Ras inhibitor salirasib (farnesylthiosalicylic acid). *Mol Cancer Ther* 6, 1765-73 (2007).

194. Shalom-Feuerstein, R., Lindenboim, L., Stein, R., Cox, A.D. & Kloog, Y. Restoration of sensitivity to anoikis in Ras-transformed rat intestinal epithelial cells by a Ras inhibitor. *Cell Death Differ* 11, 244-7 (2004).

195. Barkan, B., Starinsky, S., Friedman, E., Stein, R. & Kloog, Y. The Ras inhibitor farnesylthiosalicylic acid as a potential therapy for neurofibromatosis type 1. *Clin Cancer Res* 12, 5533-42 (2006).

196. Santen, R.J., Lynch, A.R., Neal, L.R., McPherson, R.A. & Yue, W. Farnesylthiosalicylic acid: inhibition of proliferation and enhancement of apoptosis of hormone-dependent breast cancer cells. *Anticancer Drugs* 17, 33-40 (2006).

197. Halaschek-Wiener, J., Kloog, Y., Wacheck, V. & Jansen, B. Farnesyl thiosalicylic acid chemosensitizes human melanoma in vivo. *J Invest Dermatol* 120, 109-15 (2003).

198. Jansen, B. et al. Farnesylthiosalicylic acid inhibits the growth of human Merkel cell carcinoma in SCID mice. *J Mol Med* 77, 792-7 (1999).

199. Yue, W., Wang, J., Li, Y., Fan, P. & Santen, R.J. Farnesylthiosalicylic acid blocks mammalian target of rapamycin signaling in breast cancer cells. *Int J Cancer* 117, 746-54 (2005).

200. Hanker, A.B. et al. Differential requirement of CAAX-mediated posttranslational processing for Rheb localization and signaling. *Oncogene* 29, 380-91.

201. McMahon, L.P., Yue, W., Santen, R.J. & Lawrence, J.C., Jr. Farnesylthiosalicylic acid inhibits mammalian target of rapamycin (mTOR) activity both in cells and in vitro by promoting dissociation of the mTOR-raptor complex. *Mol Endocrinol* 19, 175-83 (2005).

202. Halaschek-Wiener, J. et al. A novel Ras antagonist regulates both oncogenic Ras and the tumor suppressor p53 in colon cancer cells. *Mol Med* 6, 693-704 (2000).

203. Kho, Y. et al. A tagging-via-substrate technology for detection and proteomics of farnesylated proteins. *Proc Natl Acad Sci U S A* 101, 12479-84 (2004).

204. Tamanoi, F., Gau, C.L., Jiang, C., Edamatsu, H. & Kato-Stankiewicz, J. Protein farnesylation in mammalian cells: effects of farnesyltransferase inhibitors on cancer cells. *Cell Mol Life Sci* 58, 1636-49 (2001).

205. Jenkins, C.M. et al. Purification of recombinant human cPLA2 gamma and identification of C-terminal farnesylation, proteolytic processing, and carboxymethylation by MALDI-TOF-TOF analysis. *Biochemistry* 42, 11798-807 (2003).

206. Liu, F.T., Patterson, R.J. & Wang, J.L. Intracellular functions of galectins. *Biochim Biophys Acta* 1572, 263-73 (2002).

207. Dagher, S.F., Wang, J.L. & Patterson, R.J. Identification of galectin-3 as a factor in pre-mRNA splicing. *Proc Natl Acad Sci U S A* 92, 1213-7 (1995).

208. Wang, J.L., Gray, R.M., Haudek, K.C. & Patterson, R.J. Nucleocytoplasmic lectins. *Biochim Biophys Acta* 1673, 75-93 (2004).

209. Liu, F.T. & Rabinovich, G.A. Galectins as modulators of tumour progression. *Nat Rev Cancer* 5, 29-41 (2005).

210. Shalom-Feuerstein, R. et al. K-ras nanoclustering is subverted by overexpression of the scaffold protein galectin-3. *Cancer Res* 68, 6608-16 (2008).

211. Bermudez, O., Pages, G. & Gimond, C. The dual-specificity MAP kinase phosphatases: critical roles in development and cancer. *Am J Physiol Cell Physiol* 299, C189-202.

212. Blum, R. et al. Gene expression signature of human cancer cell lines treated with the ras inhibitor salirasib (S-farnesylthiosalicylic acid). *Cancer Res* 67, 3320-8 (2007).

APPENDIX 1

No.	Protein name	Fold change
1	6Ckine	-1.26
2	ALK-1	-1.10
3	Amphiregulin	1.01
4	Axl	2.15
5	BLC	1.04
6	Cardiotrophin-1	-1.06
7	CD27	1.68
8	CD27 L	1.02
9	CD30	1.23
10	CD30L	-1.06
11	CD36/SR-B3	1.19
12	CTLA-4	-1.30
13	CXCL16	1.51
14	Decorin	1.97
15	Dkk-1	1.78
16	E-Cadherin	-1.29
17	EGF	-1.19
18	Eotaxin	-1.13
19	Eotaxin-2	-1.16
20	Epigen	-1.32
21	E-Selectin	-1.14
22	Fas Ligand	-1.76
23	Fcg RIIB	-1.10
24	Flt-3 Ligand	-1.33
25	Fractalkine	1.09
26	Galectin-1	1.13
27	Gas6	-1.11
28	GCSF	-1.59
29	GITR	-1.23
30	GITR ligand	1.07
31	Granzyme B	1.16
32	HAI-1	1.04
33	HGF	-1.01
34	IFN gamma	-1.32
35	IGFBP-5	1.12
36	IGFBP-6	-1.32
37	IGF-II	-1.05

38	IL-1 alpha	1.12
39	IL-1 beta	1.67
40	IL-1ra	1.12
41	IL-2	1.26
42	IL-2 R alpha	1.21
43	IL-3	-1.23
44	IL-4	-1.20
45	IL-5	-1.17
46	IL-6	-4.08
47	IL-9	-1.44
48	IL-10	-2.21
49	IL-11	-1.13
50	IL-12 p40	3.76
51	IL-12 p70	-1.52
52	IL-13	-1.29
53	IL-15	1.59
54	IL-17	1.11
55	IL-17B R	-1.04
56	IL-17E	1.53
57	IL-17F	1.41
58	IL-20	1.43
59	IL-21	1.13
60	I-TAC	-1.55
61	JAM-A	-1.21
62	KC	-1.68
63	Leptin	-1.03
64	Leptin R	-1.36
65	L-Selectin	-1.32
66	Lungkine	1.26
67	Mad CAM-1	1.03
68	MCP-1	-1.07
69	MDC	-1.09
70	MFG-E8	-1.08
71	MIG	1.08
72	MIP-1 alpha	-1.69
73	MIP-1 gamma	1.08
74	MIP2	-1.90
75	MIP-3 alpha	-1.04
76	MIP-3 beta	-1.15
77	MMP-2	-1.20
78	Osteopontin	-1.16
79	Osteoprotegerin	1.86

80	Prolactin	2.44
81	SCF	-1.44
82	sTNF RI	1.88
83	sTNF RII	1.24
84	TACI	1.17
85	TARC	1.13
86	TNF alpha	-1.20
87	TPO	-1.16
88	TRANCE	-1.51
89	TROY	-1.12
90	TWEAK R	1.01
91	VCAM-1	1.14
92	VEGF	1.08
93	VEGF R1	-1.46
94	VEGF R3	1.24
95	VEGF-D	1.12

Appendix 1: Cytokine array analysis from tumours

Comparison of cytokine profiles between tumours from KPC;B+/+ and KPC;B-/- mice using an antibody-based array. The fold change listed is relative to KPC;B+/+ tissue.